Long Range Measurement and High Spatial Resolution Optical Frequency Domain Reflectometry Based on DSB-SC Modulation

By

Mudabbir Badar

Thesis submitted to the

Faculty of Graduate School of Engineering

In partial fulfillment of the requirements for the degree of

Doctor of Engineering

Kochi University of Technology, Japan

February, 2016.

Abstract

Optical reflectometry techniques are very useful instrument in optical communication systems and optical sensing networks. The fault location and fiber loss which are important factors for optical link diagnosis are analyzed by the means of optical reflectometry techniques and in optical sensing networks reflectometry techniques are used as a tool to sense the change in temperature/strain or vibration. Spatial resolution and sensitivity are the two essential factors to evaluate the performance of optical reflectometry techniques. Sensitivity sets a limit up to where measurements can be performed and spatial resolution is a precision parameter which tells how close two events can be detected separately. Despite of poor sensitivity and low spatial resolution the optical time domain reflectometry technique (OTDR) is the mainly used reflectometry technique because of long measurement range. On the other hand optical frequency domain reflectometry (OFDR) has higher spatial resolution and better sensitivity but its practice is limited to short length measurements. The laser phase noise is the main reason for short length measurement limitation in OFDR, as measurement range exceeds the laser coherence length the phase noise increases significantly and degrades the signal to noise ratio (SNR) to an undetectable level. In this research a new type of OFDR called double sideband phase noise canceled OFDR (DSB-PNC OFDR) is proposed in which laser phase noise is canceled out which made measurements beyond coherence length possible. The proposed method is simpler in configuration and does not require cumbersome computational processing. The proposed OFDR uses double sideband suppressed carrier (DSB-SC) modulation to cancel the laser phase noise. DSB-SC modulation creates two sidebands and when the sweep frequency is applied they are swept in opposite directions, the swept DSB-SC modulated signal is used as OFDR signal. After detection, two sidebands of DSB-SC modulated signal has equal phase noise but opposite in sign, therefore by separating two sidebands and multiplying them with each other cancel out the laser phase noise and remaining term is only beat frequency. The proposed method can be deployed in two sorts of arrangements heterodyne detection and phase diversity detection. The heterodyne detection works well if break point is located over far distance, however, if the break point is located over short distance the phase noise is not completely canceled out because of spectral fold back phenomenon. Phase diversity detection technique can be used as a solution to heterodyne detection spectrum fold back problem because fold back of spectrum phenomenon does not occur in phase diversity detection. The proposed method had been demonstrated by the means of experiments. In one of the demonstrations two break points 10 cm far from each other were detected in a short (120 m) and long fiber (20 km) using phase diversity detection technique. Both lengths of fiber were beyond the laser coherence length (100 m) where phase noise has significant influence. Furthermore, the high spatial resolution achievability of the

proposed OFDR was also demonstrated by measuring the fiber temperature dependence with good accuracy in a 1 km long fiber with a laser of 100 m coherence length.

Chromatic dispersion affects in the transmission optical fiber are treated as one of the impairments for the overall performance. In order to design a system which can compensate chromatic dispersion affects in the fiber link, it is required to have a precise knowledge about chromatic dispersion of the optical fiber. Phase shift method and sideband modulation are the two well-known methods for accurate chromatic dispersion measurement in the optical fiber. However, both mentioned methods are the two end methods which means both ends of the optical fiber are required to be accessible. In a scenario where optical fiber is already deployed as a part of transmission network it is always not possible to have access to both ends of the fiber. In such a condition measuring chromatic dispersion using OTDR is preferred because it is a one end measurement technique. Nevertheless, chromatic dispersion measurement accuracy of OTDR is not well appreciated because of poor spatial resolution. In this research a new method to measure chromatic dispersion with higher accuracy in long optical fibers is proposed. The proposed method uses DSB-PNC OFDR which can perform measurements in the long optical fiber beyond the laser coherence length with good spatial resolution. It was demonstrated that the proposed method can measure chromatic dispersion in a 50 km long fiber link made up of two 20 km and one 10 km long dispersion shifted fibers. The chromatic dispersion of each fiber segment was measured in connected and detached fashion. The obtained results from proposed method were compared with phase shift method and a close match was observed. The achieved spatial resolution was 7.9 mm and chromatic dispersion with accuracy as good as ± 0.096 ps/nm/km was measured. Moreover, in order to show proposed method can measure chromatic dispersion in other types of the fiber, chromatic dispersion in a 25 km long standard single mode fiber was also measured with accuracy ± 0.076 ps/nm/km.

OFDR is better known for its high spatial resolution capability. The spatial resolution in OFDR is limited by the frequency sweep span through this formula $\Delta l = \frac{c}{2n\Delta f}$ where Δf is the sweep frequency span. In some situations the available sweep span is limited by the bottlenecks imposed by the present electronics, which restricts the achievable spatial resolution. In this research a novel method to increase the available frequency sweep span up to 3-times is proposed which ultimately resulted in enhanced spatial resolution up to 3- times. The proposed method uses degenerated (FWM) with DSB-SC modulation. Usually FWM uses three laser sources (2 pumps and one signal) and this results in increased phase noise up to 3- times. The proposed method to increase frequency sweep span through FWM is using only one laser source which resulted in preserved coherence length because phase noise is not increased. Two side bands created by DSB-SC modulation are treated as two separate signals and when they travel through a non-linear

medium it results in generation of two new frequencies called FWM signals. When the sweep frequency is applied two sidebands are swept in opposite direction, as a result if sidebands are moved one unit in frequency, the FWM signals are moved 3-units because frequency difference between two sidebands increased by two times. The proposed frequency span broadening method can be used with ordinary OFDR arrangement and as well as DSB-PNC OFDR arrangement. The feasibilities of the proposed method are demonstrated by the means of experiments, around 3.4 cm spatial resolution was achieved in ordinary OFDR with only 1 GHz sweep span which corresponds to 10.2 cm spatial resolution. Moreover, phase noise cancelation with enhanced spatial resolution in DSB-PNC OFDR was also demonstrated by canceling the laser phase noise in a 10 km long fiber and achieving spatial resolution around 8.4 cm with only 400 MHZ sweep span which corresponds to 25.2 cm spatial resolution.

Wavelength converters are used in wavelength division multiplexing (WDM) networks for efficient use of wavelength resources. In presence of vast variety of modulation formats it became a requirement for network to deploy a wavelength conversion scheme which can work over all types of signal formats. In this research, a new demonstration about format independency of a wavelength conversion method based on OSSB (optical single sideband) modulation array wave guide (AWG) is also presented. The proposed scheme to increase frequency sweep span was inspired by this demonstration.

Laser phase noise is an intrinsic impairment which is linked with the presence of spectral band in the emitted light. The measurement of the laser phase noise can reveal the spectral linewidth of the laser source and laser linewidth information is essential in many situations. In this research a new method to estimate the laser phase noise is also proposed. The proposed method of laser phase noise estimation is an extension of DSB-PNC OFDR method. As described above the two detected sidebands in DSB-PNC OFDR had equal phase noise but opposite in sign, therefore if phases of two separated sidebands are estimated through signal processing and then subtracting estimated phases from each other will cancel out the beat frequency and remaining term will be purely the laser phase noise. Estimated phase noise can be used in other applications such as the laser linewidth measurement and it can be again used to cancel the laser phase noise in OFDR. If the estimated laser phase noise is multiplied with the one of the channel which has equal but opposite phase noise, it can cancel laser phase noise. With the help of experiment it is shown that the proposed method of phase noise estimation can estimate the laser phase noise correctly, it was proved by using the estimated phase noise to cancel laser phase noise in OFDR and detecting the breakpoint in a 20 km long fiber with 100 m coherence length laser. There are some advantages of canceling laser phase noise using estimated phase noise instead of multiplying two channels. Laser phase noise cancelation using estimated phase noise have same beat frequency as the original one therefore it does not require higher sampling rate, however, multiplication process converts the beat frequency to twice of the original value,

because of doubled beat frequency the minimum required sampling rate was also twice and minimum four times of the original beat frequency in order to fulfil Nyqusit rate requirement. Higher sampling rate required high speed ADC and additional noises because of high sampling rate were not favorable for overall results. Moreover higher sampling rate requirement degrades the spatial resolution between two points as is calculated by $\Delta l = \frac{cf_s}{4n\beta N}$, where f_s is the sampling frequency of A/D converter and N is the length of data point.

Acknowledgment

It would have never been possible to finish all the work presented in this thesis without support and guidance of the people around me.

I would like express my deepest gratitude to my supervisor Prof. Katsushi Iwashita for his great support and proper guidance throughout my three years of learning in kochi university of technology. I am very thankful of him for hours long discussions and finding solution for every single hindrance encountered during experiments, without which, it would had never been possible to finish my work.

I am really grateful of my second supervisor Prof. Hirokazu Kobayashi for his support throughout my course. All the discussions regarding my research with him and his help during experiments were proven fruitful. Moreover, I am very much thankful of him for taking time from his busy schedule for weekly seminar which was a great source of theoretical learning for me.

I would also like to say thanks to my friends around me for being source of energy in low and high times. Finally, I would like to say thanks to all my family members, specially my mother, Mumtaz Begum for her unconditional support and patience.

Table of Contents

List of Figures

List of Tables

List of Acronyms

OTDR	optical time domain reflectometry
C-OFDR	coherent optical frequency domain reflectometry
I-OFDR	incoherent optical frequency domain reflectometry
FWHM	full width half maxima
FUT	fiber under test
DSP	digital signal processing
DSB-SC	double sideband with suppress carrier
PNC	phase noise canceled/compensated
PN	phase noise
OC	optical coupler
PC	polarization controller
PBS	polarization beam splitter
PM	polarization maintaining
BS	backscattered
BPF	band pass filter
LPF	low pass filter
A/D	analog to digital
SNR	signal to noise ratio
DSF	dispersion shifted fiber
SPSM	standard phase shift method
FWM	four wave mixing
HNL	highly nonlinear

FBG	fiber brag grating
OSSB	optical single sideband
AWG	array waveguide grating
WDM	wavelength division multiplexing

Chapter 1 : Introduction

1.1 Background and problem statement

Optical fiber has enormous capabilities and is applied in a vast variety of industries ranging from telecommunication, medical, military, data storage, networking and broadcast industry. Optical fiber attracted a tremendous attention for past four decades and it has been remained a hot topic for researchers in all round the world, which resulted in many breakthroughs related to enhancement of optical fiber capabilities and solving bottlenecks hindering its practice. Optoelectronics industry is of another importance for making optical components easily available at steadily reduced cost.

High bandwidth, which corresponds to higher data rate [1] and low transmission loss, which guarantees better signal to noise ratio (SNR) over long distance makes optical fiber an ideal candidate to be used in high speed communication network [1,2,3]. Optical fiber is also immune to external electromagnetic interference as it carries signal in the optical form unlike its electrical counterparts. The refractive index of optical fiber core varies as the temperature or strain applied is changed, which makes it sensitive towards external perturbations like temperature, strain or vibration and opens up another window of application for optical fiber to be used as a sensor. The quality of robustness, which allows optical fiber to be used in harsh conditions and ability to perform distributed sensing make it a better choice over conventional electrical sensors [4]. Presently, optical fiber sensing is one of the actively researched topic in the field of optical fiber.

In order to diagnose or test the performance of an optical fiber link in the transmission network and optical components requires a sophisticated technique and it is known as reflectometry technique [5]. By means of reflectometry technique, we can obtain optical fiber loss [6] and fiber break point location information, which are essential parameters to keep a network healthy and uninterrupted. The basic working principle of the reflectometry technique is to inject light signal from one end of the optical fiber and inhomogeneity of fiber core reflects a fraction of input light signal back to the sending end (backscattered) throughout the fiber. The detection of backscattered light signal and its analysis based on the type of reflectometry technique can provide the information like fiber loss and breakpoint location in the fiber. Optical reflectometry has another main application in distributed optical sensing, where by detecting change in frequency, amplitude, phase and polarization of backscattered light from each point along the fiber can show accordance to the external circumstances in distributed manner [7]. Spatial resolution and sensitivity are the two characteristics to be considered in reflectometry technique to evaluate its performance. Spatial resolution determines how close two events can be detected separately and sensitivity decides the

minimum detectable signal power limit. Usually spatial resolution required for optical reflectometry in sensing system is in centimeter range to perform precise measurement, and for transmission system the usual spatial resolution required is in meters, and sensing length can range from meters to 100 kilometer [7]. Mainly there are three types of reflectometry techniques used, define as below

- Optical low coherence reflectometry (OLCR)
- Optical time domain reflectometry (OTDR)
- Optical frequency domain reflectometry (OFDR)

OLCR can achieve fine spatial resolution in millimeters range [22]. However, the length over which it can be used is limited to a few meters. OLCR uses a light source of low coherence length (white light) and its practice is limited to inspect optical components. OTDR is another reflectometry technique which is mainly used in long optical fiber such as in optical transmission network with spatial resolution in range of a few meters. Instead of low spatial resolution and poor sensitivity OTDR is the most commonly used reflectometry technique in commercial optical networks because of long measurement distance. On the other hand OFDR, which is a frequency based technique is capable of achieving higher spatial and better sensitivity than OTDR but its practice is limited by short distance applications. Short distance limitation in OFDR is imposed by the laser phase noise, which increases dramatically if the detection is performed beyond the laser coherence length, as a result spatial resolution is degraded to undetectable level. Commonly used lasers have linewidth around a few MHz, which sets the coherence length to some tens of meters. Therefore, mostly OFDR usage is limited to short distance measurement and optical component inspection. OFDR can be used in long range detection if the coherence length is extended by means of very narrow linewidth lasers [8], however, narrow linewidth lasers are not commonly available and they are very costly. Although, deployment of narrow linewidth lasers can make OFDR usage possible in long range detection but it does not set OFDR free from measurement within the coherence length limitation. The more suitable or permanent solution towards measurable distance limitation in OFDR would be to somehow compensate or cancel the laser phase noise, which is the main culprit of this limitation. Compensation or cancelation of laser phase noise will set OFDR free from measurement within coherence length limitation and high resolution and good sensitivity features of OFDR can be exploited in long range measurements regardless of laser linewidth.

Recently some work regarding phase noise compensation in OFDR have been done. A new type of OFDR called phase noise compensated OFDR (PNC-OFDR) was proposed by *xinyu et al.* [9, 10], the proposed OFDR was capable of detecting fiber break points beyond the laser coherence length. However, proposed method had issues of long computational time (10m minutes for 40-km FUT) and complexity as it was

using an extra OFDR arm known as auxiliary arm, the length of auxiliary arm was set less than laser coherence length. The phase noise of auxiliary arm was used to compensate phase noise of the real OFDR arm by means of signal processing. If the fiber length was long and linewidth of laser was broad then it requires high computational power and time to compensate phase noise of whole fiber. Therefore, PNC-OFDR was again using narrow linewidth laser to compensate laser phase noise in long fiber to reduce computational time and power. In this thesis a new type of OFDR is proposed which is quite simple in arrangement and it can perform measurements beyond the laser coherence length with high spatial resolution [11, 12]. The proposed OFDR uses broad linewidth laser and it can attain high spatial resolution, centimeter-level resolution has been demonstrated experimentally. The proposed new type OFDR uses double side band modulation to cancel the laser phase noise in OFDR, therefore, it is named as double side band phase noise canceled OFDR (DSB-PNC-OFDR) [13].

In order to design a network to cope with chromatic dispersion affects, having an accurate knowledge about chromatic dispersion coefficient of optical link is important. For optical fiber which is already deployed as a part of transmission network, chromatic dispersion measurement is best done by OTDR or OFDR because they are one end measurement technique. However, both mentioned techniques either suffer from low spatial resolution or short distance. Some methods have been proposed to measure chromatic dispersion in optical fiber using OTDR or OFDR [14, 15, 16, 17], but there accuracy is poor because of poor spatial resolution and if accuracy is improved the measurement distance becomes short. In this research a new method to measure chromatic dispersion is proposed which can measure chromatic dispersion in long optical fibers with higher accuracy. The proposed method uses DSB-PNC OFDR, since that type of OFDR is immune to laser phase noise therefore long distance measurements are possible and as it is OFDR which is capable of achieving higher spatial revolution therefore the measurement accuracy is good.

OFDR has advantages over OTDR in terms of high spatial resolution and sensitivity. The high spatial resolution in OFDR is function of the frequency sweep span, higher the sweep span better the spatial resolution. Sweeping the laser externally by RF frequency using a modulator has some advantages over internal laser wavelength tuning, such as external sweeping is linear and faster. The available frequency sweep span is limited because of some bottlenecks from the present electronics, which is the problem with external frequency sweeping technique. Some methods to increase available frequency sweep span are proposed [18, 19, 20, 21] however, proposed methods suffer from increased phase noise which shortens the measurable length. A new method to increase frequency sweep span in OFDR is proposed in this research. The proposed method can increase sweep without increasing any phase noise hence preserving

the measurement range within the laser coherence length. The proposed method to increase frequency sweep span can be used in conventional OFDR and as well as in DSB-PNC OFDR.

1.2 Research contribution

The main contribution of this thesis is to propose a new type of OFDR which is able to nullify the phase noise effects and sets OFDR free from measurement within the coherence length, as a result backscattered signal detection beyond the laser coherence length is achieved. The proposed OFDR can be implemented in two type of arrangements heterodyne detection and phase diversity detection. Since heterodyne detection is viable only if the break point is located over long distance but if break point exist at near distance the fold back of spectrum phenomenon occurs because of which phase noise is not completely canceled. In this thesis dynamic range of proposed DSB-PNC OFDR is also confirmed by deployment of phase diversity, since phase diversity has negative spectrum therefore near as well as long distance breakpoints detection is possible with phase diversity detection technique. Moreover, performance of proposed DSB-PNC OFDR is demonstrated in terms of spatial resolution by detecting two break points 10 cm apart from each other and measuring fiber temperature dependence with good accuracy. In another demonstration proposed OFDR is used to measure chromatic dispersion in a 50 km long optical fiber with spatial resolution of 7.9 mm, it is also shown that chromatic dispersion measurement by means of proposed OFDR can result in more accurate measurement than conventional method of measuring chromatic dispersion in already deployed fiber using OTDR. Proposed new type of OFDR (DSB-PNC) method was further extended to propose a new scheme to estimate the laser phase noise which was the main cause of the OFDR limitation. A new technique to cancel the phase noise using estimated laser phase noise is also presented. Low sampling rate and better spatial resolution are the advantages of canceling the laser phase noise in OFDR using estimated phase noise. Furthermore, a new demonstration about format independency of a wavelength conversion method based on OSSB modulation and AWG is also presented in this research. With the help of experiments it is verified that proposed scheme of wavelength conversion does not depend on the signal format and wavelength conversion by sideband modulation and four wave mixing (FWM) were compared. Format free wavelength conversion demonstration became an inspiration to propose a completely new idea to increase frequency sweep span in OFDR using four wave mixing (FWM) and SB-SC modulation, which resulted in increased the spatial resolution proportional to the increased sweep span. The newly proposed scheme is capable of increasing the sweep span up to 3-time, with the help of experiments it is demonstrated that the proposed scheme can be used in conventional OFDR arrangement as well as DSB-PNC OFDR arrangement to increase the spatial resolution up to 3-times. The frequency span broadening of proposed method can be increased up to 12-times if one more

stage of FWM is created , this aspect of proposed method to increase frequency sweep span is classified as the future work in the this thesis. Two more possible future works are identified in this thesis, one is application of the proposed OFDR in long range optical distributed sensing i.e. tall buildings, tunnels, bridges etc. and second is measurement of laser spectral width by laser phase noise estimation method proposed in this work.

1.3 Thesis outline

This thesis consists of 6 chapters, description is given below

Chapter 1: This chapter is based on introduction which includes background and some description about statement problem. The second part summarizes contribution of research in this thesis and last part defines the structure of the thesis.

Chapter 2: This chapter starts with types of scattering and general working principle of reflectometry technique. In following part of this chapter two mainly used reflectometry techniques OTDR and OFDR are explained briefly along with problems and limitations faced by both techniques and a comparison between both techniques is also given. This chapter ends with the main problem in OFDR which is mentioned as problem statement of this research.

Chapter 3: The proposed method to solve OFDR problem is described in this chapter. This chapter is further divided into two possible arrangements of the proposed theory. Heterodyne detection method is simple but has got a limitation and as a solution phase diversity detection was proposed. Feasibility of proposed theory is confirmed by the means of experiments and high spatial resolution capability of proposed OFDR is demonstrated by detecting two break points 10 cm apart from each other, moreover fiber temperature dependence was also measured with high spatial resolution. Moreover, a new method to measure chromatic dispersion is also presented in this chapter. This new proposed method uses DSB-PNC OFDR to measure chromatic dispersion in long optical fibers which can outperform conventional method of measuring chromatic dispersion based on OTDR. The proposed method was demonstrated using experiment where chromatic dispersion in a 50 km dispersion shifted fiber was measured with 7.9 mm spatial resolution. Measured results were compared with phase shift method and a close match was observed which confirms the accuracy of proposed method.

Chapter 4: In this chapter a new method to increase frequency sweep span is presented. The proposed method is capable of increasing the available sweep span by 3-times hence the spatial resolution by 3-times. With the help of experiments it is demonstrated the proposed method can increase sweep span in ordinary and as well as in DSB-PNC OFDR. Moreover, this chapter contains a demonstration of format

impendency of wavelength conversion scheme which was also a motivation behind the sweep span broadening method.

Chapter 5: This chapter is based on proposal of a new scheme to estimate laser phase noise. The proposed method is extension of DSB-PNC OFDR, the experimental setup and the theory is similar to that of DSB-PNC OFDR with some extra signal processing involved. The proposed scheme can estimate laser phase noise and the estimated laser phase noise can be used to cancel phase noise in OFDR with some additional advantages of reduced sampling speed required and high spatial resolution. The end of this chapter consist on discussion about the limitation of phase noise cancelation in OFDR using estimated laser phase noise.

Chapter 6: This is the last chapter which is based on discussion about one main problem with proposed scheme is discussed and a solution for that problem is also provided. Another part of this chapter talks about the possible future works and three significant future works are discussed.

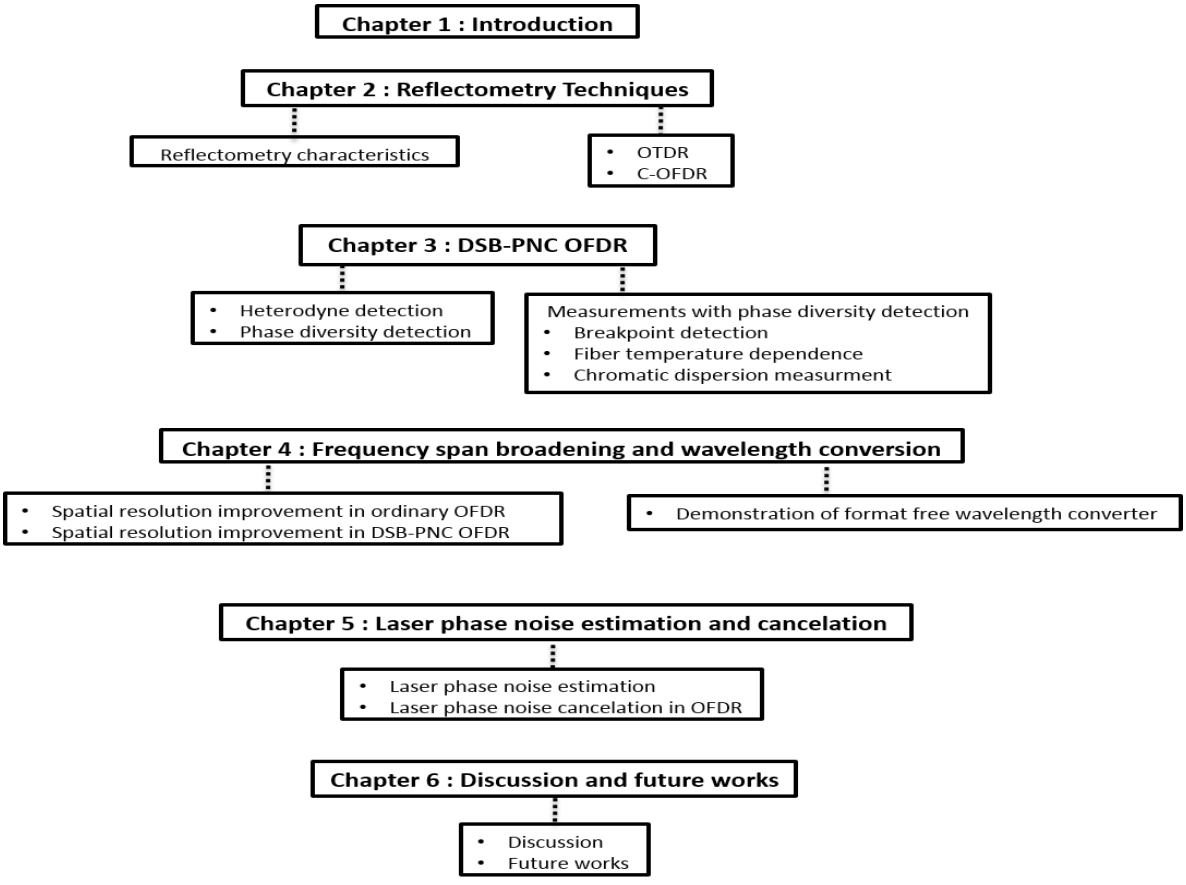

Figure 1.1 Thesis organization

1.4 References

[1] Nick Massa, "Fundamentals of Photonics", Springerfield community college, Massachusetts university of Connecticut.

[2] Govind P. Agarwal, "Lightwave Technology", Wiley.

[3]Sadakuni Shimada, "Coherent Lightwave Communication Technology", Chapman & Hall.

[4] X. Li, C. Yang, S. Yang, G. Li, "Fiber optical sensors: Basic and applications in multiphase reactors", Sensors, vol. 12, 12519-12544, 2012.

[5] P. Oberson, B. Httner, O. Guinnard, L. Guinnard, G. Ribordy, N. Gisin, "Optical frequency domain reflectometry with a narrow linewidth fiber laser", Phot. Technol. Let. Vol. 12, 2000.

[6] Govind P. Agarwal,"Nonlinear fiber optics", Academic Press.

[7] X. Bao, L. Chen, "Recent Progress in Distributed Fiber Optic Sensors", Sensors, vol. 12, 8601-8639, 2012.

[8] Jinhong Geng, Christine Spiegelberg, and Shinin Jiang, "Narrow Linewidth Fiber Laser for 100-km Optical Frequency Domain Reflectometry", *IEEE Phot. Technol. Let.* vol. 17, no.9, pp.1827-1829Sept. 2005

[9] Xinyu Fan, Y. Koshikiya, and F. Ito, "Phase-Noise-Compensated Optical Frequency-Domain Reflectometry", *IEEE J. Quant. Electron.,* vol. 45, no.6,pp.594-602, June 2009.

[10] Y. Koshikiya, Xinyu Fan and F. Ito, "40-km Range, 1-m Resolution Measurement Based on Phase-noise-compensated coherent Optical Frequency Domian Reflectometry", *ECOC 2008,* Brussels, Belgium. Sept. 2008, vol.5, pp.21-22.

[11] Mudabbir Badar, Takuya Hino, Katsushi Iwashita, "Phase noise cancelled OFDR with cm-Level Spatial Resolution Using Phase Diversity", *Phot. Tech. Let.* , 26(9), 858-861, (2014).

[12] Shuta Hiramatsu and Katsushi Iwashita, "A Novel Phase-Noise Cancelled Optical Frequency Domain Reflectometry Using Modulation Sidebands", *Photon. optoelectron. (P&O),* vol.1 Iss.3, pp. 60-64, Oct. 2012.

[13] Mudabbir. Badar, H. Kobayashi, and K. Iwashita, "Chromatic dispersion measurement with double sideband phase noise canceled OFDR*",* Opt. comm., **356**, 350-355, (2015).

[14] Scuberi Moon, and Dug Y. Kim, "Reflectometric Fiber Dispersion Measurment Using a Supercontinuum Pulse Source", *IEEE J. Quant. Electron.,* vol. 45, no.6,pp.594-602, June 2009.

[15] Alberto Rossaro, Marco Schiano, Tiziana Tambosso, and Davide D' Alessandro, "Spatially Resolved Chromatic Dispersion Measurement by a Bidirectional OTDR Technique", J. Quan. Elec. **7**(3), 375-383 (2001).

[16] Masato Yoshida, Koichiro Nakamura, and Hiromasa Ito, "A New Method for Measurement of Group velocity Dispersion in Optical Fibers by Using a Frequency-Shifted Feedback Fiber Laser", *Phot. Tech. Let.* , 13(3), 227-229, (2001).

[17] Binhao Wang, Guofeng Yan, Chunsheng Yan, "Fiber Length and Chromatic Dispersion Measurement Technology Using a Novel Optical Frequency Domain Reflectometry", OSA-IEEE-COS 2010.

[18] J. Li, J. Du, S. Wang, L. Li, L Sun, X. Fan, Q. L, Z. He, "Improving the spatial resolution of an OFDR based on recirculating frequency shifter", Phot. J. **7,** (2015).

[19] J. Li, J. Du, D. Xu, S. Wang, X. Fan, Q. Liu, and Z. He, "Broadened optical frequency sweeping for high spatial resolution OFDR based on recirculating frequency shifter", in Proc. 20th OECC, Shanghai, (2015).

[20] D. Xu, J Du, X. Fan, Q. Li, and Z. He, "10-times broadened fast optical frequency sweeping for high spatial resolution OFDR", Proc. OFC (2014).

[21] D. Xu, J Du, X. Fan, Q. Li, and Z. He, "High spatial resolution OFDR based on broadened optical frequency sweeping by four-wave-mixing", Proc. 23rd OFS (2014).

[22] M. Wegmuller, P. Oberson, J.P. Von weid, O. Guinnard, C. Vinegoni, M. Legre, N. Gisin, "Overview of coherent reflectometry techniques: Characterization of components and small systems", Ceneter of telecommunication studies, Rio de Janeiro.

Chapter 2 : Optical Reflectometry Techniques

2.1 Optical scattering

Propagation loss is the one of the most important properties of the optical fiber [1]. This is also a factor which sets a limit over which signal can be sent error free [2]. Attenuation because of Scattering and absorption are the major cause of propagation loss in optical fiber [1]. Scattering loss is the most dominant in transmission windows (850 nm, 1300 nm, 1500 nm) [3]. Scattering is the process in which light is deviated from the straight trajectory, in optical fiber this phenomenon occur because of density fluctuation due to the irregular microscopic structure in amorphous material such as glass. Light is absorbed or scattered as it interacts with the material in optical fiber in both cases, transmitted light intensity is attenuated. Therefore, total attenuation can be described as sum of attenuation coefficient due to scattering and absorption [4]

$$\alpha = \alpha_a + \alpha_s \quad (1)$$

Here $\alpha_a$is attenuation coefficient due to absorption, $\alpha_s$is attenuation caused by scattering. The optical transmitted power along the optical fiber with increasing distance z can be described as

$$I_t(z) = I_0 . e^{-\alpha z} \quad (2)$$

Where I_0 is the input optical power. Furthermore, scattering can be categorized into two groups one is linear such as Rayleigh scattering and second is non-linear such as Raman and Brillouin scattering. Measurement of Raman scattering and Brillion scattering can be used in distributed optical sensing networks [5, 6]. Since non-linear scattering is out of the scope of this research, therefore they are not further discussed.

2.1.1 Linear Scattering (Rayleigh scattering)

Rayleigh scattering is the main cause of optical loss in the fiber. The reason for Rayleigh scattering in optical fiber is density fluctuations, inhomogeneity and refractive index fluctuations in optical fiber created during the manufacturing process [7]. It is a linear type of scattering in which frequency of the scattered signal is same as that of incident signal. The photon energy in Rayleigh scattering is conserved, only its direction is changed. Rayleigh scattering can occur in liquid, solid and gases, this type of scattering is the scattering of light from particles much smaller than the light wavelength. Scattering from the particles of size comparable or larger than the wavelength of the light is called Mie scattering. Rayleigh scattering light propagates forward and backward direction inside optical fiber with same energy. This type of

scattering is highly dependent of the wavelength of propagating optical signal to proportion $\frac{1}{\lambda^4}$ [7], therefore shorter wavelength contributes more towards scattering [8] and in optical transmission window propagation losses due to scattering are dominant. The length of the fiber that give rise to the backscattered power also depends on the optical signal pulse length, for a rectangular pulse of length Δw, the backscattered power $I(z)$ from a fiber section of length equivalent to pulse length Δw at a distance z can be described as [4]

$$I(z) = S.\alpha_s.\Delta w.I_0.e^{-\alpha z} \quad (3)$$

Here S is backscattered capture power coefficient which determines how much of scattered power is captured in backward direction. Rayleigh scattering measurement is an essential process in transmission optical fiber which reveals the fiber link loss information and fiber breakpoint location. It has another application in optical distributed sensing network where change in backscattered pattern shows the accordance to change in external condition of fiber such as temperature/strain, vibration etc. following sections are dedicated for Rayleigh backscattering measurement techniques and problems related to those methods.

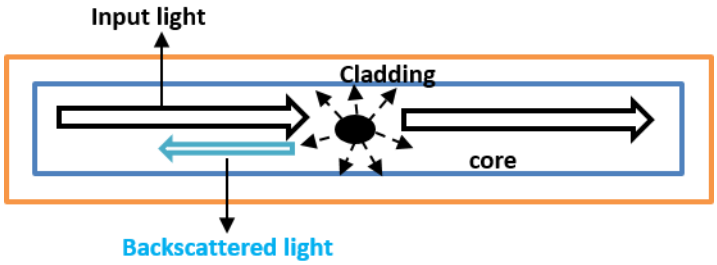

Figure 2.1 Rayleigh scattering and backscattering in optical fiber

2.2 Optical reflectometry characteristics

As mentioned above measurement of Rayleigh backscattered signal is of a great importance in optical transmission and sensing networks. The techniques used to measure Rayleigh backscattering in optical fiber are called optical reflectometry techniques. The working principle of reflectometry techniques is based on injecting an input signal in fiber under test (FUT) and detecting the backscattered signal from FUT through a circulator, configuration is shown in fig. 2.2. There are some important characteristics involved in evaluation of reflectometry techniques performance. Two of the main characteristics are described below.

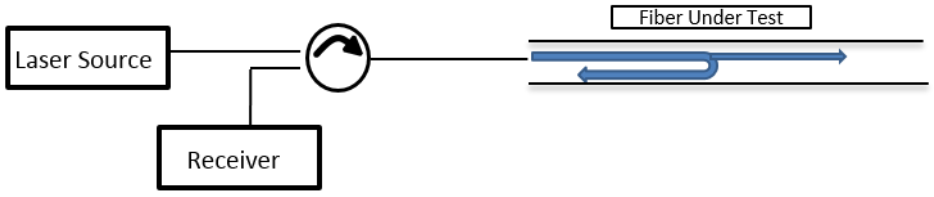

Figure 2.2 Reflectometry technique configuration

2.2.1 Sensitivity

This is one of the important characteristics of the optical reflectometry technique. Mainly this feature of optical reflectometry decides up to what length sensing or measurement can be performed. The system sensitivity puts a limit to minimum detectable backscattered power or it can also be defined as signal to noise ratio (SNR) of the system. As the signal propagates inside optical fiber it losses its power because of propagation losses and continuously backscattered power from each point along the fiber also shrinks in the power. Signals backscattered from a point not having power below the system sensitivity can be differentiated from the noises.

2.2.2 Spatial resolution

This characteristics of the optical reflectometry techniques defines how close two events can be detected separately. This value of reflectometry technique is described as full width half maxima (FWHM) of the reflection peak. Two consecutive peaks cannot be detected separately if the distance between them is less than the spatial resolution of the system.

2.3 Optical reflectometry techniques

Numerous optical reflectometry techniques have been proposed to measure backscattered power inside optical fiber to measure fiber loss as a function of fiber length, break point detection and some sensing parameters such as temperature/strain and vibration. There are mainly two practiced optical reflectometry techniques which are defined below with problems in each technique and a comparison is also given.

2.3.1 Optical time domain reflectometry (OTDR)

OTDR is simple reflectometry technique which was first proposed by Barnoski and Jensen [12] and it is also mainly used reflectometry technique for optical link monitoring. In this technique a short and high power pulse of light is incident in the fiber under test (FUT) and Rayleigh backscattered signal is detected as a function of arrival time at the input end [8], configuration shown in fig. 2.3. The amplitude of backscatter signal vs distance map is obtained to measure fiber loss and detect fault location. Since

Rayleigh backscattering is a linear process, therefore backscattered optical power at any point is linearly proportional to the optical power at that location. In OTDR a laser diode is derived by an electrical pulse generator which creates a train of short optical pulses. Incident optical pulse in FUT is backscattered which is detected in a photodiode through a circulator. The detected waveform is converted into digital format and analyzed in digital signal processing (DSP) unit, where amplitude as a function of arrival time of the backscattered signal is measure. Since the group velocity of the optical fiber is known, therefore from signal arrival time distance vs signal amplitude graph is obtained. The timing of DSP is synchronized to that of optical pulse source so that the propagation time of every backscattered signal can be calculated precisely [8], thus backscattered light location can be measured accurately, as shown in fig. 2.3. The distance information from backscattered signal detection time can be obtained by the formula below

$$z = \frac{v_g t}{2} = \frac{c}{2n} t$$

Where t the backscattered detection is time, v_g is the group velocity and z is the distance along the fiber.

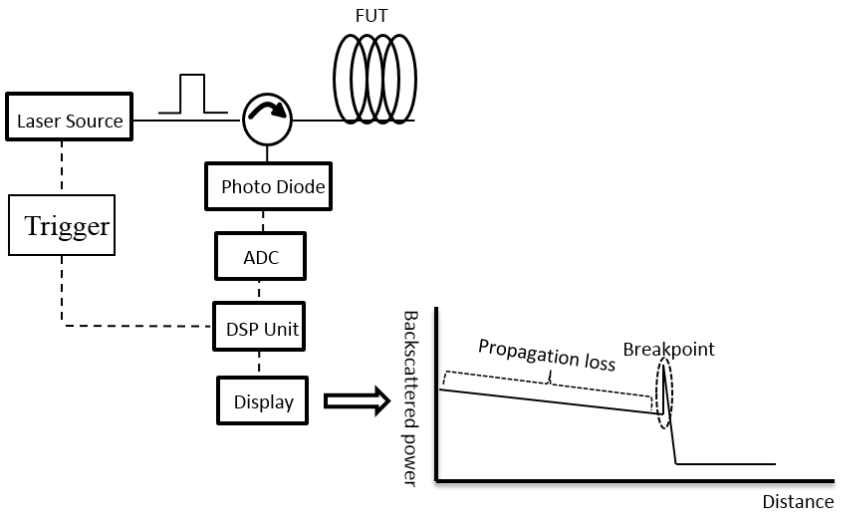

Figure 2.3 OTDR configuration and trace, DSP: digital signal processing, ADC: analog to digital converter

2.3.1.1 Spatial resolution and sensitivity trade off in OTDR

The spatial resolution in OTDR is linked to the pulse duration [3, 5, and 8]. For example if the pulse of duration τ is used then separating two events within that pulse duration would not be possible. This pulse

duration corresponds to distance $\Delta z = \frac{v_g.\tau}{2}$. Dynamic range in OTDR depends on the sensitivity of the system which again is function of pulse duration, pulse power and photodiode sensitivity. High power pulse with wider pulse width increases the signal to noise ratio (SNR), which makes the long range measurements possible. However, this enhanced sensitivity feature is achieved at the cost of low spatial resolution because wide pulse width degrades the spatial resolution. The power of backscattered signal reaching the input end decides the SNR and hence the sensitivity of OTDR systems. For example let's consider the Rayleigh backscattering from a short fiber section dz. The fraction of Rayleigh backscattered power which can make back up to the input end originated from location x will depend on various factors, described as below [8]

$$P(z)_{BS} = \frac{v_g.\tau}{2}.\eta.\alpha_s(z).P_0.\exp\{-2\int_0^z \alpha(x)dx\} \quad (4)$$

Where P_0 is the input optical power, η is the conversion efficiency from scattered light to that captured by the fiber, it can be defined as $\eta \cong \frac{1}{4.55}\frac{NA}{n}$, where NA is fiber numerical aperture and n is fiber core refractive index, $\alpha_s(x)$ is the attenuation factor due to Rayleigh scattering, $\alpha(x)$ is the total attenuation coefficient as described in Eq. (1) which is combination of attenuation due to absorption loss $\alpha_a(x)$ and attenuation due to Rayleigh scattering $\alpha_z(x) = \alpha_s(x) + \alpha_a(x)$. Considering loss $\alpha(x)$ =0.25 dB/km, $\eta = 1.19 * 10\text{^} - 3$ and input power 10 mW, the simulated backscattered power reaches the input end depends on the duration of pulse or pulse width, as it can be seen from fig. 2.4 the shorter pulse has lower backscattered power reaching the input end. Therefore in OTDR the sensitivity of the system is function of pulse width, wider the pulse width better the sensitivity, however, wider pulse width degrades the spatial resolution.

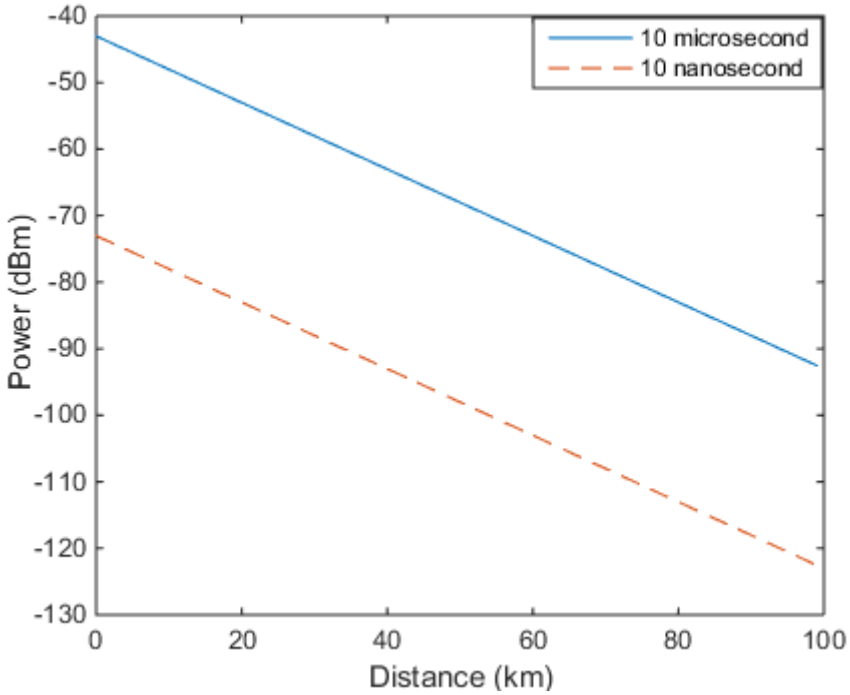

Figure 2.4 Backscattered power that reaches the input end as a function of distance with different pulse durations

2.3.2 Coherent Optical frequency domain reflectometry (C-OFDR)

OFDR is another reflectometry technique having all the capabilities as of OTDR but with high spatial resolution and better sensitivity, comparison between OFDR and OTDR can be seen in table 1. This technique can be categorized in two types incoherent OFDR (I-OFDR) and coherent (C-OFDR) in this work only C-OFDR is emphasized. In C-OFDR instead of a pulse source, continues source whose frequency is linearly swept with time is used [10] as shown in fig. 2.5. If T_s is the frequency sweep time and ΔF is the sweep span, then sweep rate (β) is defined as $\beta = \frac{\Delta F}{T_s}$. The linearly swept signal is separated into two signals probe signal and reference signal. The probe signal is sent through FUT and the light backscattered from FUT is combined with reference signal and detected coherently. As probe signal and reference signal are generated from the same source, therefore we can consider backscattered signal is time delayed version of the reference signal, when both lights are interfered at the receiver the photocurrent produced has a constant beat frequency, generated beat frequency is actually the difference of two frequencies [10]. Considering the round trip delay of backscattered signal, from the beat frequency we can deduce backscattered signal location information through spectral analysis of the detected signal by taking its Fourier transform

$$f_B = \beta . 2\tau_{FUT} \quad (5)$$

$$f_B = \beta . 2L\frac{n}{c}$$

$$L = f_B . \frac{c}{n.\beta.2} \quad (6)$$

where f_B is the beat frequency, L is the length of the reflection, $2\tau_{FUT}$is the round trip delay, n is the core refractive index and c is the speed of light.

Table 2-1 Comparison between OTDR and OFDR

Method	Sensitivity	Spatial Resolution	Measurable distance
OTDR	**Low**	**A few meters**	**Limited by sensitivity**
OFDR	**High**	**Sub-millimeter**	**Limited by coherence Length**

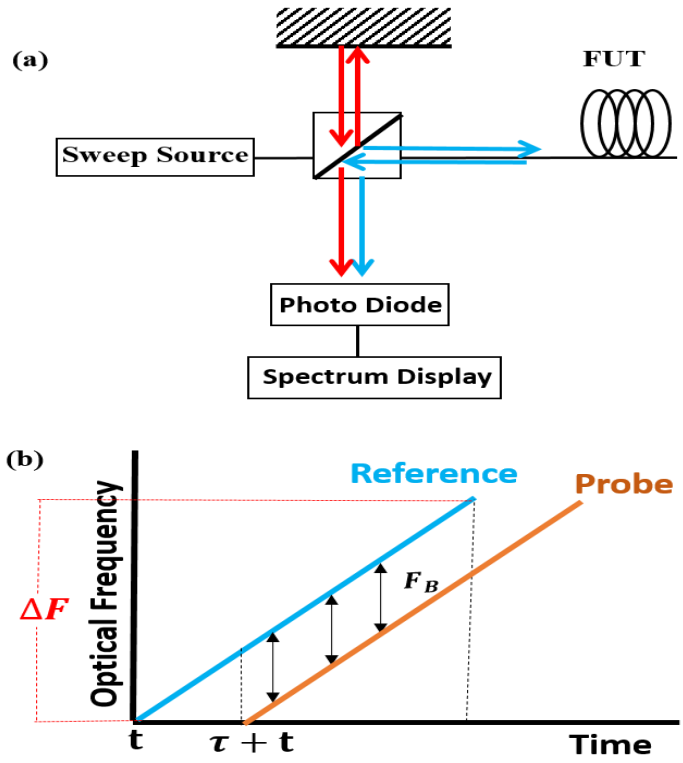

Figure 2.5 (a) OFDR Configuration, (b) Linear optical sweep

Considering a signal which is swept linearly in time, obtained optical field can be described as below

$$E(t) = E_0 e^{j(\omega_0 t + \pi t^2 \beta + \theta(t))} \quad (7)$$

Where ω_0 is initial optical frequency, β (Hz/s) is the rate at which optical frequency is swept, E_0 is the field amplitude and $\theta(t)$ is the random phase fluctuations produced by laser phase noise. Then optical swept signal is divided into two arms one arm signal is kept as local for coherent detection and the other arm signal is passed through FUT. Considering one reflection point at a distance equal to propagation delay τ_{FUT}, the backscattered signal can be represented as time delayed version of original swept signal

$$E_{FUT}(t - \tau_{FUT}) = \sqrt{R} E_0 e^{j(\omega_0 (t - \tau_{FUT}) + \pi (t - \tau_{FUT})^2 \beta + \theta(t - \tau_{FUT}))} \quad (8)$$

Where R is the reflectivity of FUT. Backscattered signal from FUT and local are mixed together and coherently detected signal is expressed as

$$I(t) = |E(t) + E_{FUt}(t - \tau_{FUT})|^2 = {E_0}^2 \left\{1 + \mathrm{R} + 2\sqrt{R} \cos\left(\omega_B t + \omega_0 t - \frac{1}{2}\omega_B \tau_{FUT} + \theta(t) - \theta(t - \tau_{FUT})\right)\right\} \quad (9)$$

Here $\omega_B = 2\pi\beta\tau$ is the beat frequency, for measurements done within laser coherence length the phase difference $\theta(t) - \theta(t - \tau_{FUT})$ is negligible and does not have any influence. By taking Fourier transform of the detected signal beat frequency value can be obtained and from beat frequency the distance of the backscattered signal can be measured as given in Eq. (6).

2.3.2.1 Spatial resolution in C-OFDR

The spatial resolution in C-OFDR is function of total frequency span, expressed by the formula given below

$$\Delta l = \frac{c}{2n\Delta F}$$

where ΔF is the total frequency sweep span. Unlike OTDR where spatial resolution was related to pulse duration and improving spatial resolution was degrading the system sensitivity, in OFDR spatial resolution improvement does not affect the system sensitivity. The two point spatial resolution in OFDR depends on sweep rate, sampling rate and number of data points, formulated as

$$\Delta L_P = \frac{c f_s}{4n\beta N}$$

Here, f_s is the sampling rate, N is the number of data points.

2.3.2.2 Influence of laser phase noise in C-OFDR

Phase noise is the main constraint behind OFDR wide practice. As the measurement distance approaches laser coherence length the laser phase noise influence gets significant and makes the detection almost impossible. Therefore, OFDR usage is mainly limited within short distance measurements and optical components diagnosis [9]. The influence of phase noise in OFDR measurement can be understood from the spectral analysis of the detected signal by taking its Fourier transform, one sided spectral density of Fourier transform of the Eq. (9) can be described as [11]

$$S_I^{(1)} = (1+R)^2\delta(f) + 2Re^{j-\left(\frac{2\tau_{FUT}}{\tau_c}\right)}\sigma(f-f_B) + \frac{2R\tau_c}{1+\pi^2\tau_c^2(f-f_B)^2}\left\{1 - e^{j-\left(\frac{2\tau_{FUT}}{\tau_c}\right)}\left(cos2\pi\left((f-f_B)\tau_{FUT}\right)\right) + \frac{sin2\pi(f-f_B)\tau_{FUT}}{\pi\tau_c(f-f_B)}\right\} \quad (10)$$

Here beat frequency is equal to $f_B = \frac{\omega_B}{2\pi} = \beta\tau$ and τ_c is the laser coherence time. In the above power spectral density of the detected signal the first term is a delta function a DC value which depends on the reflectivity R. The second term is the delta function at the beat frequency which contains the location information of the reflection peak. The amplitude of the beat frequency term is also accompanied by an exponential term $e^{j-\left(\frac{2\tau}{\tau_c}\right)}$, which tells it decays rapidly once measurement distance is approached to laser coherence length. The third terms describes the distribution of the phase noise around beat frequency which is known as phase noise term. If measurement distance exceeds the laser coherence length the phase noise terms becomes dominant and the beat frequency spectrum takes the lorentzian shape. Therefore, OFDR practice is restricted to measurement within the coherence length and commonly used lasers have spectral width around a few MHz which sets the coherence length to some tens of meters and this much length is not long enough for OFDR to be used in commercial optical transmission systems. The effect of phase noise can be seen in fig. 2.5 where measurements are done beyond the coherence length and it can be seen peak is completely buried inside the phase noise.

When operational principle of C-OFDR was explained it was assumed the optical frequency sweep is completely linear in time. However, in real scenario lasers exhibit some fluctuations in their optical frequency tuning rate. Because of non-linear tuning sampling of the interference signal with a constant spacing in time produces non-uniform sampling in optical frequency as a result the spatial resolution is degraded [13], the effect of frequency sweep non-linearity on measurement is similar to that of phase noise. Non-linear tuning problem can be solved by sampling the inference signal at equidistant instantaneous optical frequency points rather than equally time intervals [14]. Various methods have been proposed to solve non-linear frequency tuning using diverse mechanisms in an auxiliary interferometer

arm [15, 16], Hilbert transformation [17], deskew filters [18]. Mostly, optical non-linearity compensation techniques is used with laser using internal wavelength sweep mechanism but lasers with external frequency sweep using modulator and RF frequency have linear frequency sweep and in such a situation frequency non-linear compensation techniques is not required. In this research all the experiments are done by sweeping the laser frequency externally, therefore the sweep frequency was linear with time and it did not require to use any non-linear sweep compensation technique.

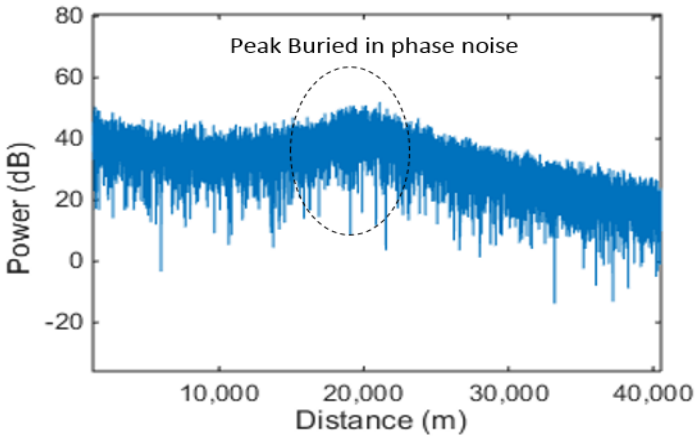

Figure 2.6 Influence of phase noise beyond the coherence length

2.4 References

[1] Govind P. Agarwal,"Nonlinear fiber optics", Academic Press.

[2] Sadakuni Shimada, "Coherent Lightwave Communication Technology", Chapman & Hall.

[3] J. Laferriere, G. Lietaert, R. Taws, S. Wolszcak, "Reference guide to fiber optic testing", vol. 1

[4] D. Derickson, "fiber optic test and measurement". Prentice Gall PTR, 1998.

[5] X. Bao, L. Chen, "Recent Progress in Distributed Fiber Optic Sensors", Sensors, vol. 12, 8601-8639, 2012.

[6] Y. Mizuno, N. Hayashi, H. Tanaka, Y. Wada, K. Nakamura, "Brillouin scattering in multi-core optical fibers for sensing applications", Scientific reports, 2015.

[7] Govind P. Agarwal, "Lightwave Technology", Wiley

[8] Rongqing Hui and Maurice O'Sullivan, *Fiber Optic Measurement Techniques (Elsevier Academic Press, 2009).*

[9] M. Wegmuller, P. Oberson, J.P. Von weid, O. Guinnard, C. Vinegoni, M. Legre, N. Gisin, “Overview of coherent reflectometry techniques: Characterization of components and small systems”, Ceneter of telecommunication studies, Rio de Janeiro.

[10] F. Ito, X. Fan, Y. Koshikiya, “Long-range coherent OFDR with light source phase noise compensation”, J. Lightw. Technol., Vol. 30, 2012.

[11] S. Venkatesh, W. V. Sorin., “Phase noise consideration in coherent optical FMCW reflectometry”, J. Lightw. Technol. 11 (1993), 1694-1700.

[12] M.K. Barnoski and S.M. Jensen, “Fiber waveguides: a novel technique for investigating attenuation characteristics”, Apl. opt. vol. 15, 2112-2115, 1976.

[13] K. Yuksel, M. Wuilpart, V. Moeyaert, P. Megret, “Optical frequency domain reflectometry: A Review”, ICTON, 2009.

[14] U. Glombitza and E. Brinkmeyer, “Coherent frequency-domain reflectometry for characterization of single-mode integrated-optical waveguides,” J. Lightwave Technol, vol. 11, no. 8, pp. 1377-1384, 1993.

[15] L.-T. Wang et al.: Loss measurements in optical waveguide devices by coherent frequency modulated continuous-wave reflectometry, Optics Letters, vol. 18, no. 13, pp. 1095-1097, 1993.

[16] K. Iiyama, et al.: Linearizing optical frequency-sweep of laser diode for FMCW reflectometry, J. Lightwave Technol, vol. 14, no. 2, pp. 173-178, 1996.

[18] T. J. Ahn, J. Y. Lee, D. Y. Kim, “Supression of nonlinear frequency sweep in an optical frequency-domain reflectometry by use of Hilbert transformation”, Apl. Opt. vol. 44, 7630-7634, 2006.

[19] Y. Du, T. Liu, Z. Ding, B. Feng, X. Li, K. Li, J. Jiang,”Method for improving spatial resolution and amplitude by optimized deskew filter in long-range OFDR”, Phot. J., vol.6, 2014.

Chapter 3 : Double Sideband Phase Noise Canceled OFDR (DSB-PNC-OFDR)

3.1 Introduction

Since OFDR has capable of achieving high spatial resolution and better sensitivity than OTDR, however, its measurement range is limited to half of the laser coherence length (considering round trip delay). Measurement range can be increased if the narrow linewidth laser is deployed [1] but narrow linewidth lasers are not commonly used and they are expensive as well. Moreover, narrow linewidth laser does not set OFDR free from the measurement within coherence length limitation. Appropriate solution to this limitation would be to somehow cancel or compensate the laser phase noise, in doing so measurements beyond the coherence length can be acquired. Recently, a new method to compensate laser phase noise has been proposed called phase noise compensated OFDR (PNC-OFDR), in which measurements beyond the laser coherence length was demonstrated, backscattered signal detection up to 40 km was reported [2, 3]. PNC-OFDR uses an auxiliary OFDR arm to compensate phase noise which increases the complexities in the systems, moreover it require a narrow linewidth laser with high computational processing and time. In this research a new method to cancel laser phase noise in OFDR is proposed, the proposed scheme is called double sideband phase noise canceled OFDR (DSB-PNC-OFDR) [4] which is simpler in configuration and does not require cumbersome computational processing and time. In proposed method the laser light is modulated by double sideband with suppress carrier (DSB-SC) modulation to cancel the laser phase noise [5, 6]. After modulation the light signal is dived into two arms called as reference and probe arm. The probe arm signal is sent through FUT and backscattered signal from FUT is coupled with the reference arm. Later, two sidebands present in the coupled light are separated as low and high frequency channels using a separation mechanism. The two separated channels have equal phase noise but opposite in sign, therefore on multiplying two channels laser phase noise was canceled out and remaining terms were the beat frequency and some constants. The principle and configuration of proposed scheme is shown in fig. 3.1.

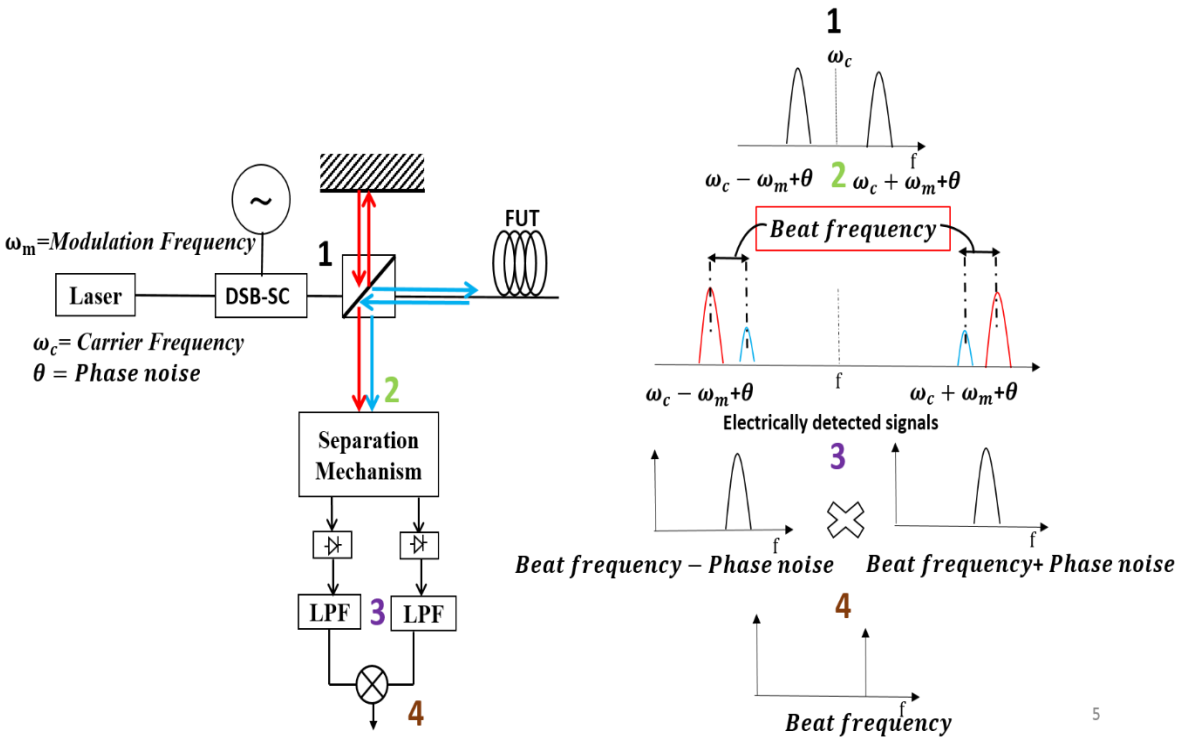

Figure 3.1 Configuration and principle of proposed DSB-PNC-OFDR

The proposed DSB-PNC OFDR can be implemented into two types of arrangements heterodyne detection and phase diversity detection [5, 6]. The principle of each detection technique along with problems is described in the below section.

3.2 Heterodyne detection principle

This type of detection technique is simpler to implement setup is shown in fig. 3.2. The laser source is modulated by DSB-SC modulation which creates two sidebands to both sides of carrier frequency. The optical filed of modulated signal can be expressed as below

$$E(t) = \frac{E_0}{2}\left[e^{j(\omega_+ t+\pi\beta t^2+\theta(t))} + e^{j(\omega_- t-\pi\beta t^2+\theta(t))}\right] \quad (1)$$

where E_0 is the field amplitude, $\omega_+ = \omega_c + \omega_m$, $\omega_- = \omega_c - \omega_m$, ω_c is the carrier angular frequency, ω_m is modulation angular frequency, β is the linear sweep rate and $\theta(t)$ is random phase produced by phase noise. Later the modulated light was divided into two arms as a reference and a probe arm. Probe arm

signal was sent through FUT and backscattered signal from FUT considering a reflection at propagation delay τ_{FUT} could be represented by

$$E_{FUT}(t-\tau_{FUT}) = \frac{\alpha E_0}{2\sqrt{2}} \{e^{j(\omega_+(t-\tau_{FUT})+\pi\beta(t-\tau_{FUT})^2+\theta(t-\tau_{FUT}))} + e^{j(\omega_-(t-\tau_{FUT})-\pi\beta(t-\tau_{FUT})^2+\theta(t-\tau_{FUT}))} \quad (2)$$

Here α is fiber loss and reflectivity of the signal. Two sidebands present in the reference arm are separated using a bandpass optical filter as high and low frequency channels. Then backscattered signal is divided into two arms using a 3 dB optical coupler. The low frequency channels of reference light is coupled with one of the backscattered light arms signal and high frequency channels is coupled with remaining backscattered signal arm. The two coupled channels are detected by photodiode, the detected currents can be expressed as (detailed calculations can be seen in appendix A)

$$I_h(t) \propto \cos(2\pi\beta\tau_{FUT}t + \theta(t) - \theta(t-\tau_{FUT}) + \omega_+\tau_{FUT} - \pi\beta{\tau_{FUT}}^2) \quad (3)$$

$$I_l(t) \propto \cos(2\pi\beta\tau_{FUT}t - \{\theta(t) - \theta(t-\tau_{FUT})\} - \omega_-\tau_{FUT} - \pi\beta{\tau_{FUT}}^2) \quad (4)$$

As it can be seen from the above equations two detected channels have equal phase noise but with opposite sign, therefore on multiplying two detected currents cancel out the phase noise, as expressed below

$$I_h(t) * I_l(t)\ ) \propto \cos(4\pi\beta\tau_{FUT}t - -\omega_-\tau - \pi\beta{\tau_{FUT}}^2) \quad (5)$$

In above equation the phase noise term has been canceled out and the remaining terms are beat frequency with some constants.

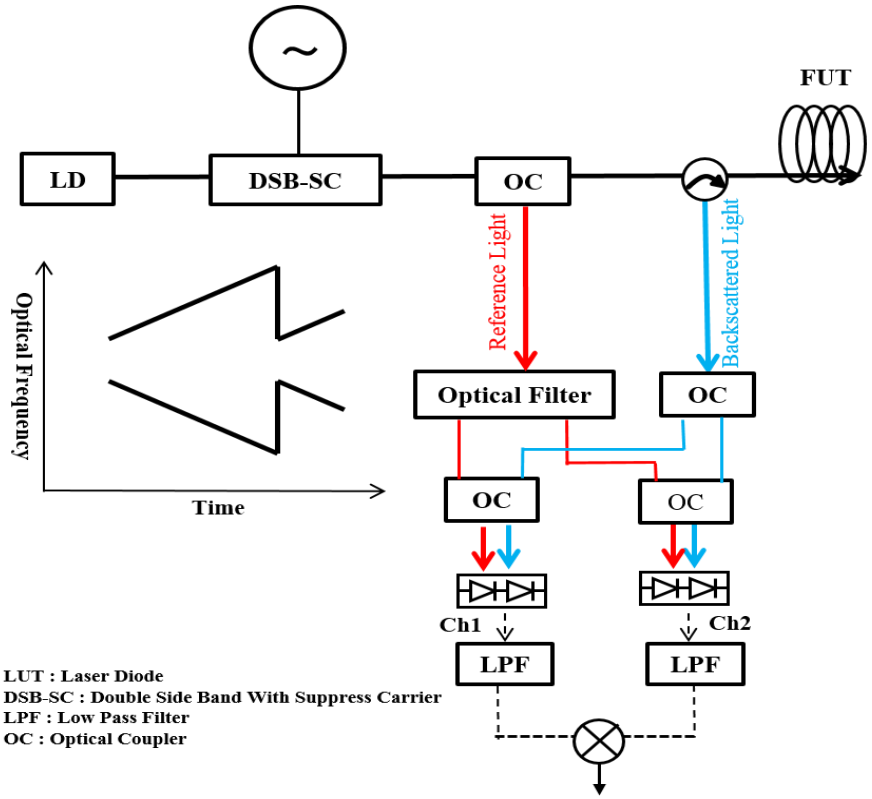

Figure 3.2 Heterodyne detection configuration

3.2.1 Heterodyne detection experimental results

Feasibility of the proposed method with heterodyne detection method was confirmed by the means of experiments. Distributed feed-back (DFB) laser diode of linewidth around 1.5 MHz (200 m coherence length in air) was modulated by double side band with a suppress carrier (DSB-SC). $LiNbO_3$ dual drive MZM intensity modulator was used to achieve DSB-SC modulation by applying opposite signals produced by sweep generator to two arms of intensity modulator using 180 degree hybrid. The frequency of opposite signals applied to two arms of the intensity modulator was swept linearly, hence the two sidebands with sweeping frequency in opposite direction appeared. The sweep span used in the experiment was 8 GHz (6-12 GHz) and sweep time 100 ms, which corresponds to sweep rate of 80 GHz/s. By adjusting bias voltage of modulator carrier components were suppressed up to 18 dB, see fig. 3.3. The drawn output power of laser diode was 1 dBm, modulation process contributed total loss of ~ -20 dB, therefore DSB-SC modulated light was amplified using an optical amplifier. Then amplified light signal was divided into two arms using 3 dB coupler, one arm signal was fed into 20 km long FUT and the second arm known as reference arm signal was used as a local oscillator for coherent detection. Two sidebands of reference light

were separated into two channels as higher frequency and lower frequency channels using a bandpass optical filter with 25 GHz channel spacing. Backscattered light from fiber was divided into two signals using 3 dB optical coupler and then one arm signal was coupled with higher frequency channel signal of reference light and another arm signal was combined with lower frequency channel of reference light. Then two combined lights were detected by two balance photo detectors of bandwidth around 10 MHz as higher frequency and lower frequency channels. Signal from each channel was converted into digital format using 16 bit A/D convertor with sampling rate 200 MSa/s and passed through low pass filters, where higher frequency components were filtered out.

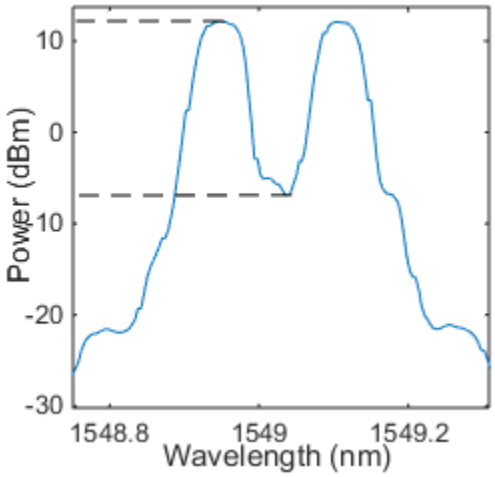

Figure 3.3 Double sideband with a suppress carrier (DSB-SC)

Two detected channels were multiplied as the beat frequency becomes twice of the original value and phase noise was canceled out. In fig. 3.4 it can be seen after multiplication of two channels the peak becomes sharp which was very broad before multiplication as can be seen in each channel.

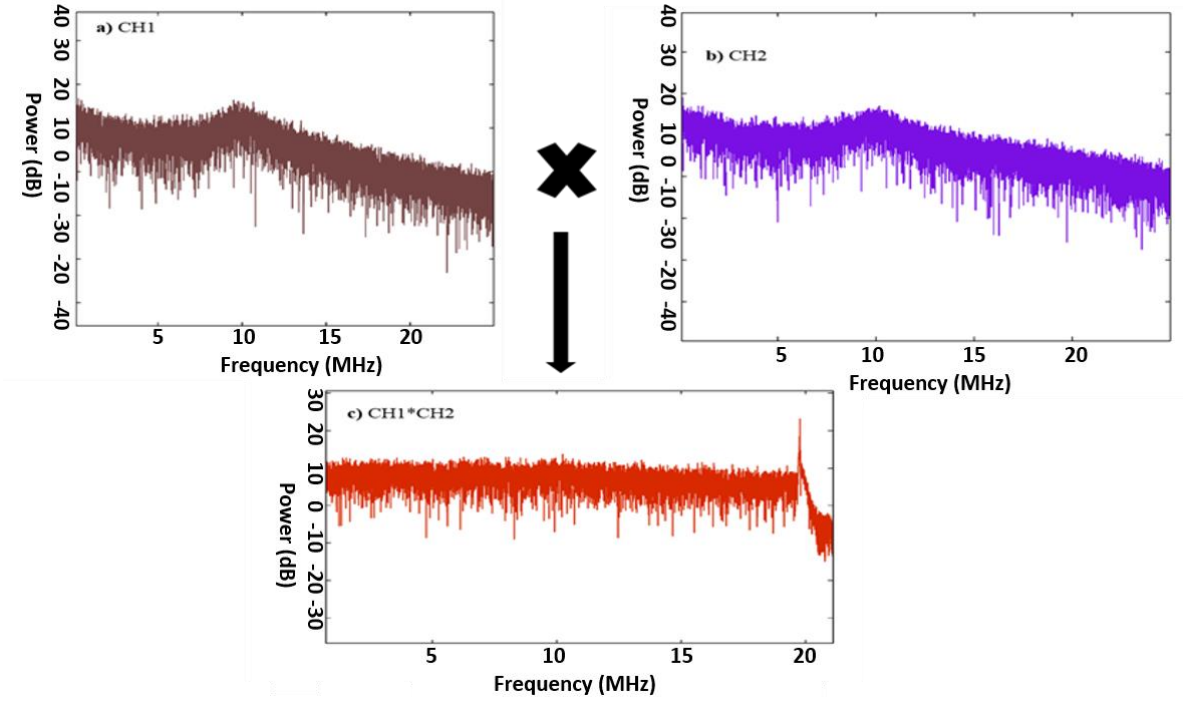

Figure 3.4 Phase noise cancelation with heterodyne detection, (a) channel 1, (b) channel 2, (c) multiplication of channel 1 and channel 2

3.2.2 Limitations with heterodyne detection

Proposed method with heterodyne detection works well when reflection is located at long distance, however, if the reflection exists at a short distance the peak frequency is close to zero frequency and because of phase noise the peak is broader as a result, part of the peak spectrum crosses the zero frequency, since heterodyne detection does not have a negative spectrum, therefore, part of the spectrum crosses the zero frequency is folded back into positive side. Because of this fold of spectrum phenomenon the phase noise is not completely canceled and break point at short distance cannot be detected clearly. Fold back of spectrum phenomenon can be understood from fig. 3.5. Phase diversity detection can be deployed as a solution to this problem because phase diversity has a negative spectrum so if a reflection exist at short distance part of the spectrum is not folded back to positive side. Another limitation with heterodyne detection is that it uses optical filters to separate two sidebands, it needs to be tuned every time if the wavelength of the laser source is changed for other kind of measurements such as chromatic dispersion measurement and again phase diversity detection technique could be the best option to eliminate need of

optical filter to separate two sidebands because phase diversity detection technique uses optical 90 degree hybrid to perform the task optical filter do in heterodyne detection.

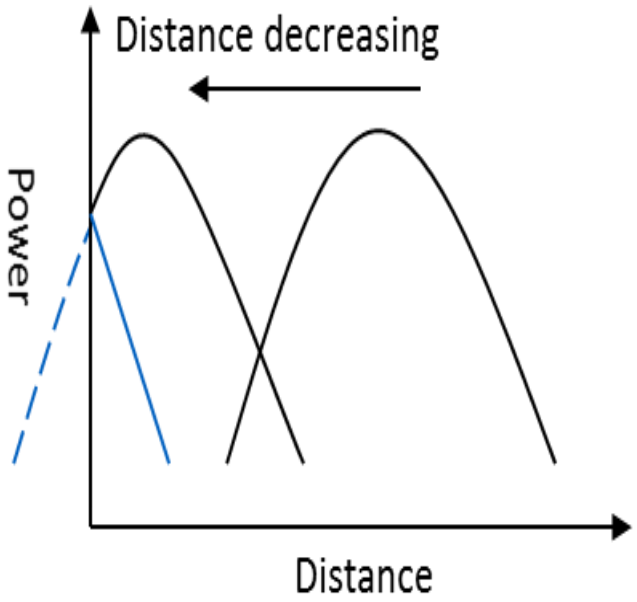

Figure 3.5 Fold back of spectrum phenomenon in heterodyne detection

3.3 Phase diversity detection principle

Phase diversity detection could be the right solution for the fold back of spectrum and optical filter limitation problems in heterodyne detection. The phase noise cancelation principle with this technique is same to that of heterodyne detection, only instead of using optical filters in this technique optical 90 degree hybrid is used to separate two sidebands, principle can be understood from fig. 3.6 (a) and configuration shown in fig. 3.6 (b). The optical 90 degree hybrid consist of one polarization maintaining (PM) coupler and two polarization beam splitters (PBS). Linearly polarized reference light and circularly polarized backscattered light from FUT are coupled into PM coupler of optical 90 degree hybrid where reference light is broken into two in phase signals (E_{refA}, E_{refB}) and backscattered light is divided into two 90 degree out of phase signals (E_{FUTA}, E_{FUTB}). The DSB-SC modulated light can be expressed same as given in Eq. (1), and two inphase reference lights and two 90 degree out of phase lights can be expressed as below

$$E_{ref}(t)_A = E_{ref}(t)_B \sim \frac{E_0}{2}\left[e^{j(\omega_+ t + \pi\beta t^2 + \theta(t))} + e^{j(\omega_- t - \pi\beta t^2 + \theta(t))}\right] \quad (5)$$

$$E_{FUT}(t-\tau_{FUT})_A \sim \frac{\alpha E_0}{2\sqrt{2}}\{e^{j(\omega_+(t-\tau_{FUT})+\pi\beta(t-\tau_{FUT})^2+\theta(t-\tau_{FUT}))} + e^{j(\omega_-(t-\tau_{FUT})-\pi\beta(t-\tau_{FUT})^2+\theta(t-\tau_{FUT}))}\} \quad (6)$$

$$E_{FUT}(t-\tau_{FUT})_B \sim \frac{\alpha E_0}{2\sqrt{2}}\{e^{j(\omega_+(t-\tau_{FUT})+\pi\beta(t-\tau_{FUT})^2+\theta\left(t-\tau_{FUT})+\frac{\pi}{2}\right)} + e^{j(\omega_-(t-\tau_{FUT})-\pi\beta(t-\tau_{FUT})^2+\theta\left(t-\tau_{FUT})+\frac{\pi}{2}\right)}\} \quad (7)$$

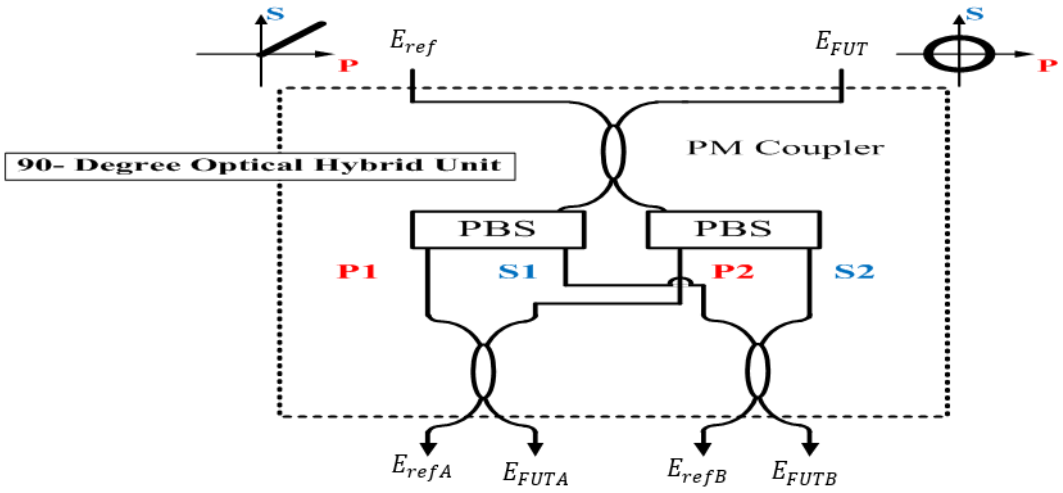

Figure 3.6 Optical 90 degree hybrid

Then one of the reference light signal is detected with inphase signal of backscattered light as I phase channel and remaining reference signal is detected with 90 degree out of phase signals of backscattered light as a Q phase channel. Photocurrents of two detected channels are expressed as below (detailed calculations are presented in appendix B)

$$I_I(t) \sim \left|E_{refA} + E_{FUTA}\right|^2$$

$$\sim \alpha E_0^2(\cos(A) + \cos(B)) \quad (8)$$

$$A = 2\pi\beta\tau_{FUT}t - \theta(t) + \theta(t-\tau_{FUT}) + \emptyset_1,\ B = 2\pi\beta\tau_{FUT}t + \theta(t) - \theta(t-\tau_{FUT}) + \emptyset_2$$

$$\emptyset_1 = -\omega_-\tau_{FUT} - \pi\beta{\tau_{FUT}}^2,\ \emptyset_2 = \omega_+\tau_{FUT} - \pi\beta{\tau_{FUT}}^2$$

Above equations are derived after ignoring DC components, Similarly for Q channels

$$I_Q(t) \sim \left|E_{refB} + E_{FUTB}\right|^2$$

$$\sim \alpha E_0^2(\sin(A) + \sin(B)) \quad (9)$$

Then In-phase and Q-phase signals are electrically combined in the form of $I_I + jI_Q$ and $I_I - jI_Q$

$$I_I + jI_Q \propto e^{jA} + e^{-jB} \quad (10)$$

Similarly $I_I - jI_Q$

$$I_I - jI_Q \propto e^{-jA} + e^{jB} \quad (11)$$

Now multiplication of $I_I + jI_Q$ and $I_I - jI_Q$ can cancel phase noise completely as and beat signal obtained is like below

$$(I_I + jI_Q)(I_I - jI_Q) \sim \cos(A + B)$$

$$\sim \cos(4\pi\beta\tau_{FUT}t + 2\omega_m - 2\pi\beta{\tau_{FUT}}^2) \quad (12)$$

In above derived equation the phase noise has been canceled after multiplying two created signals and remaining term is again beat frequency and some constants.

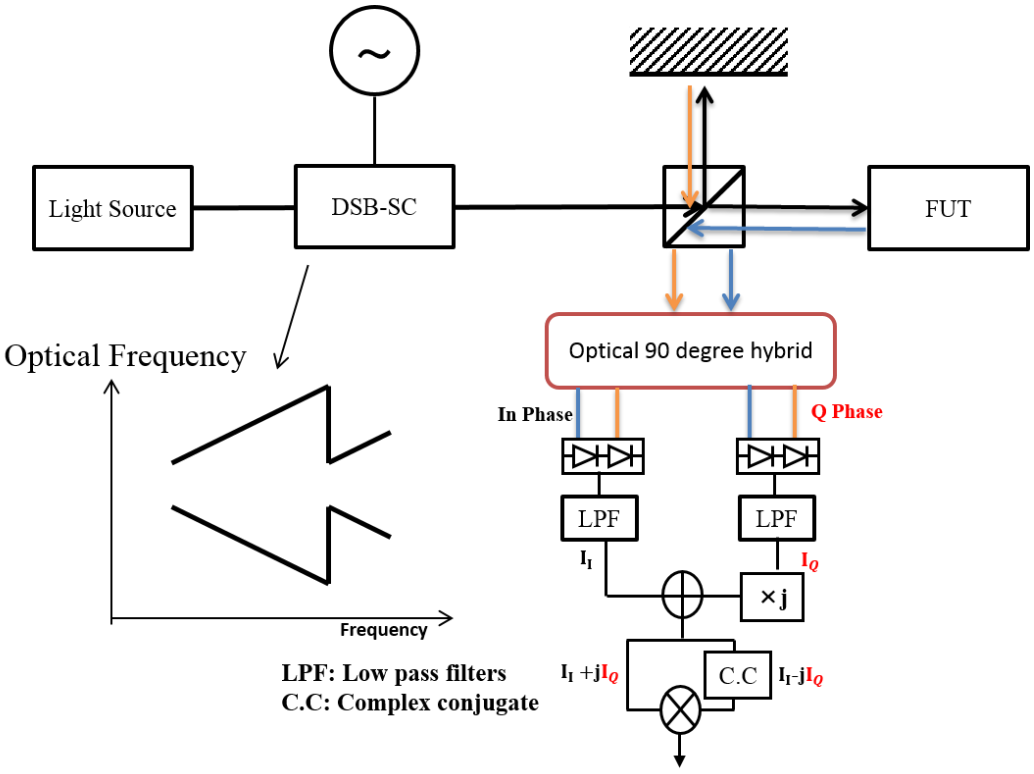

Figure 3.7 (b) Phase diversity configuration

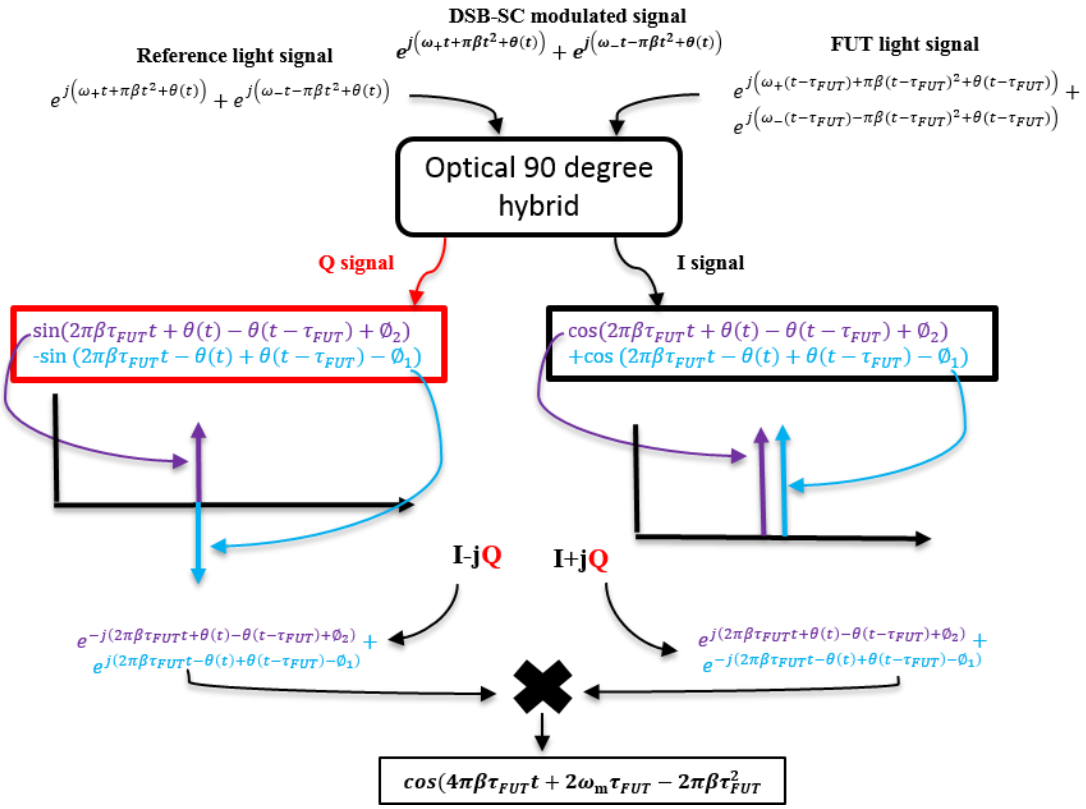

Figure 3.7 Phase diversity principle

3.4 Breakpoint detection in short and long fiber using phase diversity

The DSB-SC modulation procedure for phase diversity is same as that with heterodyne detection. After amplifying the modulated signal to compensate modulation losses, it was divided into FUT and reference arms. Reference arm light and backscattered light from FUT arm are combined using optical 90 degree hybrid and detected by two balanced photo detectors as In-phase and Q phase signals. Detected signals are then converted to digital signals using A/D converters. Q channel signal is multiplied by j (imaginary unit) then added to I channel signal. The resultant signal and its complex conjugate are multiplied with each other. Proposed method with phase diversity was demonstrated to verify short range and long range break point detections. Two experiments with different FUT lengths were conducted one with short fiber where 120 m long fiber was used as a short range fiber (results in fig. 3.8) and in second experiment FUT was replaced by 20 km long fiber to show long range break point detection (results in fig. 3.9). To show the high spatial resolution capability of the proposed method in each experiment two peak at 10 cm apart from each other were detected. In each experiment first peak at the end of FUT was detected and then 10 cm long fiber was attached and peak with addition 10 cm length was detected. In the last part two peaks

10 cm apart from each other were detected by lose coupling between two fiber sections. Sweep span selected in the experiments was 3 GHz (6-9 GHz) and sweep time was 62 ms which sets sweep rate at 48.3 GHz/s. The spatial resolution of the experiment was around 3.4 cm which was calculated by $\Delta l = \frac{c}{2n\Delta F}$ where ΔF is the total frequency sweep span.

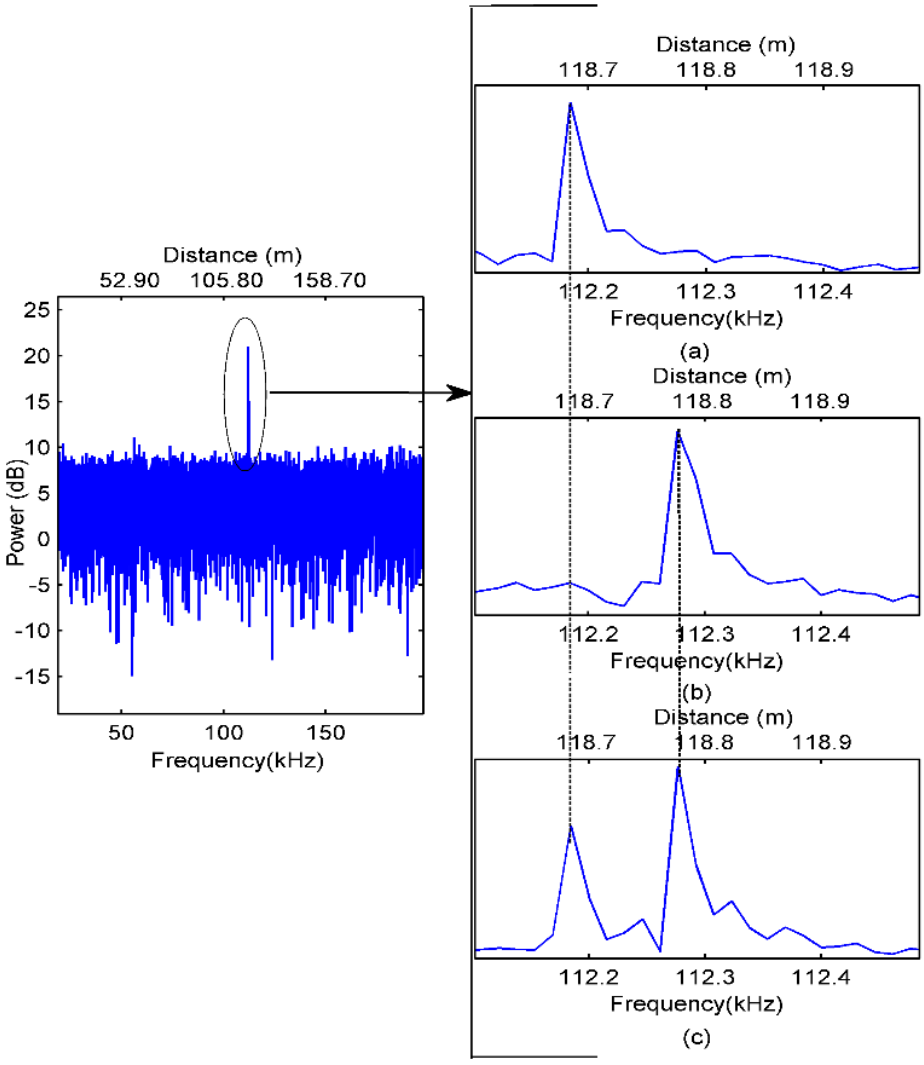

Figure 3.8 Short range break point detection using phase diversity

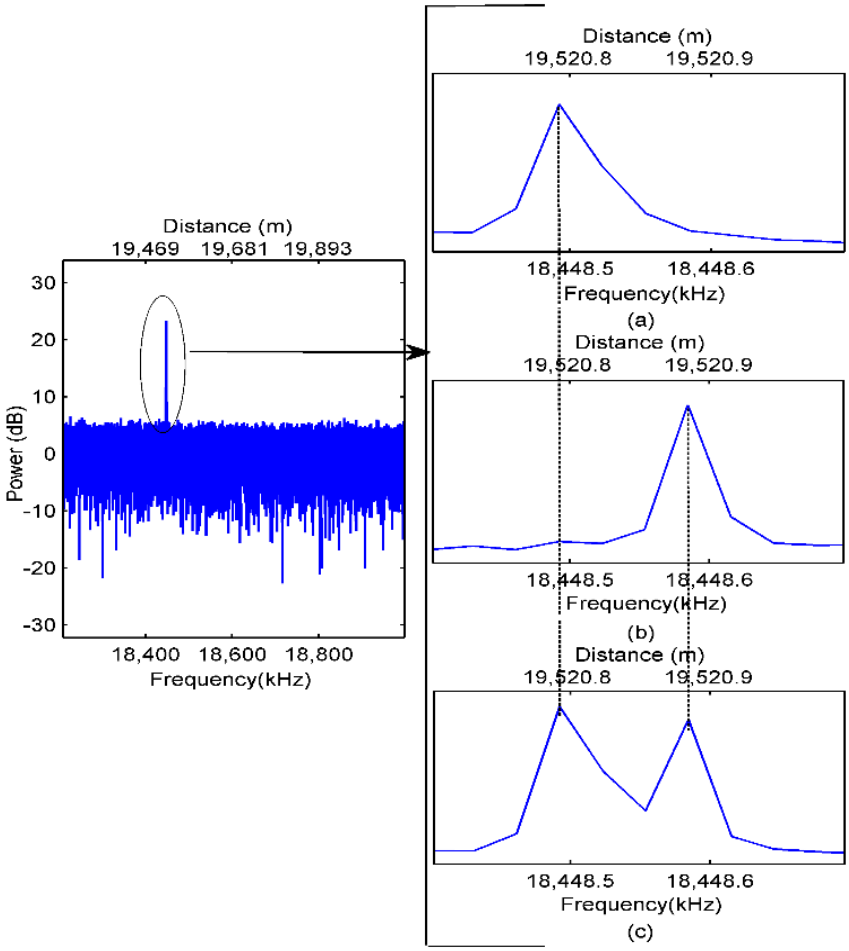

Figure 3.9 Long range breakpoint detection using phase diversity

3.4.1 Dependency on polarization state in phase diversity detection

As described in the principle of phase diversity detection technique the circularly polarized backscattered light is coupled with linearly polarized reference light into 90 degree optical hybrid, this requirement of the scheme makes it sensitive towards polarization of the backscattered light. Since polarization of backscattered light from FUT is arbitrary which changes at every point, therefore achieving same polarization at every point is very difficult. Because of arbitrary nature of backscattered light polarization, it was not possible to measure optical loss. Circular polarization was achieved using polarization controllers over a single point which was the point from where reflection was originated therefore phase noise was canceled at the reflection point and peak was crystal clear but other points have different polarization state because of which phase noise could have not been canceled as a result propagation loss

information was lost. The problem of polarization sensitivity in phase diversity detection technique can be solved by deploying polarization diversity scheme, since polarization diversity will make the system independent of polarization state and phase noise can be canceled over all the backscattered point along the FUT and loss information will be achievable.

3.5 Fiber temperature dependence

Furthermore to demonstrate the high spatial resolution of the proposed scheme fiber temperature dependence of an optical fiber was measured with phase diversity detection technique with spatial resolution around 1.5 cm. 1 km long optical fiber was placed in an incubator and temperature of inside incubator was changed for 5 to 40 ℃. The measured results are shown in fig. 3.10. The experimentally obtained temperature dependence of the measured single-mode fiber is 0.73×10^{-5}m/(m/°C). For standard commercial single mode fiber at wavelength $\lambda = 1550\ nm$, and keeping other parameters as $n = 1.4675$, $\alpha_T = 5.5 \times 10^{-7}/℃$ and $C_T = 0.811 \times 10^{-5}$ [7], where α_T is thermal expansion and C_T is the change of refractive index of the fiber core due to temperature change. The calculated length expansion obtained is 0.811×10^{-5}m/(m/°C). This value is in good agreement with experimental result. This can express our proposed method has confirmed high spatial resolution.

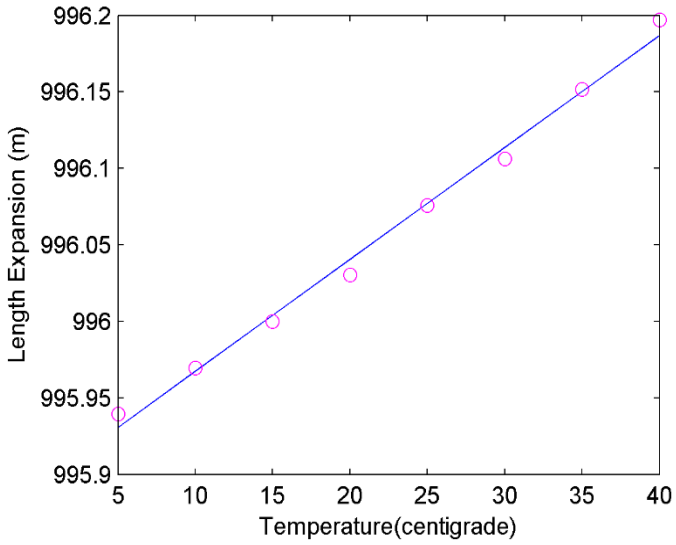

Figure 3.10 Fiber temperature dependence measurement using proposed scheme

3.6 Chromatic dispersion measurement

Chromatic dispersion is one of the significant characteristics of an optical fiber to be taken into consideration. The typical effect of chromatic dispersion in high speed transmission is pulse broadening.

Moreover, dense wavelength division multiplexing (DWDM) systems work on high power with many channels, which may cause four wave mixing, cross phase modulation and stimulated Raman scattering phenomenon. In order to design a system to cope with those effects, an accurate knowledge of the chromatic dispersion is required. Mainly two methods are used to measure chromatic dispersion in a long fiber [8]; time-of-flight mechanism, which measures the propagation delay of signals at different wavelength and phase shift method [9], which measures the difference in phases of signals as the function of wavelength.

In the phase shift measurement method, an amplitude modulated signal is sent through fiber under test (FUT) and group delay difference (propagation delay due to wavelength change) is calculated from the phase shift measurement at various wavelengths, first time demonstrated using LED [10]. Another method is baseband AM response method, which measures the chromatic dispersion based on interference of modulation sidebands [11]. Phase shift method is an accurate method and that is why it is widely used by manufacturers to measure fiber chromatic dispersion. However, phase shift method is a two end measurement method, which means one unit at each fiber end is required, moreover signal phase information is needed at the receiving end, provided by a reference signal. The accuracy of AM response method is not as excellent as phase shift method, though it does not require any reference signal but still it is a two end method. Above mentioned methods are viable techniques to measure chromatic dispersion in optical fiber, when both fiber ends are easily accessible but in other scenario if a fiber is already deployed as a part of an optical transmission network, it is always not possible to have access to both terminating ends of the fiber, because they are usually several tens of kilometers far from each other. Other problem with two end techniques is that, they cannot measure chromatic dispersion of each segment if fiber link is made up of multiple fiber segments. Moreover, those techniques do not provide length information. Thus, if length of deployed fiber link is not known, the optical time domain reflectometry (OTDR) has to be used to obtain length information before starting chromatic dispersion measurement [9]. In such a scenario, chromatic dispersion measurement using OTDR, which is based on time-of-flight mechanism is the best solution. This is because OTDR is a one end measurement technique, which can also provide length and loss information without using any other additional measurement process [9]. Another advantage of OTDR method is, if the fiber link is made up of multiple fiber segments connected together, OTDR method can measure chromatic dispersion of each fiber segment (distributed measurement), provided there is a reflection present at each connector. However, OTDR has some severe limitations. Because of its poor spatial resolution, the measurement accuracy is not very good. Commercially available OTDR based chromatic dispersion measurement equipment have spatial resolution in meters. Optical frequency domain reflectometry (OFDR), which has better spatial resolution

and better sensitivity can be the optimal solution for OTDR limitations. However, the measurable distance of OFDR is limited by the coherence length of the laser, because beyond the coherence length, significantly increased laser phase noise makes detection almost impossible. Increasing measurable range by the means of narrow linewidth lasers can be an option to detect long range backscattered signal [13]. However, narrow linewidth lasers are not commonly available and they are expensive as well, moreover using narrow linewidth lasers do not solve OFDR problem of measurement within coherence length. Another method to solve this problem is to somehow cancel or compensate the laser phase noise. This method can set OFDR free from measurement within coherence length limitation and long distance measurements can be possible [14, 15]. Previously various works have been done on chromatic dispersion measurement in long fibers using OTDR and OFDR but mentioned techniques suffer from either small dynamic range or poor spatial resolution. A comparative table of previous works can be seen in table 1.

Table 3-1 Comparison of previous works to measure chromatic dispersion using OTDR and OFDR

Method	Spatial Resolution	Length	Reference
Supercontinuum pulse source OTDR	Centimeter level	4.2 km	[16]
Bidirectional OTDR	Tens of meters	70 km	[17]
Frequency shifted laser based OFDR	A few meters	20 km	[18]
DSB-PNC OFDR	Millimeters	50 km	[4]

In this research, a new method to measure chromatic dispersion using OFDR in long optical fibers is proposed with spatial resolution around 8 mm (Limited by hardware availability in the Lab.). The proposed method uses DSB-PNC-OFDR to measure chromatic dispersion in fibers much longer than laser coherence length (not possible with ordinary OFDR) with good accuracy. OFDR can be used in long fiber lengths with high spatial resolution if it is set free from measurement within the coherence length and DSB-PNC OFDR is capable of performing measurements beyond the coherence length, therefore chromatic dispersion in long optical fibers can be measured accurately if DSB-PNC OFDR with high spatial resolution is used.

3.6.1 Chromatic dispersion measurement method

The proposed scheme can be implemented using two types of arrangements; one is a heterodyne detection method and the other is phase diversity detection method as described earlier in this chapter. In heterodyne detection method two side bands of combined light are separated using optical filter and then separated sidebands are detected using two photo detectors as two separate channels. Finally, multiplication of two channels results in cancelation of laser phase noise [6]. Since the heterodyne method has simple configuration, but requires optical filter, which needs to be tuned every time if wavelength of laser source is changed for chromatic dispersion measurement. Therefore, for chromatic dispersion measurement phase diversity detection technique is recommended.

The chromatic dispersion in a fiber is measured by simply shifting the source wavelength and measuring the group delay. The propagation delay difference between two wavelengths is measured as below

$$\Delta\tau_{FUT}(\lambda_m,\lambda_r) = \tau_{FUT}(\lambda_m) - \tau_{FUT}(\lambda_r) = \frac{f_m - f_r}{4\beta} \tag{13}$$

where $\Delta\tau_{FUT}(\lambda_m,\lambda_r)$ is the propagation delay difference between two wavelengths λ_m,λ_r $f_m = 4\beta\tau_{FUT}(\lambda_m)$ and $f_r = 4\beta\tau_{FUT}(\lambda_r)$ are the beating frequency, which is obtained by taking FFT of the measured beating signal. The group delay is determined by the difference of beating frequency at two different wavelengths. The chromatic dispersion $D(\lambda)$ in FUT is the function of wavelength, which is obtained by differentiating the group delay with respect to wavelength and dividing by FUT length [18], as formulated below

$$D((\lambda_m + \lambda_r)/2) = \frac{1}{L}.\frac{\Delta\tau_{FUT}(\lambda_m,\lambda_r)}{\lambda_m - \lambda_r} \tag{14}$$

Minimum measurable dispersion depends on minimum detectable group delay and this depends on the spatial resolution of the OFDR. If the spatial resolution of OFDR is very high, even small change in propagation delay of different wavelengths results in observable change in beat frequency. In OFDR, spatial resolution depends on sweep frequency span and the micrometer (μm) level spatial resolution is achievable as determined by the formula below

$$\Delta L = \frac{c}{2n\Delta F} \tag{15}$$

where c is the speed of light, n is the refractive index of the fiber core and ΔF is the sweep frequency span. Moreover, the experimentally achievable spatial resolution depends on the sweep rate, sampling rate and number of data points, formulated as

$$\Delta L_P = \frac{c f_s}{4n\beta N} \quad (16)$$

Here, f_s is the sampling rate, N is the number of data points. The accuracy of total optical dispersion depends on beat frequency accuracy error, which can be minimized with increased sweep span, hence the better spatial resolution [18]. On the other hand, OTDR spatial resolution depends on pulse width and reducing pulse width can increase spatial resolution but at the same time signal to noise ratio of the signal drops down, thus the system sensitivity. Therefore, averaging for several thousand is required and still gaining less than a meter spatial resolution in OTDR is a challenging task.

3.6.2 Chromatic dispersion measurement results

The chromatic dispersions in optical fibers is measured by DSB-PNC-OFDR which makes a long range backscattered detection possible without using very narrow linewidth lasers. The laser phase noise cancelation principle was same as described in DSB-PNC OFDR with phase diversity detection technique. A 50 km long optical link was created which was made up of two 20 km and one 10 km long dispersion shifted fiber (DSF) and chromatic dispersion in each fiber segment was measured in connected and detached fashion, as shown in fig. 3.11. The theoretical spatial resolution of the OFDR for all the experiments was limited by the frequency sweep span of the sweep generator. The available sweep range was 13 GHz, which corresponds to 7.9 mm spatial resolution limit, which was calculated by Eq. (15). Detected signals were sampled at the sampling rate of 2 Msa/s. The length of data points was 1027397, while sweep rate was 20 GHz/s. This sets a 5 mm spatial difference between two points. It was then calculated using Eq. (16). In experiments presented in this research, signals were under sampled in order to increase the spatial resolution between two points. Since the balance photo detectors used in the experiment had low bandwidth (10 MHz), increasing the sweep rate resulted in the beat frequency from a long fiber ($4\beta * \tau_{FUT}$) exceeding the minimum detectable frequency range of balance photo detectors. Also, since the length of the fibers was already known, the exact beat frequency information was not necessary. The important task was to track the propagation delay difference as a function of wavelength change.

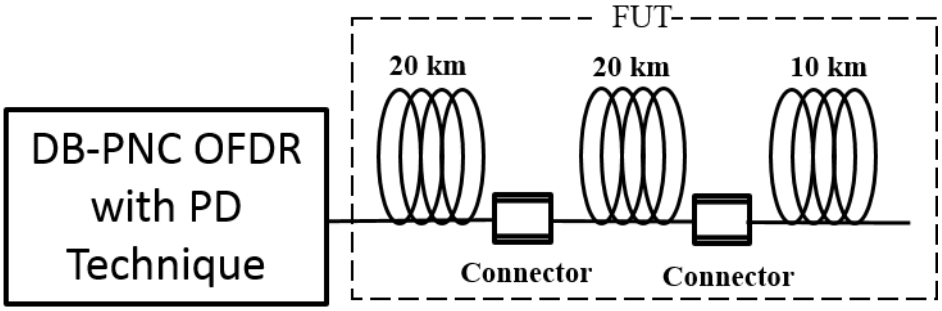

Figure 3.11 Experimental arrangement for chromatic dispersion measurement using phase diversity detection DSB-PNC OFDR

In the first part of the experiment, the chromatic dispersion along with zero dispersion wavelength in three different length of fibers (two 20 km with 1549 nm and 1554 nm as zero dispersion wavelengths and one 10 km 1540 nm as zero dispersion wavelength) were measured individually. Also, in order to confirm the accuracy of the proposed method, chromatic dispersion measured in all the fibers were compared with standard phase shift method. In addition, chromatic dispersion of a standard single mode fiber of length 25.2 km is also measured. In the second part of the experiment, a fiber link of 50 km was constructed by connecting the three fiber segments and again, chromatic dispersion of each segment was measured in connected fashion. In all the experiments the wavelength of the optical signal was changed from 1500 to 1570 nm, with 10 nm each step size. As the wavelength was changed, a shift in frequency (Distance) was observed and group delay was calculated as described in Eq. (13). Fig. 3.12 shows the peak shift in distance as the wavelength was changed in one of the 20 km long dispersion shifted fiber and fig. 3.13 is the measured group delay.

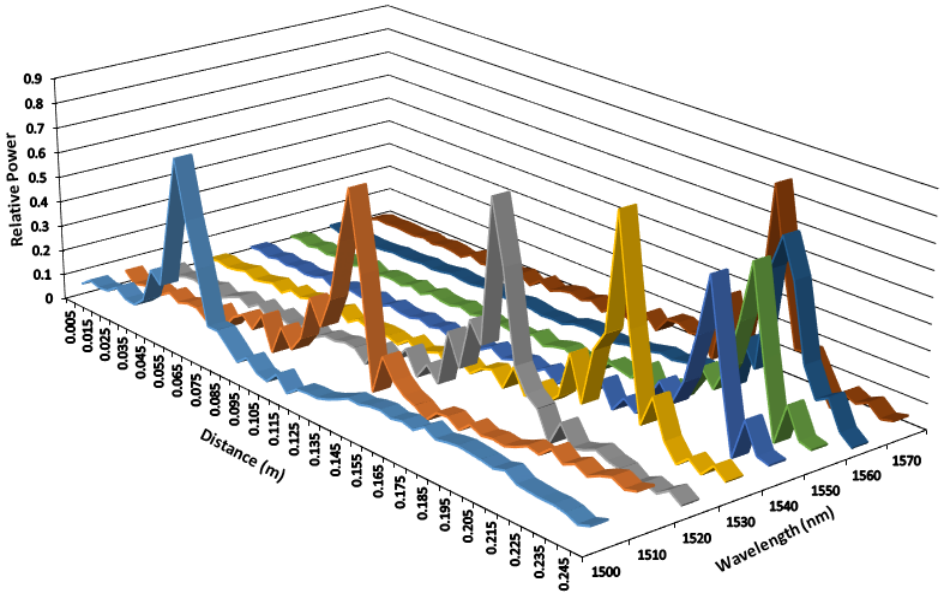

Figure 3.12 Shift in beat frequency (Distance) as a function of wavelength, where 19963 m is subtracted from distance axis

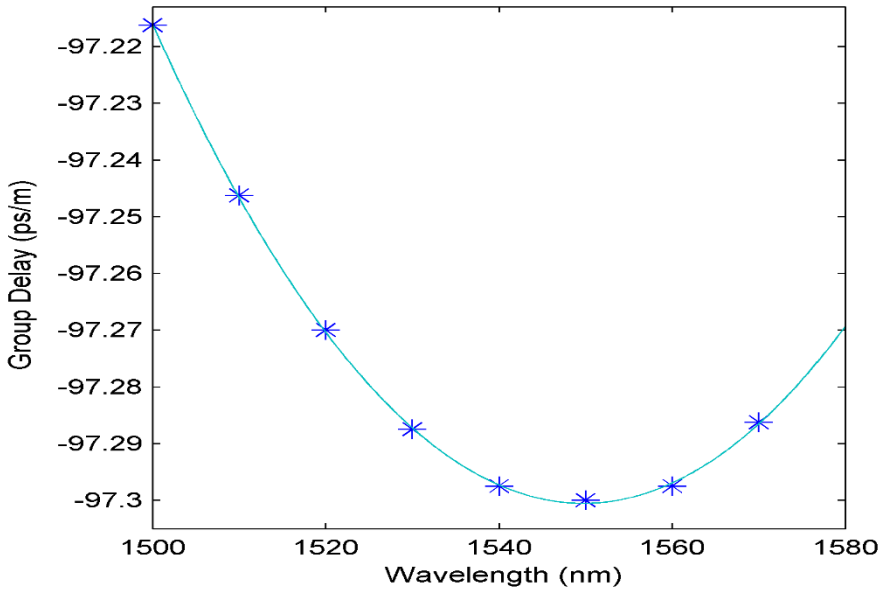

Figure 3.13 Measured group delay in one of the 20 km long fiber

To calculate the dispersion of FUT, first group delay data is fit over theoretical curve and then, the best fit group delay curve is differentiated with respect to wavelength. Chromatic dispersion is dominated by

material dispersion in dispersion of non-shifted fibers around 1.55μm. In such a scenario, group delay is well defined by the Sellmeier equation. According to fiber optic test procedure (FOTP)-169, group delay fit should be a three-term Sellmeier equation as given below [21].

$$\tau(\lambda) = a\lambda^2 + \mathrm{b}\lambda^{-2} + \mathrm{c} \tag{17}$$

The group delay in a dispersion shifted fiber has a different functional form due to a large waveguide contribution to dispersion. For such a case, FOTP-169 recommends that group delay data should be fit to a quadratic equation

$$\tau(\lambda) = a\lambda^2 + \mathrm{b}\lambda + \mathrm{c} \tag{18}$$

There are many kinds of equations for fitting group delay data, 5 term Sellmeier, various polynomials and fits with terms involving natural logarithm, fit classification for wavelength range and fiber type can be found in [9,21]. For different types of fibers, each functional form best describes the group delay.

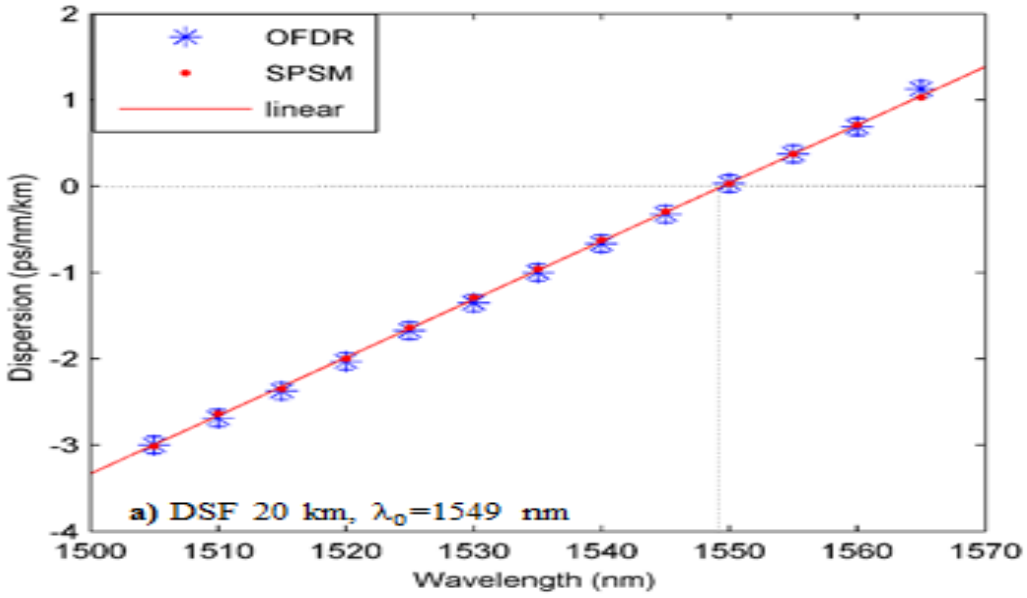

Figure 3.14 Chromatic dispersion of a dispersion shifted fiber.

Chromatic dispersion can be calculated from differentiation of group delay with respect to wavelength as in Eq. (14). Fig. 3.14 shows measured dispersion of a 20 km DSF fiber. The dispersion coefficient goes through zero which is known as “zero dispersion wavelength”. By using calculated dispersion values, dispersion slope can also be measured, which is derivative of calculated dispersion. In order to confirm the accuracy of the proposed measurement method, chromatic dispersion in same fibers was measured

with standard phase shift method (SPSM). Conventional SPSM was constructed by using network analyzer, tunable laser source, intensity modulator and photo detector [12]. Modulation frequency was 1 GHz and wavelength change step was same as for proposed method, which was 10 nm. The compared results in Table 2 show that there is an excellent agreement between calculated dispersion coefficients by both methods. The accuracy of the proposed measurement method can be increased with increasing wavelength shift span, but since the chromatic dispersion is not completely straight, on increasing accuracy some discrepancies appeared when compared with phase shift method over some wavelengths.

Table 3-2 Dispersion coefficient comparison between OFDR and SPSM at wavelength 1545 nm

Fiber	Dispersion ($\frac{ps}{nm}/km$) with OFDR	Dispersion ($\frac{ps}{nm}/km$) with SPSM	Zero Dispersion Wavelength in nm (λ_0)	Slope $ps/(nm^2 \times km)$
1st DSF 20 km	-0.25$\pm$0.096	-0.29±0.007	1549$\pm$1.4	0.069
2nd DSF 20 km	-0.625$\pm$0.096	-0.68±0.007	1554$\pm$1.4	0.064
3nd DSF 10 km	0.25$\pm$0.19	0.38±0.013	1540$\pm$2.8	0.073
Standard Single Mode Fiber	16.25$\pm$0.076	16.19±0.005	—	0.049

To check the measurement accuracy in other types of fibers, chromatic dispersion in a 25.2 km long standard single mode fiber was measured with proposed method. Measured dispersion results were compared with results obtained by standard phase shift method and again very good match was observed as can be seen in table 1.

In order to measure chromatic dispersion of each fiber segment in a connected fashion, three fiber segments in which chromatic dispersion was already measured were connected together using SPC connections to construct a 50 km long fiber link without any splice. Subsequently, chromatic dispersion was measured in each segment by detecting the fraction of reflected light from the SPC connections, usually return loss of SPC connection is -30 to -40 dB. In present condition splice points along the fiber are not detectable, increased sensitivity by means of averaging might make splice point detection possible.

Calculated dispersion, zero dispersion wavelength and the dispersion slope were almost equal to when they were measured in each fiber segment separately. Table 3 shows comparisons of calculated dispersion coefficient by the proposed method in connected and detached arrangements.

Table 3-3 Dispersion coefficient Comparison in connected and separate arrangements at wavelength 1545 nm

Fiber	Dispersion ($\frac{ps}{nm}/km$) when separate	Dispersion ($\frac{ps}{nm}/km$) when connected
1st DSF 20 km	-0.25±0.096	-0.25±0.096
2nd DSF 20 km	-0.625±0.096	-0.75±0.096
3nd DSF 10 km	0.25±0.19	0.5±0.19

3.6.3 Accuracy

In proposed method experiment, theoretical spatial resolution limit was 7.9 mm, which corresponds to detectable group delay of 38.5 ps ($\Delta\tau = \frac{\Delta L}{v_g}, v_g = c/n$) , and with 10 nm wavelength shift in a 20 km long fiber gave dispersion value $0.192\ \frac{ps}{nm}/km$, calculated using Eq. (14) and accuracy was $\pm 0.096\ \frac{ps}{nm}/km$. For 10 km long fiber accuracy became $\pm 0.19\ \frac{ps}{nm}/km$. The group delay in phase shift method can be calculated from formula below

$$\Delta\tau = \frac{\Delta\theta}{360.f_m}$$

where $\Delta\theta$ is phase difference and f_m is the modulation frequency. Modulation frequency for phase shift method experiment conducted in this research was set at 1 GHz and minimum phase difference could be of one degree, which corresponds to minimum group delay of 2.7 ps, and 10 nm wavelength change in 20 km contributed dispersion of value $0.0138\ \frac{ps}{nm}/km$ and the accuracy was around $\pm 0.007\ \frac{ps}{nm}/km$. For 10 km fiber it became $\pm 0.0138\ \frac{ps}{nm}/km$.

3.7 References

[1] Jinhong Geng, Christine Spiegelberg, and Shinin Jiang, "Narrow Linewidth Fiber Laser for 100-km Optical Frequency Domain Reflectometry", *IEEE photonics technology letters,* vol. 17, no.9, pp.1827-1829Sept. 2005.

[2] Xinyu Fan, Y. Koshikiya, and F. Ito, "Phase-Noise-Compensated Optical Frequency-Domain Reflectometry", *IEEE J. Quant. Electron.*, vol. 45, no.6,pp.594-602, June 2009.

[3] Y. Koshikiya, Xinyu Fan and F. Ito, "40-km Range, 1-m Resolution Measurement Based on Phase-noise-compensated coherent Optical Frequency Domian Reflectometry", *ECOC 2008,* Brussels, Belgium. Sept. 2008, vol.5, pp.21-22.

[4] Mudabbir. Badar, H. Kobayashi, and K. Iwashita, "Chromatic dispersion measurement with double sideband phase noise canceled OFDR*",* Opt. comm., **356**, 350-355, (2015).

[5] Mudabbir Badar, Takuya Hino, Katsushi Iwashita, "Phase noise cancelled OFDR with cm-Level Spatial Resolution Using Phase Diversity", *Phot. Tech. Let.* , 26(9), 858-861, (2014).

[6] Shuta Hiramatsu and Katsushi Iwashita, "A Novel Phase-Noise Cancelled Optical Frequency Domain Reflectometry Using Modulation Sidebands", *Photon. optoelectron. (P&O),* vol.1 Iss.3, pp. 60-64, Oct. 2012.

[7] L. B. Yuan, J. Yang: "Multiplexed Mach-Zehnder and Fizeau tandem white light interferometric fiber optic strain/temperature sensing system*", Sens. and Actuat. A*, vol. 105, p. 40, 2003.

[8] P.Hlubina, M.Kadulova, D.ciprian, "Spectral interferometry-based chromatic dispersion measurement of fiber including the zero-dispersion wavelength",J. Europ. Opt. Soc. Ra. Pub. 7, 12017 (2012).

[9] Brandon Collings, Fred Heismann, Gregory Lietaert, *Reference Guide to fiber optics testing col 2 (JDS uniphase cooperation, 2010).*

[10] Bruno Costa, Daniele Mazzoni, Mario Puleo, and Emilio Vezzoni, "Phase shift Technique for the Measurement of Chromatic Dispersion in Optical Fibers Using LED's", IEEE Trans. Microwave. And Technol., 30(10), 1497-1503 (1982).

[11] F. Devaux, Y. Sorel and J.F. Kerdiles, "Simple Measurement of Fiber Dispersion and of Chirp Parameter of Intensity Modulated Light Emitter", J. Lightwave. Technol. 11(12), 1937-1940, 1993.

[12] Rongqing Hui and Maurice O'Sullivan, *Fiber Optic Measurement Techniques (Elsevier Academic Press, 2009)*.

[13] Jinhong Geng, Christine Spiegelberg, and Shinin Jiang, "Narrow Linewidth Fiber Laser for 100-km Optical Frequency Domain Reflectometry", *IEEE photonics technology letters*, 17(9), 1827-1829, (2005).

[14] Y. Koshikiya, Xinyu Fan, and F. Ito, "Long Range and cm-Level Spatial Resolution Measurement Using Coherent Optical Frequency Domain Reflectometry with SSB-SC Modulator and Narrow Linewidth Fiber Laser", *J. lightw. Technol.*, vol.26, no.18, pp.3287-3294, Sept. 15, 2008.

[15] Xinyu Fan, Y. Koshikiya, and F. Ito, "Phase-Noise-Compensated Optical Frequency-Domain Reflectometry", *Phot. Tech. Let.* , 21(17), 1262-1264, (2009).

[16] Scuberi Moon, and Dug Y. Kim, "Reflectometric Fiber Dispersion Measurment Using a Supercontinuum Pulse Source", *IEEE J. Quant. Electron.*, vol. 45, no.6,pp.594-602, June 2009.

[17] Alberto Rossaro, Marco Schiano, Tiziana Tambosso, and Davide D' Alessandro, "Spatially Resolved Chromatic Dispersion Measurement by a Bidirectional OTDR Technique", J. Quan. Elec. **7**(3), 375-383 (2001).

[18] Masato Yoshida, Koichiro Nakamura, and Hiromasa Ito, "A New Method for Measurement of Group velocity Dispersion in Optical Fibers by Using a Frequency-Shifted Feedback Fiber Laser", *Phot. Tech. Let.* , 13(3), 227-229, (2001).

[19] Binhao Wang, Guofeng Yan, Chunsheng Yan, "Fiber Length and Chromatic Dispersion Measurement Technology Using a Novel Optical Frequency Domain Reflectometry", OSA-IEEE-COS 2010.

[20] *Tae-Jung Ahn, Yongmin Jung, Kyunghwan Oh, and Dug Yound Kim,* "Optical frequency-domain chromatic dispersion measurement method for higher order modes in an optical fiber", Opt. Exp., 13(25), 10040-10048, (2005).

[21] S.E. Mechels, J.B. Schlager, and D.L. Franzen, "Accurate Measurement of the Zero-Dispersion Wavelength in Optical Fibers", J. Res. Natl. Inst. Stand. & Technol., 102(3), 333-347, (1997).

Chapter 4 : Spatial Resolution Improvement in OFDR with Sweep Span Broadening and Format Free Optical Wavelength Conversion

4.1 Optical frequency sweep span broadening

Optical time domain reflectometry (OTDR) is mainly used reflectometry technique because of longer measurable distance. Though, OTDR is widely used technique, it faces the problem of low spatial resolution and poor sensitivity as emphasized in earlier chapters. On the other hand optical frequency domain reflectometry (OFDR) has better spatial resolution and sensitivity, and this is the reason it is mostly used in high spatial resolution applications such as optical component diagnosis [2]. In OFDR the spatial resolution is linked with frequency sweep span, broader the frequency span, higher the spatial resolution. Usually light source in OFDR can be swept in two ways, one is by using tunable laser source and the second is external sweep by the means of modulator by RF frequency. Sweeping by tunable laser source can provide broad sweep span, some tens of nm has been demonstrated, however broad sweep through tunable laser restrict the measurement to small distance because of broader spectral width. Moreover, Sweep through tunable laser is slow and sweep nonlinearity can degrade the OFDR performance [3]. External light source sweep by the means of external modulator modulated by RF frequency can realize long range measurement without degrading OFDR performance and this kind of sweep is also linear up to several GHz. However, the available RF sweep span frequency is limited because bottlenecks imposed by electronics. Moreover, commonly available modulators have operating frequency up to 40 GHz and cost soar with the broader frequency components. Therefore it is desired to find some other way to increase sweep span in high spatial resolution OFDR applications.

Recently, some new methods to broaden available sweep span are proposed which can increase the sweep span for multiple times. Frequency span broadening using recirculating frequency shifter has demonstrated increased spatial resolution up to 1.46 cm with sweep span of 712 MHz [3,4] but additional phase noise was the main problem with mentioned technique as the frequency broadening was increased with higher side band. Another method which uses higher order modulation sidebands reported 10-times broadening with 1.5 cm achieved spatial resolution [5], latter technique was further modified and used with degenerated four wave mixing (FWM) to increase two times sweep span [6]. The reported technique with

degenerated FWM was using two laser sources one for the pump and other for the signal, because of two laser sources the laser phase noise was increased up to 3-times, hence the coherence length was reduced up to 3- times which can result in short measuring distance.

In this research a novel method to increase available sweep span up to 3-times has been proposed. The proposed technique is using degenerated FWM created by double side band with a suppress carrier modulation (DSB-SC). The advantage of using DSB-SC modulation is that two created sidebands behave as separate signals for degenerated FWM, since they are generated from the single light source, therefore the phase noise is not increased to 3-times and coherence length of the light source is preserved. Furthermore, DSB-SC modulation technique can be used to cancel the laser phase noise (DSB-PNC OFDR) [7, 8] and measurement beyond the laser coherence length can be achieved. In this part of research it is also confirmed if DSB-SC modulation is used with degenerated FWM we can cancel the laser phase and perform measurement beyond laser coherence length with 3-times higher spatial resolution. The proposed method's sweep frequency span broadening capability can be increased up to 12-times if one more stage of FWM is included [9, 10].

4.2 Frequency sweep span broadening principle

OFDR is the best choice over OTDR especially in high spatial resolution measurements. The theoretical spatial resolution in an OFDR system is linked with the sweep frequency span by the formula given below

$$\Delta l = \frac{c}{2n\Delta F} \tag{1}$$

where ΔF is the frequency sweep span, n is core refractive index and c is the speed of light. A new method to expand sweep span using DSB-SC modulation and degenerated FWM is proposed. DSB-SC modulation creates two side bands which work as two individual signals, both sidebands are passed through the nonlinear medium to create new frequency components (FWM signals) which are located next to each sideband, configuration can be seen in fig. 4.1. When the sweep frequency is applied two sidebands are swept in opposite directions and as a result if sidebands move one unit in frequency, the FWM signal is moved 3-units because frequency difference between two sidebands increased two times. The light signal from the source is modulated by DSB-SC modulation, the optical field of modulated signal can be described as

$$E(t) = \frac{E_0}{2}\left[e^{j((\omega_c+\omega_m)t+\pi\beta t^2+\theta(t))} + e^{j((\omega_c-\omega_m)t-\pi\beta t^2+\theta(t))}\right] \tag{2}$$

where E_0 is the field amplitude , ω_c is the carrier angular frequency, ω_m is modulation angular frequency, β is the linear sweep rate and $\theta(t)$ is random phase produced by phase noise. Each sideband is treated as separate light source and they can be expressed as below

$$E(t)_1 \propto \frac{E_0}{2}\left[e^{j((\omega_c+\omega_m)t+\pi\beta t^2+\theta(t))}\right] \quad (3)$$

$$E(t)_2 \propto \frac{E_0}{2}\left[e^{j((\omega_c-\omega_m)t-\pi\beta t^2+\theta(t))}\right] \quad (4)$$

where $E(t)_1$ and $E(t)_2$ denotes two signals to be used for degenerated FWM. As two signals travels through a non-linear medium two new FWM frequency components are generated. There will be two 1st order FWM frequencies generated at opposite frequency locations from the center frequency as shown in fig. 4.2. Newly generated frequency components can be represented as

$$E(t)_{FWM} = E_1^2 . E_2^* \propto |E_i|^2\left[e^{j((\omega_c+3\omega_m)t+3\pi\beta t^2+\theta(t))}\right] \quad (5)$$

$$E(t)_{FWM'} = E_2^2 . E_1^* \propto |E_i'|^2\left[e^{j((\omega_c-3\omega_m)t-3\pi\beta t^2+\theta(t))}\right] \quad (6)$$

where E_i *and* E_i' are the degenerated optical fields. As it can be seen from the above equations newly generated frequency components are modulated 3-times farther than the originally applied modulation frequency, moreover the sweep rate is also increased by 3- times. Here, it can also be seen that the phase of newly generated frequency components is same as that of original source without being increased to 3-times because two sidebands has exactly same phase as they were generated from the same laser source. Further, other end of the non-linear medium is connected to an optical filter, where one of the FWM signal is filtered out and used as the OFDR signal. The filtered out FWM signal is divided into two arms and one arm signal is kept as reference signal for coherent detection, while the other arm signal is sent through fiber under test (FUT) as a probe signal. The backscattered signal form the FUT is combined with reference signal and detected coherently.

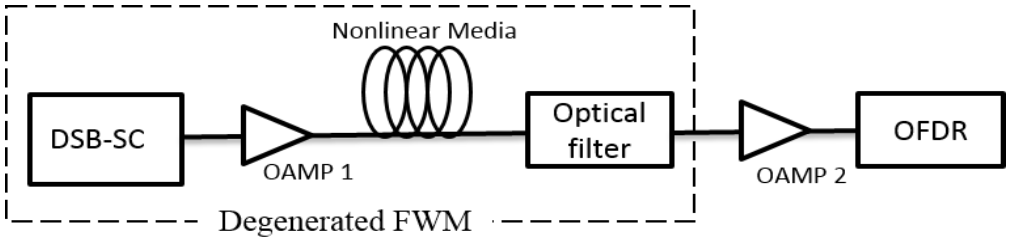

Figure 4.1 Configuration of proposed method

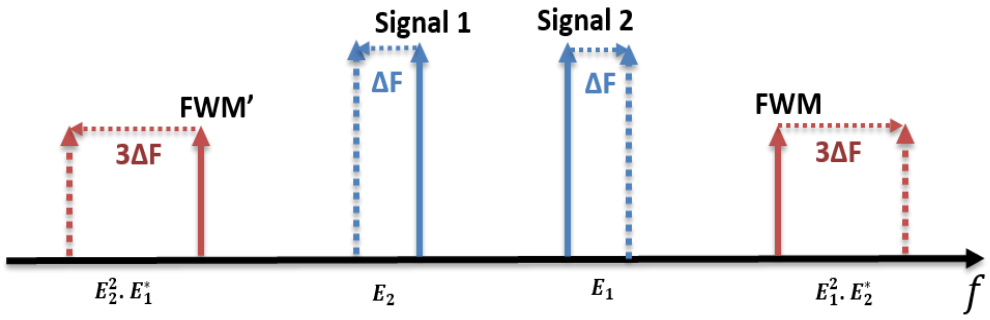

Figure 4.2 Schematic illustration of optical sweep span broadening using proposed method, ΔF is the sweep frequency span

Laser phase noise is the main constrained in OFDR measurement range, normally measurable distance of OFDR is limited to half of the laser coherence length. In order to perform measurements beyond the laser coherence length some methods have been proposed [11, 12]. Proposed OFDR (DSB-PNC OFDR) to cancel the laser phase noise and conduct measurements beyond the laser coherence length is based on DSB-SC modulation [7, 8, and 13]. The DSB-PNC OFDR was using two sidebands created after DSB-SC modulation to cancel the laser phase noise in OFDR. The proposed method presented in this research is also using DSB-SC modulation to increase the frequency sweep span and newly created FWM signals (Eq. (5) and Eq. (6)) are identical to two side bands created from DSB-SC modulation as in Eq. (2), only with 3-times higher sweep span. Therefore, if two FWM signals are treated as two sidebands of DSB-SC we can cancel the laser phase noise with 3-times higher spatial resolution. In order to use the proposed method to cancel the laser phase noise both FWM signals are filtered out and coupled together using an optical coupler. After amplification the coupled FWM signals are divided into two arms and one arm signal is kept as reference arm and the other arm signal is probed into the FUT. The coupled FWM signals and backscattered signal from the FUT arm with single peak at a delay τ_{FUT} can be described as below

$$E(t)_{FWM+FWM'} \propto |E_i|^2\left[e^{j((\omega_c+3\omega_m)t+3\pi\beta t^2+\theta(t))}\right] + |E_i'|^2\left[e^{j((\omega_c-3\omega_m)t-3\pi\beta t^2+\theta(t))}\right] \quad (7)$$

$$E(t-\tau)_{FWM+FWM'} \propto |E_i|^2\left[e^{j((\omega_c+3\omega_m)(t-\tau_{FUT})+3\pi\beta(t-\tau_{FUT})^2+\theta(t-\tau_{FUT}))}\right] + |E_i'|^2\left[e^{j((\omega_c-3\omega_m)(t-\tau_{FUT})-3\pi\beta(t-\tau_{FUT})^2+\theta(t-\tau_{FUT}))}\right] \quad (8)$$

Then reference arm signal was passed through optical filter, where two FWM signals were separated into two channels as higher and lower frequency channels. Later, each separated channel from reference light was coupled with the backscattered light and detected by two balance photodiodes as higher frequency and lower frequency channels. The photo current of each channel is given below

$$I_l(t) \propto \cos(6\pi\beta\tau_{FUT}t + \theta(t-\tau_{FUT}) - \theta(t) + \emptyset_1) \quad (9)$$

$$I_h(t) \propto \cos(6\pi\beta\tau_{FUT}t - \{\theta(t-\tau_{FUT}) - \theta(t)\} + \emptyset_2) \quad (10)$$

Above equations are derived after ignoring DC components. Here $I_l(t)$ and $I_h(t)$ are photo currents of low frequency and high frequency channel, $\emptyset_1 = -(\omega_c - 3\omega_m)\tau_{FUT} - 3\pi\beta{\tau_{FUT}}^2 and\ \emptyset_2 = (\omega_c + 3\omega_m)\tau_{FUT} - 3\pi\beta{\tau_{FUT}}^2$. In above equation the beat frequency is 3-times higher than the original because the sweep span was broadened 3-times. As it can be seen from derived equations the phase noise present in one channel is same to that of other channel but opposite in sign, therefore on multiplying Eq.(9) and Eq.(10) the phase noise is canceled out and remaining terms are beat frequency and some constants, defined below

$$I_h(t) * I_l(t) \propto \cos(12\pi\beta\tau_{FUT}t + \emptyset_1 + \emptyset_2) \quad (11)$$

where the first term is beat frequency, $\emptyset_1$ and $\emptyset_2$ are constants without phase noise. Therefore, proposed method can also be used to cancel laser phase noise in OFDR with 3-times enhanced spatial resolution.

4.3 Frequency span broadening experimental arrangements

The proposed method to enhance frequency sweep span was demonstrated by the means of experiments. Two types of experiments were conducted to check feasibilities of the proposed method. First experiment was carried out with ordinary OFDR and frequency span broadening was confirmed. The second experiment involved phase noise cancelation and checking of frequency span broadening.

4.3.1 Ordinary OFDR

This experiment was carried out to show frequency sweep span can be increased in normal OFDR arrangement. The experimental setup is shown in fig. 4.3. The proposed method involves only one laser source which was distributed feed-back (DFB) laser diode of linewidth around 3 MHz. The laser source was modulated by DSB-SC modulation with center wavelength 1549 nm and maximum power was derived from the laser which was around +7 dBm. $LiNbO_3$ dual drive MZM intensity modulator was used to achieve DSB-SC modulation by applying opposite signals produced by sweep generator to two arms of intensity modulator using 180 degree hybrid. The career components were suppressed by more than 18 dB. After modulation two sidebands appeared which were used as two individual signals for degenerated FWM. In order to compensate modulation losses and increase the power high enough for efficient conversion, sidebands power was raised up to +10 dBm using EDFA. After amplification modulated light was passed through a nonlinear medium, we have used 20 km dispersion shifted fiber (DSF) with 1549 nm as zero dispersion wavelength for non-linear media which is same as wavelength of laser source. After

degenerated FWM conversion the two sidebands power was around +4 dBm and FWM signal power was around -12 dBm. The other end of DSF fiber was connected with an optical bandpass filter where one of the FWM signal was extracted to be used as OFDR signal. A 25 GHz channel spacing optical bandpass filter was used with 5 dB insertion loss and 3 dB bandwidth was 17.5 GHz. The FWM signal extracted from optical bandpass filter had power around -17 dBm. In order to boost the FWM signal power it was amplified using EDFA which was followed by another optical band pass filter to reduce ASE noises. Later, amplified FWM signal was divided into two arms by an optical coupler. One of the arm signal was kept as reference signal, while other arm signal was sent through FUT as a probe signal. The backscattered light from the FUT and reference signal were combined through an optical coupler and detected by a balance photo detector. Then detected signals were converted into digital format by a 16 bit A/D converter. The OFDR measured trace was analyzed in the computer, the fresnel peak width was measured with normal sweep and with sweep through proposed method and both results were compared.

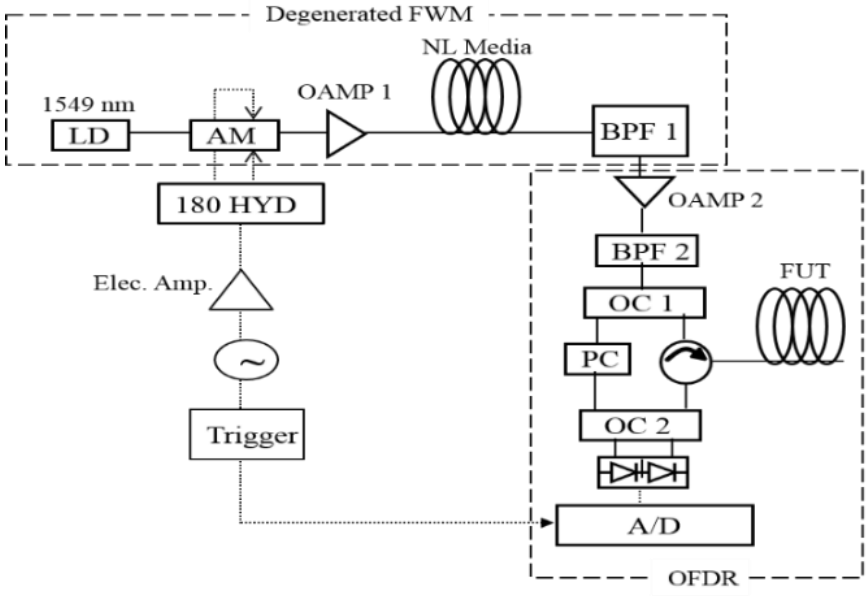

Figure 4.3 Experimental setup for ordinary OFDR

4.3.2 DSB-PNC OFDR

This experiment was conducted to show proposed method can be further used to cancel the laser phase noise with three times increased sweep span, (setup in fig. 4.4). The frequency broadening method for this experiment is same as that for ordinary OFDR. Only instead of filtering out single FWM signal in this experiment two FWM signals at opposite frequency from the center frequency were filtered out. Later,

filtered FWM signals were coupled together in an optical coupler and amplified using EDFA, followed by bandpass filter to reduce ASE noises. After amplification the coupled signal was divided into two arms as reference and probe arms. The backscattered signal from FUT was further divided into two arms using an optical coupler. Two FWM signals in reference arm signal were separated using another optical filter as high and low frequency signals. Later high frequency reference signal was combined with one of the backscattered signal arm and detected in balance photo detector. Similarly, low frequency reference signal was combined with remaining backscattered light arm and detected in another balance photo detector. Both detected signals were converted into digital format using 16 bit A/D convertor and passed through low pass filter. Finally, multiplication of two detected signals canceled out the phase noise. The obtained results were analyzed and the width of peak detected by proposed method sweep was compared with normal sweep.

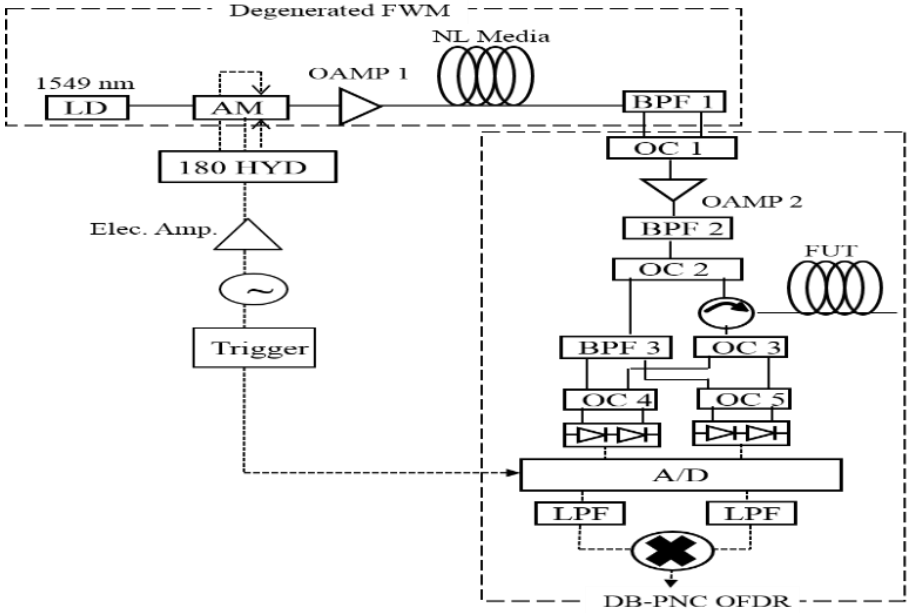

Figure 4.4 Experimental setup for DSB-PNC OFDR

4.4 Frequency sweep span broadening experimental results

For two experiments described in the above section the sweep span selected was 1 GHz (10 GHz to 11 GHz) and 400 MHz (10 GHz to 10.4 GHz) which corresponds to around 10 cm and 25 cm spatial resolution respectively, calculated by Eq. (1). Fig. 4.5 (a) shows the DSB-SC modulation in which two side bands are created and applied sweep moves them in opposite direction. FWM spectrum was checked at starting and stopping sweep frequency. The 4 GHz change in sweep frequency resulted in each side band to move

around 0.03 nm in wavelength as it can be seen in fig. 4.5 (b) where modulation frequency is 10 GHz and 5 (c) where modulation frequency is changed to 14 GHz. While the FWM signal was moved around 0.1 nm in wavelength with 4 GHz sweep change which is equal to around 12 GHz change in frequency again it can be seen in fig. 4.5 (b) at 10 GHz modulation frequency and 5 (c) at 14 GHz modulation frequency. In fig. 4.5 (d) and (e) two separated FWM signals at frequency 10 GHz and 14 GHz are shown, respectively.

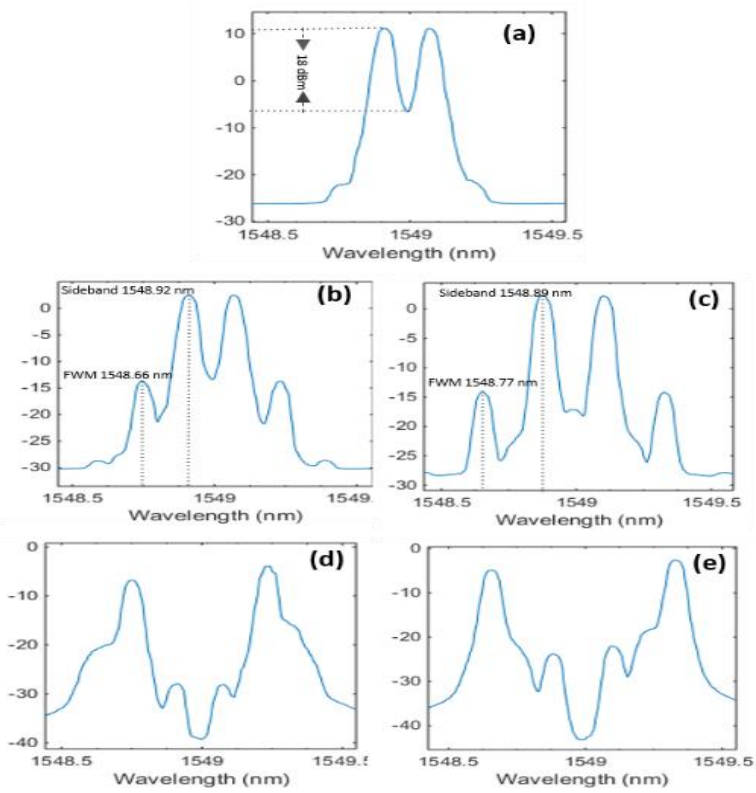

Figure 4.5 (a) DSB-SC Modulation at 1549 nm center frequency; (b) degenerated FWM at modulation frequency 10 GHz; (c) degenerated FWM at modulation frequency 14 GHz, (d) separated FWM signals at 10 GHz, (e) separated FWM signals at 14 GHz

4.4.1 Ordinary OFDR results

In this experiment the sweep time was set at 5 ms which makes the sweep rate 200 GHz with 1 GHz sweep span. The FUT length was around 5 m. The sampling rate selected for this experiment was 20 Msa/s and data points were 510000. The spatial difference between two points was around 1 cm which was calculated by $\Delta l = \frac{cf_s}{4n\beta N}$, where f_s is the sampling frequency of A/D converter, N is the length of data point, n core refractive index and c is the speed of light. Two experiments were conducted one with normal sweep and

the other with proposed method. As it can be seen in fig. 4.6 (a) the measured peak width is 10.3 cm and it matches well with calculated width with 1 GHz sweep. Further, it can be seen in fig. 4.6 (b) the peak width is reduced to 3-times smaller around 3.4 cm with sweep span provided by the means of proposed method and the spatial difference between two points also reduced to 3.3 mm from 1 cm because sweep rate was increased up to 3-times. A clear difference in peak width can also be seen in fig. 4.6 (c) where both results are superimposed in logarithmic scale.

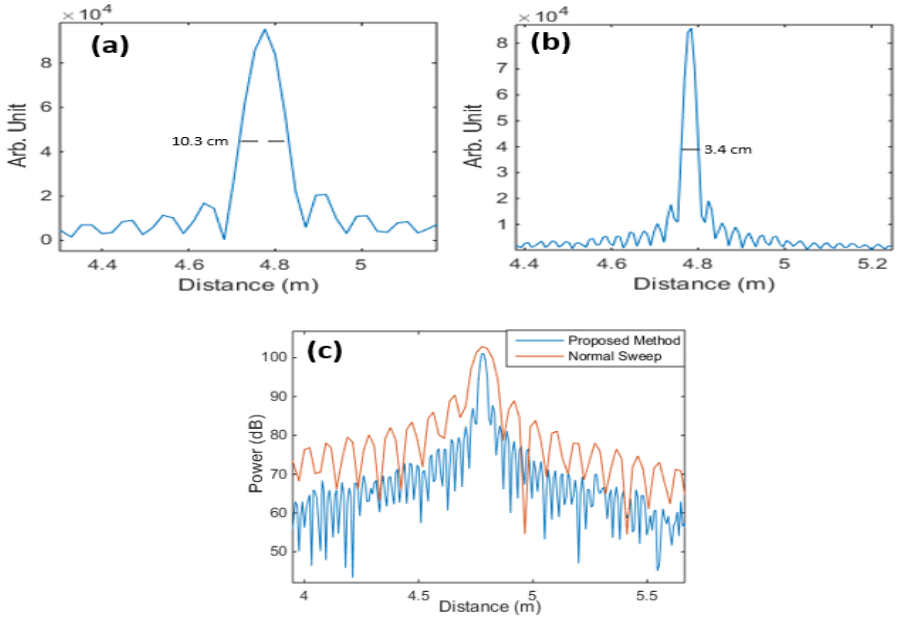

Figure 4.6 Ordinary OFDR results; (a) Normal sweep with 1 GHz sweep span; (b) proposed method sweep with 1 GHz sweep span equivalent to 3 GHz sweep span; (c) two methods superimposed

Furthermore, different sweep span was checked with proposed method varying from 200 MHz up to 5 GHz and measured width was in good agreement with the calculated one, it is shown in fig. 4.7.

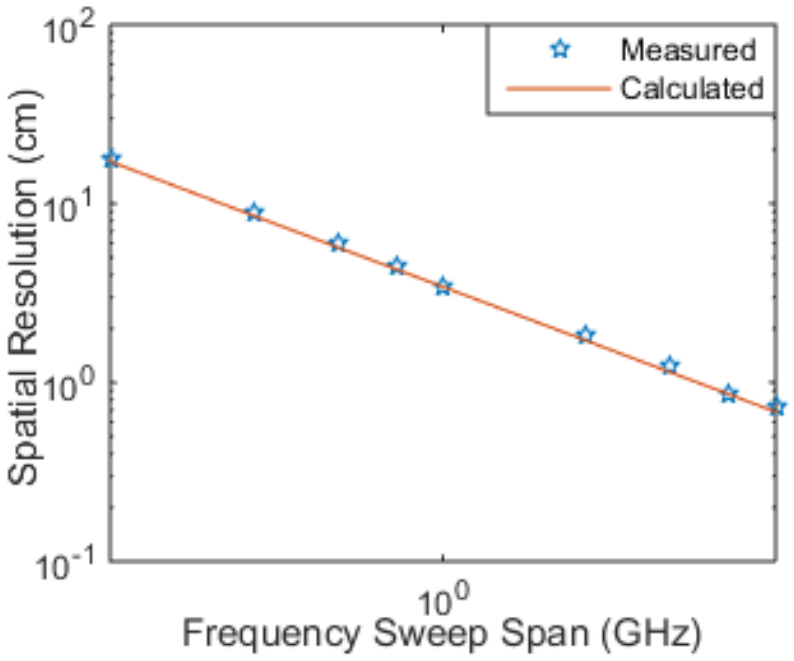

Figure 4.7 Sweep Span vs spatial resolution, calculated spatial resolution and measured spatial resolution as a function of frequency sweep span

4.4.2 DSB-PNC OFDR results

In this experiment a long fiber of length around 10 km is used to show measurement beyond the coherence length. The sweep time was set 10 ms which sets sweep rate of 40 GHz with 400 MHz sweep span. The spatial difference between two points in this experiment was around 10 cm. The sampling speed was 50 Msa/s and number of data points were 650000. Similarly, two experiments were conducted with DSB-PNC OFDR one with normal sweep and one with proposed method. It can be seen in fig. 4.8 the measured width of peak is around 25.2 cm after canceling the laser phase noise with normal sweep, while the peak width was improved to around 8.4 cm when sweep was provided through proposed method. Hence, confirming the proposed method can be used in DSB-PNC OFDR as well to improve the spatial resolution. Longer fiber measurement could have been possible but photo detectors used in the experiment were low bandwidth detectors around 10 MHz.

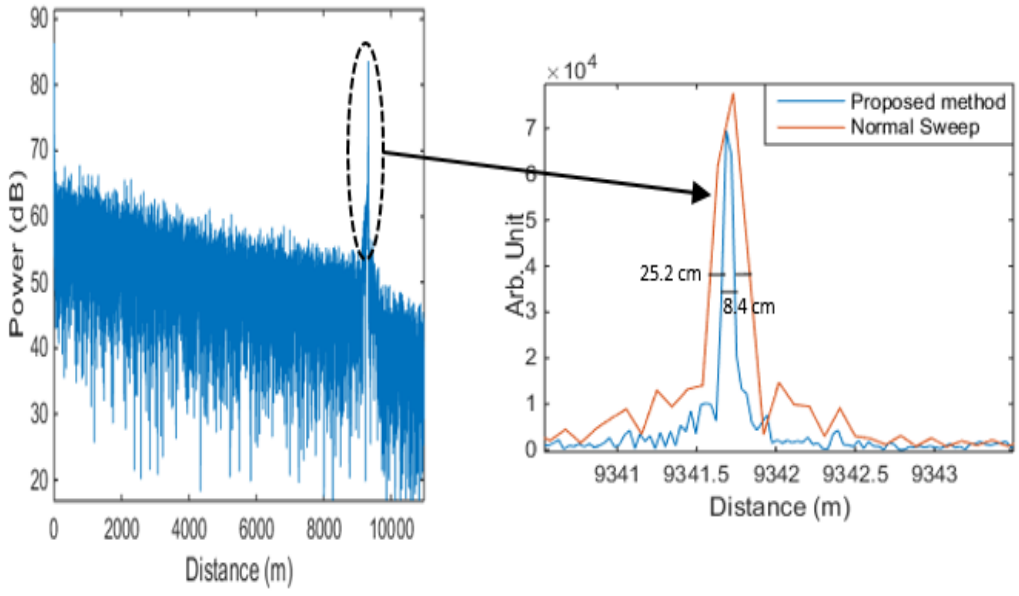

Figure 4.8 DSB-PNC OFDR with sweep by proposed method and normal sweep

4.5 Discussion for frequency sweep span broadening method

Since in the proposed method the frequency is continuously swept therefore two signals are not static in the frequency, which can induce the phase mismatching and changes the FWM conversion efficiency with respect to frequency sweep. The FWM conversion efficiency of proposed method is discussed. The conversion efficiency in FWM depends on various factors, as given below

$$\eta = \frac{\alpha^2}{\alpha^2+(\Delta\beta)^2}\left[1+\frac{4e^{-\alpha L}sin^2(\Delta\beta/2)}{\{1-e^{-\alpha L}\}^2}\right] \quad (12)$$

here α is fiber loss, L is the length of fiber and $\Delta\beta$ is the phase mismatch. The phase matching condition is called satisfied when $\Delta\beta = 0$, in this situation efficiency η takes the maximum value. In degenerated FWM case where only single pump is used, the $\Delta\beta = 0$ condition is satisfied by coinciding the pump frequency with zero dispersion frequency of the nonlinear medium. Usually in FWM if the pump frequency is moved away from the zero dispersion frequency the phase mismatch is introduced and efficiency drops down [14], the rate of drop in efficiency also depends on the separation between two signals [14, 15]. Since in proposed method both FWM signal (FWM and FWM') are used, therefore it is important that amplitude of two FWM signals should be same $|E_{FWM}| = |E_{FWM'}|$. Amplitude of generated FWM signals depends upon the efficiency and same amplitude can be achieved if $\eta_{FWM} = \eta_{FWM'}$. Again efficiency of two FWM signals will be same if both signal experience equal phase mismatch ($|\Delta\beta_{FWM}| =$

$|\Delta\beta_{FWM'}|$). Equal phase mismatch condition can be satisfied if two sidebands created are equally far from the zero dispersion frequency, it can be possible if carrier frequency is matched with zero dispersion frequency ($f_c = f_0$, where f_c carrier frequency, f_0 is zero dispersion frequency) as shown in fig. 4.9. Therefore in proposed method the laser source is modulated at the zero dispersion wavelength which sets two sidebands equally far in opposite direction from the zero dispersion frequency. Signal at $f_c + f_m$ frequency works as a pump for right side FWM signal and signal $f_c - f_m$frequency works as a pump for left side FWM signal (FWM'). When the modulation frequency is changed (swept) the separation from the zero dispersion wavelength of both pumps is increased according to the modulation frequency and the frequency separation between two signals becomes twice of the modulation frequency as two signal are moved in opposite direction. Therefore, the derived phase mismatch equation for the proposed method can be written as below when $f_c = f_0$ [14]

$$\Delta\beta_{FWM} = -\frac{\lambda^2\pi}{c^2}\frac{dD_c}{d\lambda}2\big((f_c + f_m) - (f_c - f_m)\big)^2(f_c + f_m - f_0) = -\frac{\lambda^2\pi}{c^2}\frac{dD_c}{d\lambda}2(2f_m)^2(f_m) \quad (13)$$

$$\Delta\beta_{FWM'} = -\frac{\lambda^2\pi}{c^2}\frac{dD_c}{d\lambda}2\big((f_c - f_m) - (f_c + f_m)\big)^2(f_c - f_m - f_0) = \frac{\lambda^2\pi}{c^2}\frac{dD_c}{d\lambda}2(2f_m)^2(f_m) \quad (14)$$

In above equation, $\frac{dD_c}{d\lambda}$ is the dispersion slope and f_m is the modulation frequency, the separation between two signals is $2f_m$ and the frequency difference between pump and zero dispersion frequency is f_m. As the f_m is increased the separation between two signals and difference between zero dispersion and pump frequency increases as a result the phase mismatch increases and efficiency drops down. From Eq. (13) and (14) it can be seen the phase mismatch for both FWM signals has same absolute value, therefore efficiencies of two FWM signals are same. Assuming the experimental conditions presented in this paper such as 20 km DSF fiber with dispersion slope 0.07 $ps/km.nm^2$, fiber loss 0.2 dB/km and changing the modulation frequency from 1 GHz to 1000 GHz, the phase mismatch was simulated as shown in fig. 4.10. The results show FWM efficiency dropped to 0.95 around 80 GHz. Another study shows that the phase matched bandwidth is broader if short length fiber is deployed [14, 15], in order to increase phase matched bandwidth a comparison was carried out with a short length highly nonlinear fiber (HNL). Assuming HNL fiber with fiber loss 1.53 dB/km, affective fiber length 2.8 km and dispersion slope 0.013 $ps/km.nm^2$ [10], the simulated efficiency dropped to 0.95 around 270 GHz as shown in fig. 4.10. Therefore, in proposed method phase match can be extended to broader bandwidth if short length HNL fiber is used and it is also desirable to start sweep from low frequency so that phase matched condition can be realized up to broader frequency range.

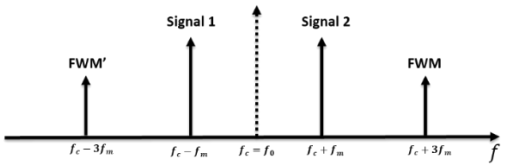

Figure 4.9 Frequency relationship of signals and zero dispersion wavelength

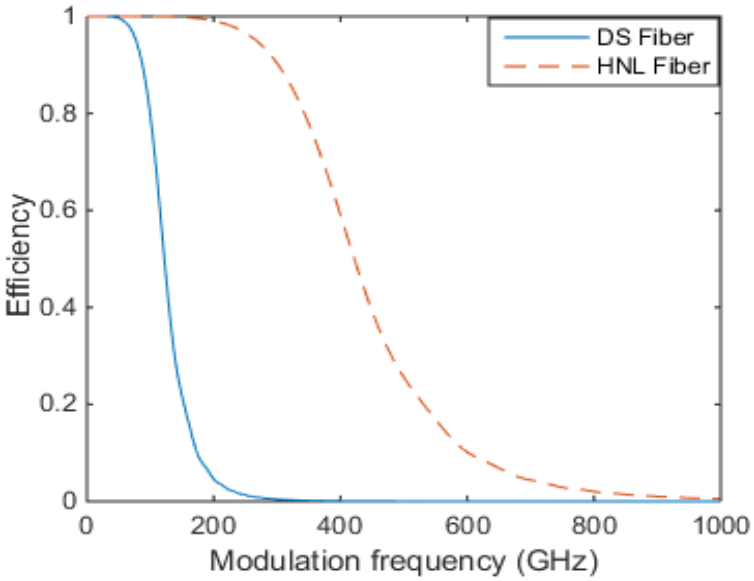

Figure 4.10 Efficiency vs modulation frequency, 20 km DSF (solid line) and 2.8 km HNL fiber (dashed line).

The normal sweep span can be described as $\Delta F = f_{start} - f_{stope}$, while using proposed method the applied sweep span is extended as $\Delta F = 3f_{start} - 3f_{stope}$. Since proposed method is based on FWM and a bandpass optical filter is used to separate FWM signal to be used as OFDR signal. The FWM signal is separated well if the channel spacing of the filter matches with the frequency separation between FWM signal and sidebands. As the frequency is swept linearly with time, therefore there is possibility that sideband frequency and FWM signal frequency range can overlap during frequency sweep in such a condition it becomes difficult to separate FWM from the sidebands. Such a condition can be possible if f_{stope} frequency is more than 3 times of f_{start}, for example if the sweep span is selected from 5-20 GHz, the FWM signal sweep will be equal to 15-60 GHz in such a situation at least 5 GHz of frequency portion of FWM signal will be overlapped with one sideband. Even though the frequency span is selected in a way that f_{stope} is slightly less or equal to 3 times of the f_{start} still separating FWM signal from the sidebands

would be not easy as practically the frequency response of filters is not quite sharp. There has to be enough separation between FWM signal frequency span and sidebands frequency span in order to separate FWM signal throughout the sweep. The possible solution for this problem could be to use a tunable optical filter which is linearly tuned in time with the same speed as that of the sweep rate. In doing so FWM signal can be separated from the sidebands throughout the sweep. There are various kinds of tunable optical filters available, usually sweep time in OFDR is order of milliseconds or less, therefore selecting a tunable filter with high speed is important. High speed tunable optical filters have been demonstrated with tuning range as large as 16 nm and wavelength switching time in nanoseconds [16].

4.6 Format free optical wavelength conversion

An overwhelming increase in demands of telecommunication services in the form of internet and high speed mobile networks, made wavelength division multiplexing (WDM) an indispensable need to fulfil demands of high speed networks. Effective utilization of optical fiber bandwidth is one of the attribute of WDM networks, and wavelength conversions are very important in order to use wavelength resource efficiently. There are many wavelength conversion methods, which can be mainly categorized in optoelectronic (O/E-E/O), optical gating and four wave mixing (FWM) methods [17, 18]. The optical gating contains large number of wavelength conversion methods e.g. semiconductor optical amplifier cross-gain modulation, semiconductor optical amplifier with cross-phase modulation, semiconductor lasers with saturable absorption. [18]. FWM exploits the nonlinear nature of the medium to convert signal wavelength. Although it is a simple and useful method, however spectrum inversion in this technique imposes limitation of signal format usability. Recently, some methods to eliminate the spectrum inversion has been demonstrated such as two stages of FWM [3] and dual pump FWM [19].

Format independency in the network has become more essential as recent optical networks work over vast variety of optical formats e.g. intensity modulation direct detection (IM-DD), dual-polarization differential quadrature phase shift keying (DP-DQPSK), quadrature amplitude modulation (QAM), quadrature phase shift keying (QPSK), and orthogonal frequency multiplexing (OFDM). Optical single side-band (OSSB) offers format independent wavelength conversion and capable of realizing appropriate wavelength conversion without increased phase noise [20, 21], while in FWM the phase noise is three times higher than OSSB method because three sources are used in FWM (two pump and one signal). A new method was proposed to convert optical wavelength using optical single side band modulator (OSSB) and array wave guide grating (AWG) and demonstrated the feasibility with IM-DD format [21].

In this part of the research, format independency of the proposed method has been demonstrated experimentally, the proposed idea to increase sweep span broadening in OFDR was inspired by the demonstration presented in this research.

4.7 Format free wavelength conversion principle

The proposed method to convert wavelength, is mainly comprised of an OSSB modulator and an AWG as shown in fig. 4.11. The OSSB and the AWG are connected through a closed loop, which is created by connecting "k" port of the AWG to a circulator, furthermore the circulator was connected to the input and the output of the OSSB. When the signal of wavelength "λ_i" is provided into "i" port of the AWG, the signal is transferred to the "k" port of the AWG, which is followed by the OSSB via the closed loop. The modulation frequency of the OSSB modulator is equivalent to the AWG channel spacing and signal going through OSSB modulator experiences the wavelength conversion equal to modulation frequency and wavelength shifts to"$\lambda_{i+1}\ or\ \lambda_{i-1}$" depending on the wavelength conversion direction (up-or down-conversion). The wavelength converted signal is then incident into the "k" port of the AWG through the circulator, which is appeared at the adjacent port (left or right) "$i+1\ or\ i-1$" of the input signal. If converted signal requires more conversion, then the signal is reflected back into the same port of the AWG using a mirror and signal is again transferred at the "k" port of AWG and same procedure is repeated once again. The wavelength conversion of the input signal is carried out again and again by passing the signal through OSSB modulator, until desired wavelength converted signal is achieved. Once the wavelength of the signal becomes required wavelength "λ_j", the wavelength converted signal is obtained from "j" port of the AWG and detected. The proposed method can convert wavelength up to required amount by using mirrors and furthermore up and down wavelength conversion is also possible by controlling the bias voltage of OSSB and selecting the appropriate side band.

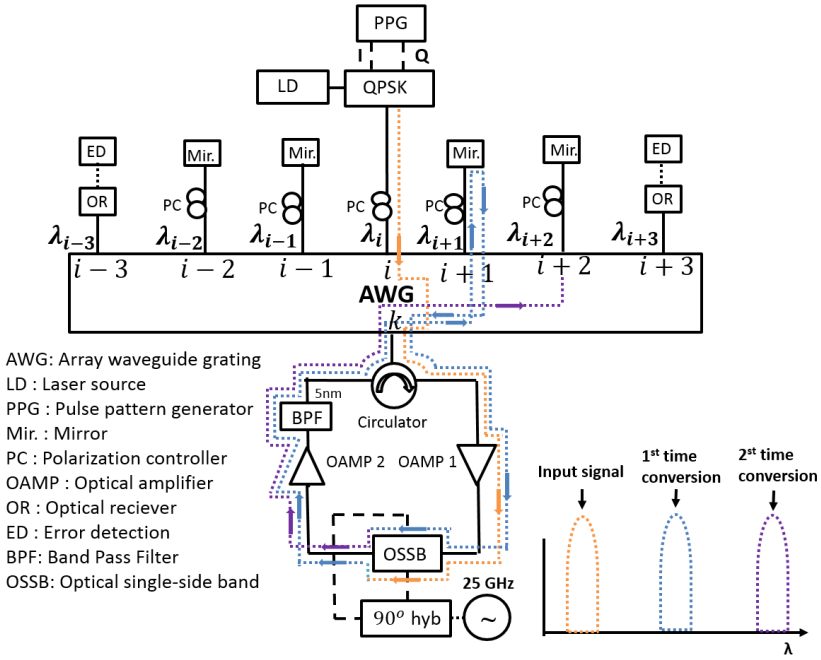

Figure 4.11 Experimental setup

Here if the input phase modulated optical signal is described as

$$E_{in}(t)=A(t)\, e^{j(\omega_c t+\varphi(t))} \tag{15}$$

where A is the amplitude, ω_c is the optical carrier frequency, and φ is the phase of the signal. Then, OSSB wavelength converted signal can be expressed as

$$E_{OSSB}(t) \propto J_1(m)A(t)e^{j[(\omega_c \pm n\omega_m)t+\varphi(t)]} \tag{16}$$

where $J_1(m)$ is the Bessel function of the first kind of order one , m is the modulation index, n is number of conversions, and ω_m is the modulating frequency. The total amount of frequency conversion can be controlled by number of conversions.

On the other hand, FWM scheme converts the wavelength of the signal by mixing pump and signal waves, and nonlinear response of the medium results in generation of another wave with preserved amplitude and phase of interacting waves [17].

The FWM scheme can be expressed as

$$E_{ijk}=E_iE_jE_k* \tag{17}$$

where E_{ijk} is FWM produced optical signal, E_i ,E_j, and E_k are input optical fields for nonlinear media and * denotes complex conjugate. The converted optical angular frequency has the following relation [18]

$$\omega_{ijk} = \omega_i + \omega_j - \omega_k$$

where $\omega_{ijk}, \omega_i, \omega_j, and\ \omega_k$ are the angular frequencies of each signal. For the broad range wavelength conversion, E_i and E_j are degenerated (E_i=E_j) and its wavelength is set at zero dispersion wavelength of the nonlinear medium to realize phase matching condition. The FWM converted signal can be described with the input signal E_{in}(t)

$$E_{ijk}(t) = A\left|E_p\right|^2 e^{j\{(2\omega_p - \omega_c)t - \varphi(t)\}} \quad (18)$$

where E_p is the degenerated optical field with the frequency ω_p .

It can be seen that the signal frequency is changed but with inverted phase. This spectrum inversion doesn't affect IM-DD, BPSK signals, while the advanced modulation/demodulation schemes, such as QPSK, OFDM, and QAM can be affected. Comparison of two methods, OSSB and FWM, in terms of spectrum inversion is depicted in fig. 4.12. It can be seen FWM wavelength converted signal gets inverted as shown in fig. 4.12 (a), while signal converted by OSSB method has same spectrum in up-and down conversion of the signal frequency as shown in fig. 4.12 (b). Spectrum inversion effect on constellation for QPSK case can be seen in fig. 4.13. In this case, the phase of signal is inverted, that is π/4, 3π/4, -3π/4, -π/4 to -π/4, -3π/4, 3π/4, π/4, respectively. Spectral inversion did not affect I signal but Q signal got affected and bits corresponding to Q signal were transposed.

Spectrum inversion problem can be solved by encoding input signal with differential code. However, it needs a decoder at the destination end and the performance can be degraded.

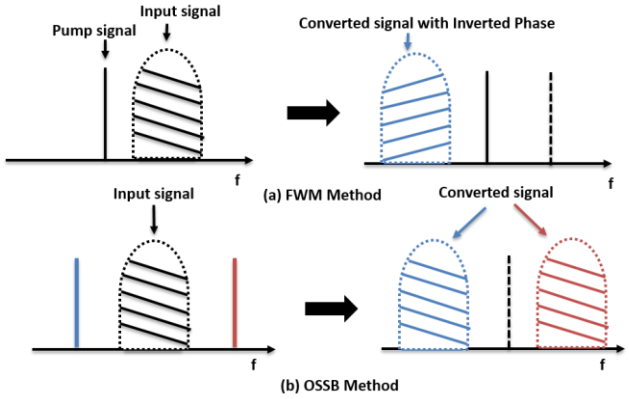

Figure 4.12 Spectra comparison of wavelength converted signal by (a) OSSB method (b) FWM method

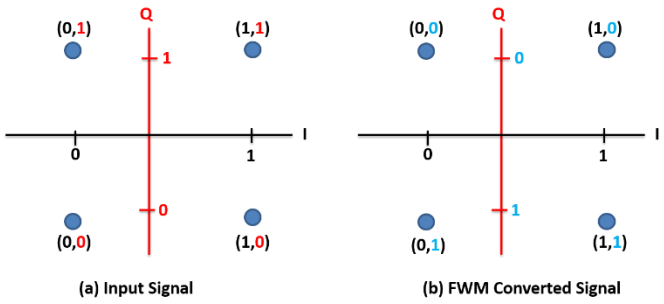

Figure 4.13 Spectrum Inversion Phenomenon (a) input QPSK modulated signal (b) FWM wavelength converted QPSK modulated signal

Previously IM-DD optical format was converted using proposed method [20]. In this research, to show proposed method is independent of format, a QPSK formatted signal is used to convert the wavelength and successful wavelength conversion up to 75 GHz is demonstrated. Moreover, obtained results are compared with FWM wavelength conversion method to verify spectrum inversion does not occur in proposed scheme.

4.8 Format free wavelength conversion experimental results

An AWG with 25 GHz (0.2 nm) channel spacing was used. The 3 dB and 1 dB bandwidth of the AWG was 17.5 GHz and 10 GHz respectively and insertion loss was 5.5 dB. The input light was incident into "i" port of the AWG and output signal after 75 GHz conversion was taken from port "$i+3$" and port "$i-3$" for up-and down-converted signals, respectively.

The modulation frequency for OSSB modulator was set equivalent to the channel spacing of the AWG, which was 25 GHz. The frequency conversion efficiency was 25 dB, and unwanted side-band suppression ratio was more than 28 dB. The 3 dB optical bandwidth of OSSB modulator was more than 12 GHz and V_π was 4 V, the input power measured at k port of AWG was around -10 dBm and every time converted signal power in AWG was around 0 dBm measured at port $i+1$ to $i+3$ and $i-1$ to $i-3$, as shown in fig. 4. The optical signal of input power around +7 dBm was QPSK modulated at 10 Gbps (5 Gsymbol/s) PRBS (pseudorandom binary sequence) and placed in OSSB as input signal via AWG and circulator. The modulated signal was incident into "i" port of the AWG, which was transferred to the "k" port of AWG and connected to a circulator. Then signal from circulator was amplified using optical amplifier and input to the OSSB. The output signal from OSSB was amplified before connecting to the AWG via circulator. In order to compensate insertion losses of AWG and OSSB modulator, the signal was amplified before and after the OSSB. Moreover, a band pass filter (BPF) with pass band range 5 nm was inserted at the output of OSSB to reduce ASE noise from amplifiers and to pass all signals. The output signal of OSSB

was sent to AWG via circulator appeared at adjacent port "$i+1\ or\ i-1$" (up or down wavelength conversion) of the original signal in AWG. The wavelength converted signal was then reflected back by the means of mirror for further conversion and next time the converted signal appeared at "$i+2\ or\ i-2$". This procedure was repeated two times up to 75 GHz conversion. The final wavelength converted signal was obtained from "$i+3\ or\ i-3$"port of the AWG. The wavelength converted signals were detected with heterodyne detection with 7.5 GHz as intermediate frequency. The detected signal were sampled at 40 Gsa/s with 400k number of points and demodulated, and subsequently constellation, eye diagram, and bit error rate was measured. In heterodyne detection, signal wavelength was kept higher than the local wavelength.

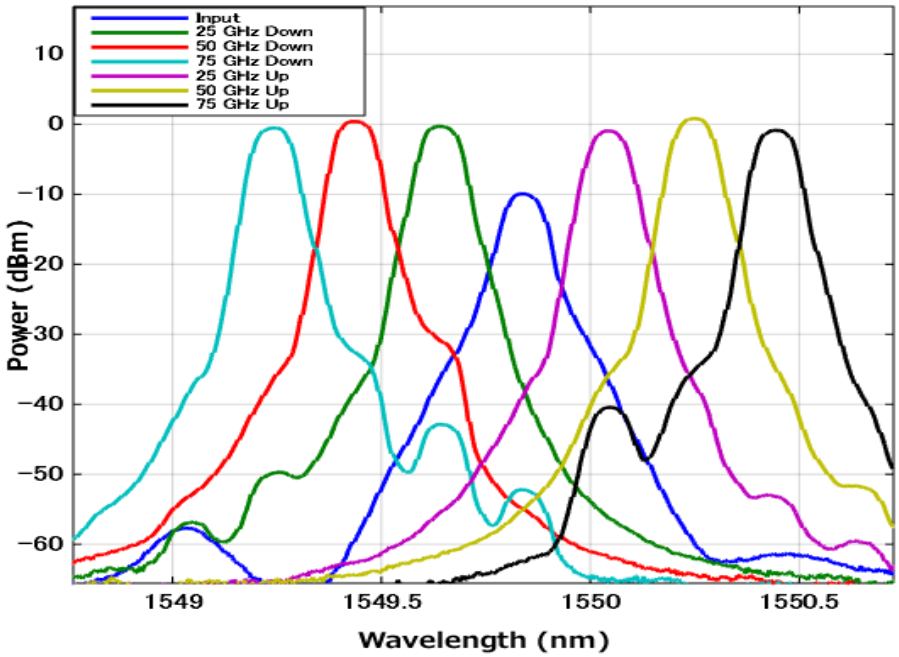

Figure 4.14 Input and converted wavelength spectra's

The experimentally obtained wavelength converted spectra are shown in fig. 4.14. The input wavelength was converted to both sides (up-and down-conversion). Error free (BER $<10^{-5}$ for 50k symbols) wavelength converted signal up to 75 GHz, up and down conversion was achieved. The eye diagram and constellation of 75 GHz converted signal is shown in fig. 4.15.

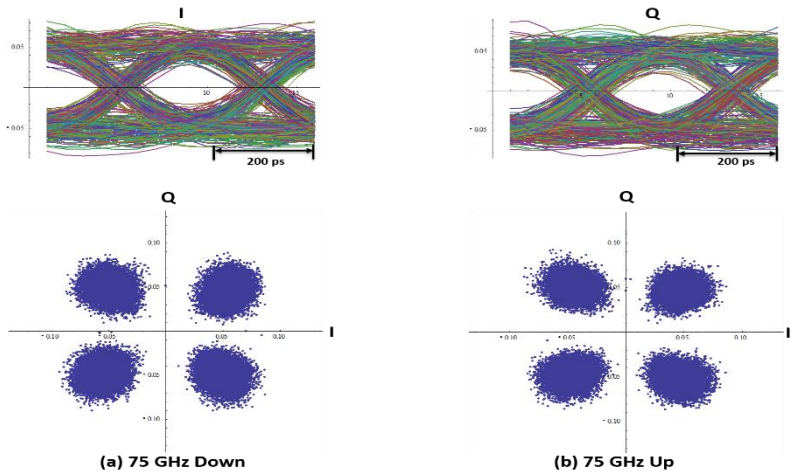

Figure 4.15 Eye diagram and constellation 75 GHz conversion (a) down conversion (b) up conversion

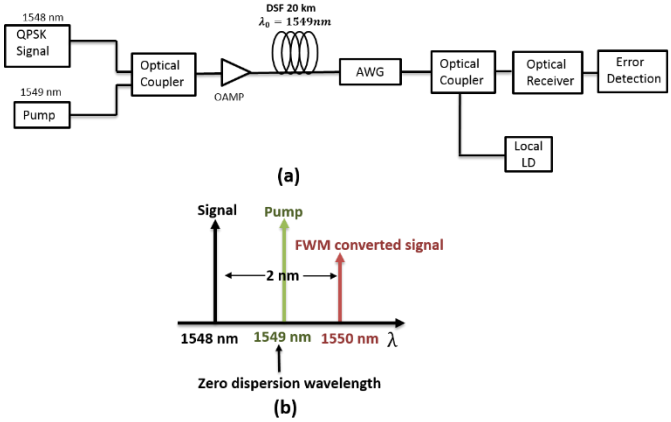

Figure 4.16 (a) FWM experimental setup (b) FWM wavelength relationship

To confirm that the spectral inversion does not occur in proposed method of wavelength conversion, patterns of demodulated I and Q signals were compared with FWM method. Wavelength of QPSK modulated signal was converted by FWM method (setup shown in fig. 4.16 (a)), wavelength for signal was set at 1548 nm and pump was set at 1549 nm for the nonlinear media, a 20 km long fiber with 1549 nm zero dispersion wavelength was used as a non-linear medium, which resulted in 2 nm wavelength conversion and converted signal had 1550 nm wavelength, wavelength relationship can be seen in fig. 4.16 (b). The FWM wavelength converted signal was detected with the heterodyne detection, which was the same with OSSB case (signal wavelength was set higher than the local wavelength). Detected FWM wavelength converted signal was demodulated and measured error rate was very high (BER=0.5) because of spectrum inversion. Patterns of demodulated I and Q signals of OSSB and FWM methods were

compared with input signal in fig. 4.17. It can be seen waveform of Q signal of FWM method went through inversion, while converted signal by the means of proposed method had the same pattern as the input.

In order to confirm the spectrum inversion, by opposing the order of signal and local in heterodyne detection (local wavelength was set higher than the signal wavelength), it inverts the spectrum for one more time and signal become error free.

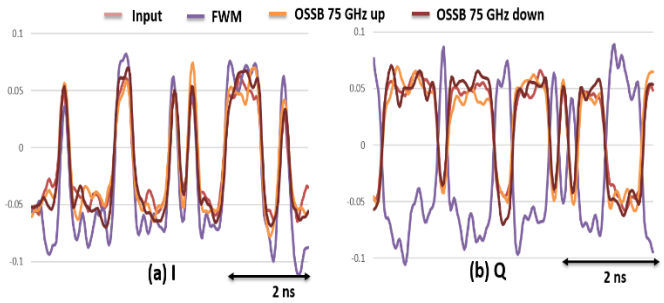

Figure 4.17 Waveform comparison (a) I signal (b) Q signal

In order to convert large amount of wavelength using proposed scheme it is desired to use high frequency optical modulator with high modulation frequency and an optical filter of channel spacing equivalent to modulation frequency. In doing so each time in the loop amount of wavelength conversion would be higher and desired conversion can be acquired with a few number of rounds in the loop. If the modulation frequency is kept low for large amount of wavelength conversion, it will require many rounds in the loop before the targeted wavelength conversion could be achieved, however, each time light signal rounding the loop will result in narrowing of bandwidth caused by AWG which will ultimately degrade the waveform. Another factor which can affect the performance is SNR degradation by optical amplifiers in the loop, SNR degradation can be improved by improving the conversion efficiency of OSSB modulator and increasing the allowable input power [21]. Moreover wavelength of other formats can also be converted using proposed scheme such as QAM, it can be understood from wavelength converted signal as described in Eq. (16). Wavelength of polarization multiplexed QAM for high speed can also be converted using proposed scheme if two polarizations are separated and wavelength of each polarization is converted separately, however, the most challenging part would be to recombine two polarization of wavelength converted signal with same phase.

4.9 References

[1] M. froggat and J. Moore, “High-spatial-resolution distributed strain measurement in optical fiber with Rayleigh scatter”, Appl. Opt. **47**, 1735-1740 (1998).

[2] B. J. Soller, D. K. Gifford, > S. Wolfe and M. E. Froggatt, “High resolution optical frequency domain reflectometry for characterization of components and assemblies”, Opt. Exp., **13**, 666-674, (2005).

[3] J. Li, J. Du, S. Wang, L. Li, L Sun, X. Fan, Q. L, Z. He, “Improving the spatial resolution of an OFDR based on recirculating frequency shifter”, Phot. J. **7,** (2015).

[4] J. Li, J. Du, D. Xu, S. Wang, X. Fan, Q. Liu, and Z. He, “Broadened optical frequency sweeping for high spatial resolution OFDR based on recirculating frequency shifter”, in Proc. 20th OECC, Shanghai, (2015).

[5] D. Xu, J Du, X. Fan, Q. Li, and Z. He, “10-times broadened fast optical frequency sweeping for high spatial resolution OFDR”, Proc. OFC (2014).

[6] D. Xu, J Du, X. Fan, Q. Li, and Z. He, “High spatial resolution OFDR based on broadened optical frequency sweeping by four-wave-mixing”, Proc. 23rd OFS (2014).

[7] M. Badar and I. Katsushi, “Phase noise cancelled OFDR with cm-Level Spatial Resolution Using Phase Diversity”, Phot. Tech. Let. , **26**, 858-861, (2014).

[8] S. Hiramatsu and K. Iwashita, “A Novel Phase-Noise Cancelled Optical Frequency Domain Reflectometry Using Modulation Sidebands”, Photon. & optoelectron. , **1**, 60-64, (2012).

[9] J. Du, Lu. Li, X. Fan, Q. Li, and Z. He, “Sensitivity enhancement for fiber Bragg grating sensors by four wave mixing”, Photo. **2,** 426-439, (2015).

[10] S. Petit, T. Kurosu, M. Takahashi, T. Yagi, and S. Namiki, “Low penalty uniformly tunable wavelength conversion without spectral inversion over 30 nm using SBS-suppressed low-dispersion-slope highly nonlinear fibers,” Phot. Tech. Let. **23,** 546-548, (2011).

[11] Y. Koshikiya, X. Fan, and F. Ilto, “40-km range, 1-m resolution measurement based on phase-noise-compensated coherent optical frequency domain reflectometry”, Proc. 34th ECOC, (2008).

[12] X. Fan, Y. Koshikiya, and F. Ito, “Phase-Noise-Compensated Optical Frequency-Domain Reflectometry”, *IEEE J. Quant. Electron.*, **45**,594-602, (2009).

[13] M. Badar, H. Kobayashi, and K. Iwashita, “Chromatic dispersion measurement with double sideband phase noise canceled OFDR*”,* Opt. comm., **356**, 350-355, (2015).

[14] K. Inoue, “Four-wave mixing in an optical fiber in the zero-dispersion wavelength region”, J. Lightwav. Tech., **10**, 1553-1561, 1992.

[15] N. Shibata, R. P. Braun, and G. Waarts,"Phase-mismatch dependence of efficiency of wave generation through four-wave mixing in a single-mode optical fiber", *IEEE J. Quant. Electron.,* **23,** 1205-1210, 1987.

[16] T. Segawa, S. Matsuo, T. Ishii, Y. Ohiso, Y. Shibata, and H. Suzuki, "High-speed wavelength-tunable optical filter using cascaded mach-zehnder interferometers with apodized sampled gratings", *IEEE J. Quant. Electron.,* **44,** 922-930, 2008.

[17] S. J. B. Yoo, "Wavelength Conversion Technologies for WDM Network Applications ", *IEEE J. Lightwave Technol.,* vol. 14, no.6, pp.955-966, 1996.

[18] Byrav Ramamurthy, and Biswanath Mukherjee, "Wavelength conversion in WDM Networking", *IEEE, J. Selected areas Comm*., vol 16, no.7, pp.1061-1073, 1998.

[19] Xinying Li, Jianjun Yu, Ze Dong, and Nan Chi, "Wavelength conversion of 544-Gbit/s dual-carrier PDM-16QAM signal based on the co-polarized dual-pump scheme", *opt. exp*., vol.20, no.19, pp.21324-21330, 2012.

[20] Hiroyuki Mima and Katsushi Iwashita, "A Novel Wavelength Converter Based of Optical Single-sideband Modulator and Array Waveguide Grating", *17th* Opto-electronics and communication (OECC), P1-10, Busan, July 2012.

[21] Hiroyuki Mima and Katsushi Iwashita, "Dual-Channel Simultaneous Wavelength Conversion With OSSB Modulator and AWG", *IEEE Photon. Technol. Lett.,* vol.26, no.14, pp.1462-1465, 2014.

Chapter 5 : Laser Phase Noise Estimation and Cancelation in OFDR

5.1 Introduction

Laser phase noise is an intrinsic phenomenon which is mainly caused by optical phase fluctuation because of spontaneous emission of the gain medium. Ideally the spectral width of a laser source should be very small some fraction of Hz but because of phase noise this is always not the case and linewidth of laser is much broader. The phase fluctuations (phase noise) in laser has been studied from long time [1, 2] and its effect on the laser line shape and, thus, the linewidth [3, 4]. Correct laser linewidth information which can be obtained from the laser phase noise is essential in many laser applications i.e. interferometric application of laser. This laser phase noise is the very same reason restricting the measurable distance in OFDR and for which a new method to cancel the laser phase noise in OFDR was proposed in this research. In this part of the thesis a new method to estimate the laser noise is proposed. The proposed method to estimate laser phase noise is actually extension of DSB-PNC OFDR with some extra signal processing involved. Since, in DSB-PNC OFDR two detected channels had equal but opposite laser phase noise, therefore if we estimate the phase of each channel and subtract them, in doing so the same beat frequency term present in each channel will be canceled out and the remaining term will be purely the laser phase noise. There could be a few main applications of this estimated phase noise such as it can be used to measure the laser linewidth and other application could be laser phase noise cancelation in OFDR with some extra advantages as compare the conventional way of canceling the phase noise by multiplying two channels. The experimental configuration of phase noise estimation is same to that of DSB-PNC OFDR with heterodyne detection only extra signal processing is used to estimate the phase of each channel and estimate the laser phase noise, configuration is shown in fig. 5.1.

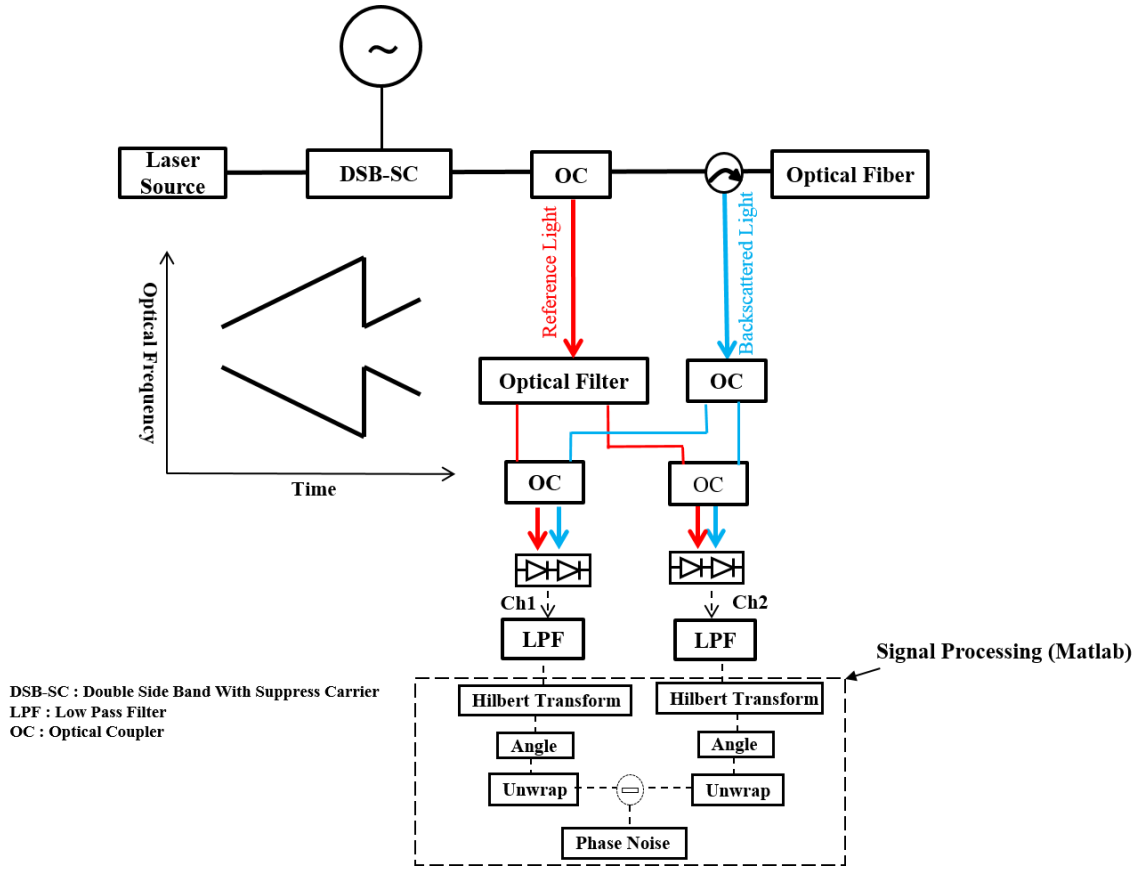

Figure 5.1 Laser phase noise estimation configuration

5.2 Laser phase noise estimation principle

As discussed earlier the experimental configuration is exactly same as for DSB-PNC OFDR using heterodyne detection, therefore two obtained channels photocurrent would be same as described in heterodyne detection, given below

$$I_h(t) \propto \cos(2\pi\beta\tau_{FUT}t + \theta(t) - \theta(t-\tau_{FUT}) + \omega_+\tau_{FUT} - \pi\beta{\tau_{FUT}}^2) \quad (1)$$

$$I_l(t) \propto \cos(2\pi\beta\tau_{FUT}t - \{\theta(t) - \theta(t-\tau_{FUT})\} - \omega_-\tau_{FUT} - \pi\beta{\tau_{FUT}}^2) \quad (2)$$

where $\omega_+, \omega_-, \omega_c$, ω_m, β and $\theta(t)$ are same as described in theory of DSB-PNC OFDR. The instantaneous phase of two detected channels were obtained by converting into analytical form. The Hilbert transform of Eq. (1) and (2) provided the imaginary part ($I_h{}^*(t)$ *and* $I_l{}^*(t)$) for the complex form [5, 6, 7]

$$I_h{}^*(t) = H\{I_h(t)\} = \sin(2\pi\beta\tau_{FUT}t + \theta(t) - \theta(t-\tau_{FUT}) + \omega_+\tau_{FUT} - \pi\beta{\tau_{FUT}}^2) \quad (3)$$

And complex form $Z_h(t)$ becomes

$$Z_h(t) = I_h(t) + iI_h{}^*(t) = e^{i(2\pi\beta\tau_{FUT}t + \theta(t) - \theta(t-\tau_{FUT}) + \omega_+\tau_{FUT} - \pi\beta\tau_{FUT}{}^2)} = e^{i\emptyset_h} \quad (4)$$

Once complex form is obtained, instantaneous phase can be found by

$$\emptyset_h = \arctan\left[\frac{I_h{}^*(t)}{I_h(t)}\right] = 2\pi\beta\tau_{FUT}t + \theta(t) - \theta(t-\tau_{FUT}) + \omega_+\tau_{FUT} - \pi\beta\tau_{FUT}{}^2) \quad (5)$$

Similarly for lower frequency channel

$$\emptyset_l = \arctan\left[\frac{I_l{}^*(t)}{I_l(t)}\right] = 2\pi\beta\tau_{FUT}t - \{\theta(t) - \theta(t-\tau_{FUT})\} - \omega_-\tau_{FUT} - \pi\beta\tau_{FUT}{}^2) \quad (6)$$

Where $\emptyset_h$ and $\emptyset_l$ represent instantaneous phases of higher frequency and lower frequency channels respectively. As it can be seen from Eq. (7) and (8) two estimated phases have same beat frequency terms and equal but opposite phase noise terms, therefore on subtracting two phases from each other cancelled out frequency terms and remaining is purely twice of the laser phase noise, which can be divided by two to cancel the double effect, described as

$$\frac{\emptyset_l - \emptyset_h}{2} \propto (-\theta(t) + \theta(t-\tau_{FUT}) - \omega_c\tau_{FUT}) \quad (7)$$

Where $\omega_c t$ is a constant term and it can be ignored. The above derived is purely laser phase noise. The relative phase or phase difference of $I_h(t)$ and $I_l(t)$ can also be obtained directly by [x]

$$\emptyset_l - \emptyset_h \propto \arctan\left[\frac{I_l{}^*(t)I_h(t) - I_l(t)I_h{}^*(t)}{I_l(t)I_h(t) + I_l{}^*(t)I_h{}^*(t)}\right] \quad (8)$$

We can use estimated phase noise to cancel the laser phase noise in OFDR by multiplying Eq. (6) by Eq. (9)

$$Z_h(t) = e^{i\emptyset_h} * e^{i\left(\frac{\emptyset_l - \emptyset_h}{2}\right)} \propto e^{i(2\pi\beta\tau_{FUT}t + \omega_m\tau_{FUT} - \pi\beta\tau_{FUT}{}^2)} \quad (9)$$

As can be seen from above equation phase noise term has been cancelled out and only remaining term is the beat frequency and other terms are constants. In this paper phase noise cancellation principle described was same as in previously proposed methods [8, 9] but employed technique for phase noise cancellation is new. Previously two channels were directly multiplied (Eq. (3) and (4)). The multiplication process converted the beat frequency to twice of the original beat frequency, because of doubled beat frequency the minimum required sampling rate was also twice and minimum four times of the original beat frequency in order to fulfil Nyqusit rate requirement. Higher sampling rate required high speed ADC and additional noises because of high sampling rate were not favorable for overall results. Moreover higher sampling rate

requirement degrades the spatial resolution between two points as is calculated by $\Delta l = \frac{c f_s}{4n\beta N}$, where f_s is the sampling frequency of A/D converter and N is the length of data point. The phase noise cancellation using estimated phase noise gives the beat frequency same as original, hence eliminate requirement of higher sampling rate.

Phase noise estimation method was checked using simulation, shown in fig. 5.2. Two channels like Eq. (3) and (4) were assumed and theoretically generated phase noise was introduced, the sweep rate set was 1000 GHz and instantaneous phase of each channel was estimated as described in Eq. (7) and (8). The relative difference of two extracted phases provided estimated laser phase noise as in Eq. (9) and comparison with the applied phase noise was in a good agreement.

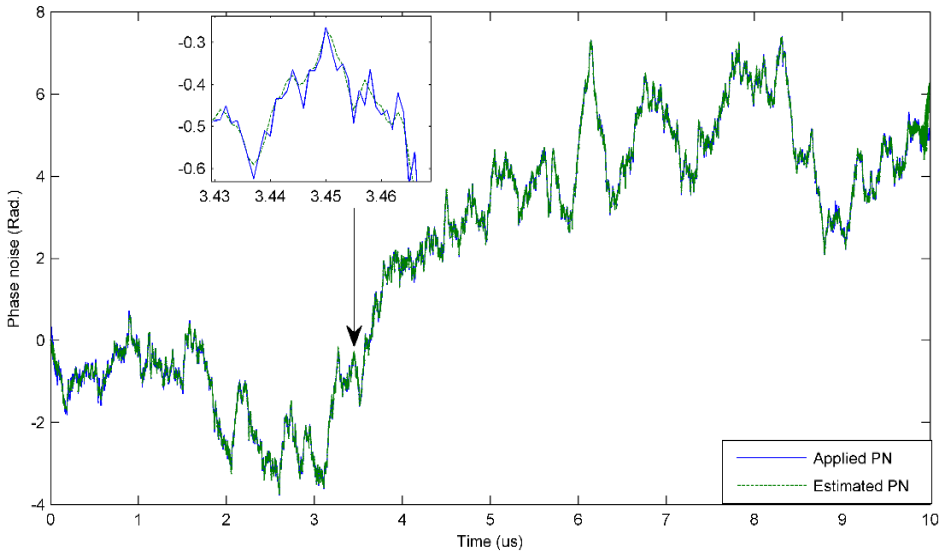

Figure 5.2 Theoretically generated phase noise (blue) and estimated phase noise (green)

5.3 Phase noise estimation experimental results

Since proposed method to estimate laser phase noise is based on DSB-PNC OFDR, therefore DSB-SC modulation and its treatment is same as mentioned in the heterodyne detection technique. The proposed scheme of laser phase noise estimation was verified with experiment. The photocurrent of two channels was detected in the experiment which was converted into digital format using 16 bit A/D converter. The obtained data of two channels was saved into computer for further processing. The instantaneous phase of each channel data was estimated using Hilbert transformation same as shown in the configuration. The recovered phase was confined between π and $-\pi$, an unwrapping process was needed to remove the

discontinuities and retrieve continues phase. Estimated phase noise was the relative phase of two detected signals as shown in Eq. (7). The accuracy of the estimated phase noise was confirmed with cancelation of the phase noise in OFDR using the estimated laser phase noise.

4.3.1 Laser phase noise estimation

The digital data generated from photocurrent of each channel was brought into computer for further signal processing. Phase information of each channel was obtained by taking their Hilbert transform. Since two channels had same frequency components but opposite phase noise as in (3) and (4), therefore on subtracting unwrapped version of phase of one channel from the unwrapped version of phase of another channel, cancelled out all the frequency components, leaving only phase noise, shown in fig. 5.3.

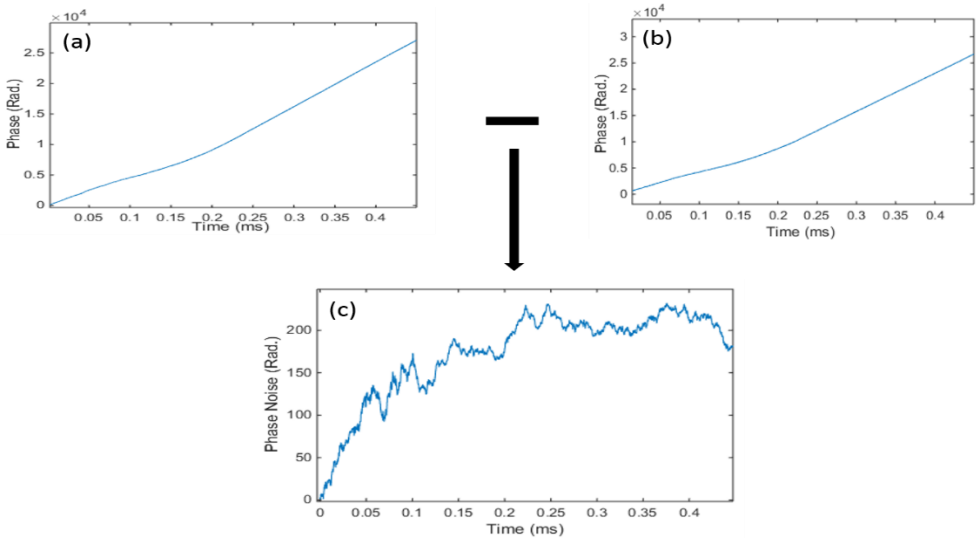

Figure 5.3 Phase noise estimation (a) Phase of channel 1. (b) Phase of channel 2. (c) Estimated phase noise

4.3.2 Laser phase noise cancelation using estimated phase noise

Subtracting estimated phases of two channels cancelled out frequency terms and the remaining was purely laser phase noise as described in Eq. (9). The subtrahend channel in the process of phase estimation has same phase noise as estimated one but opposite in sign. Therefore if we multiply estimated phase noise with subtrahend channel, phase noise is cancelled out and the remaining is the only beat frequency same as Eq. (11), shown in fig. 5.4.

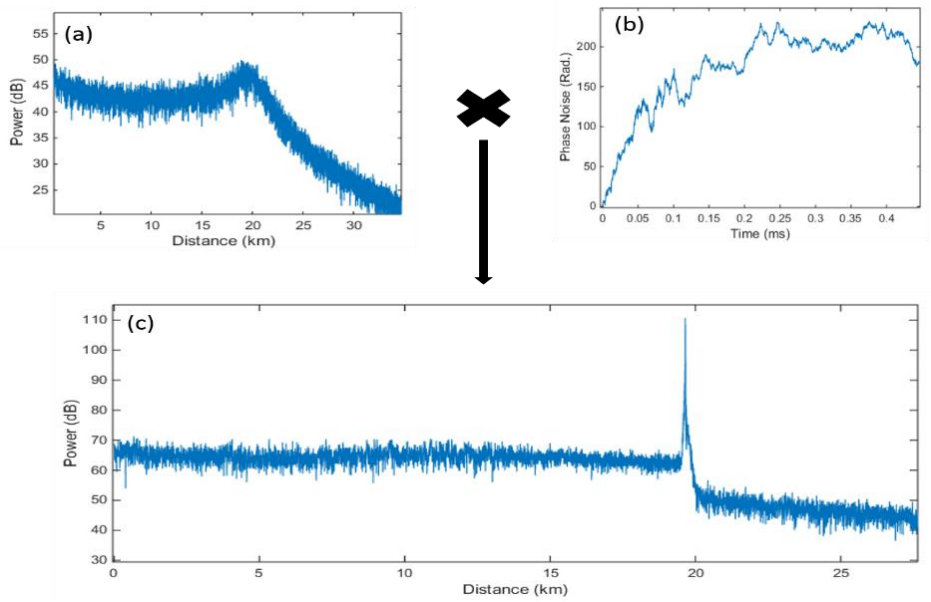

Figure 5.4 Phase noise cancellation in OFDR (a) Subtrahend channel (b) estimated phase noise (c) phase noise cancellation in 20 km long fiber

As it can be seen from the fig. 5.4 (a) the reflection peak is very broad and completely buried inside the phase noise. After multiplying the same channel signal with estimated phase noise, the present phase noise in that channel cancelled out completely and reflection peak become very clear and sharp. The obtained beat frequency is same as original without double effect, therefore does not require higher sampling rate. Moreover, phase noise cancellation through estimated laser phase noise also confirms the accuracy of proposed method of laser phase noise estimation.

5.4 Discussion

The proposed scheme to estimate lase phase noise can be used mainly for measuring spectral width of laser source. Laser phase noise cancelation in OFDR by estimated phase noise can also be another application of the proposed method and it is also demonstrated there are some advantages if the laser phase noise is canceled by estimated laser phase noise. However, there are some limitation with proposed scheme to cancel laser phase noise in OFDR using estimated phase noise. Proposed technique can cancel the phase noise in OFDR only if single reflection peak exist. Therefore this technique can only be used in OFDR applications involving single reflection peak i.e. fiber sensing, chromatic dispersion measurement. If more than one reflection peak exist the estimated phase noise will be composed of phase noise from all the reflection points and on multiplying with one of the channel each reflection will be multiplied with phase

noise from all the reflections. In such a case, when more than one reflection exist the only way to cancel laser phase noise is to multiply two channels and in doing so an additional peak (ghost peak) will appear between real reflection peaks. The ghost peak problem can be solved by using phase modulation with spread code [10].

5.5 References

[1] J. A. ARMSTRONG, "Theory of Interferometric Analysis of Laser Phase Noise*", J. Opt. Soc. Am. **56**(8), 1024-1031 (1966).

[2 CHARLES H. HENRY, "Phase Noise in Semiconductor Lasers", J. Lightwave Technol**. 4**(3), 298-31 (1986).

[3] R.W Tkach and A.R Chraplyvy, "Phase noise and linewidth in an InGaAsP DFB laser", J. Lightwave Technol. **4**(1), 1711-1716 (1986).

[4] E. D. Hinkley and Charles Freed, "DIRECT OBSERVATION OF THE LORENTZIAN LINE SHAPE AS LIMITED BY QUANTUM PHASE NOISE IN A LASER ABOVE THRESHOLD*", Phys. Rew. Lett. **2**(6), 277-280 (1969).

[5] JAIDEVA c. Goswami, Albert E. Hoefel, "Algorithms for estimating instantaneous frequency", Sig. Pro., 84 (8), 1423-1427, 2004.

[6]Lanbo Liu, "GPRS signal analysis: Instantaneous parameter estimation using the wavelet transform", Proc. 7th Int. Conf. Ground Penetrat. Rad.

[7]Miuchael Rosenblum, and Jurgen Kurths, "Analyzing synchronization phenomena from bivariate data by means of the Hilbert transform", Nonlin. Ana. Phys. Dat., springer 19988, 91-99.

[8] Mudabbir Badar, Takuya Hino, Katsushi Iwashita, "Phase noise cancelled OFDR with cm-Level Spatial Resolution Using Phase Diversity", *Phot. Tech. Let.* , 26(9), 858-861, (2014).

[9] Shuta Hiramatsu and Katsushi Iwashita, "A Novel Phase-Noise Cancelled Optical Frequency Domain Reflectometry Using Modulation Sidebands", *Photon. optoelectron. (P&O),* vol.1 Iss.3, pp. 60-64, Oct. 2012.

[10] S. Hiramatsu and K. Iwashita, "Spatial Resolution Improved Phase-Noise Cancelled Optical Frequency Domain Reflectometry Using Spreading Code", P1-41, *17th Opto-electron. commun. Conf. (OECC 2012) Tech. Digest, Busan, Korea 2012,* pp.389-390.

Chapter 6 : Discussion and Future Works

6.1 Discussion

Proposed DSB-PNC OFDR is capable of performing measurements beyond the laser coherence length. The feasibility of the proposed OFDR has been demonstrated through various experiments such as detecting breakpoints, measuring fiber temperature dependence, chromatic dispersion measurement. If there is more than one breakpoint exist in FUT, the backscattered power will have reflections from more than one location, in normal case when the spectrum of OFDR backscattered signal is obtained it shows two reflections at their corresponding originating locations. However, in the DSB-PNC OFDR this is not the case, since two channels are multiplied in order to cancel the laser phase noise therefore if each channels contains reflection power from more than one location and when two channels are multiplied with each other, as a result an unwanted peak (cross term) appears between two reflection peaks. It can be understood from fig. 6.1, where reflection peaks from same breakpoint location are multiplied with each other as a result phase noise is canceled out but at the same time reflection peaks from two different location are also multiplied with each other, as a result an unwanted peak appears between them with the phase noise equal to the difference of phase noises in two real peaks. In order to understand the mathematical explanation, let's consider DSB-SC modulated signal as described in chapter 3 Eq. (1), then backscattered signal considering from two breakpoints at propagation delay τ_1 and τ_2 can be described as below

$$E_{BS}(t) = \frac{\alpha_1 E_0}{2\sqrt{2}} \left\{ e^{j(\omega_+(t-\tau_1)+\pi\beta(t-\tau_1)^2+\theta(t-\tau_1))} + e^{j(\omega_-(t-\tau_1)-\pi\beta(t-\tau_1)^2+\theta(t-\tau_1))} \right\} + \frac{\alpha_2 E_0}{2\sqrt{2}} \left\{ e^{j(\omega_+(t-\tau_2)+\pi\beta(t-\tau_2)^2+\theta(t-\tau_2))} + e^{j(\omega_-(t-\tau_2)-\pi\beta(t-\tau)^2+\theta(t-\tau_2))} \right\} \quad (1)$$

And obtained photo currents of low frequency and high frequency channels only considering beat frequency and phase noise without constants can be derived as

$$I_h(t) \propto \alpha_1 \cos(2\pi\beta\tau_1 t + \emptyset_1) + \alpha_2 \cos(2\pi\beta\tau_2\, t + \emptyset_2) \quad (3)$$

$$I_l(t) \propto \alpha_1 \cos(2\pi\beta\tau_1 t + \emptyset_3) + \alpha_2 \cos(2\pi\beta\tau_2 t + \emptyset_4) \quad (4)$$

Where $\emptyset_1 = \theta(t) - \theta(t-\tau_1)$, $\emptyset_2 = \theta(t) - \theta(t-\tau_2)$, $\emptyset_3 = -\{\theta(t) - \theta(t-\tau_1)\}$ and $\emptyset_4 = -\{\theta(t) - \theta(t-\tau_2)\}$, when two channels are multiplied the obtained signal is like below

$$I_h(t) * I_l(t)\ ) \propto {\alpha_1}^2 \cos(4\pi\beta\tau_1 t) + {\alpha_2}^2 \cos(4\pi\beta\tau_2 t) + \alpha_1\alpha_2 \cos(4\pi\beta(\tau_1-\tau_2)t + \emptyset_1 - \emptyset_4) + \alpha_2\alpha_1 \cos(4\pi\beta(\tau_2-\tau_1)t + \emptyset_2 - \emptyset_3) \quad (5)$$

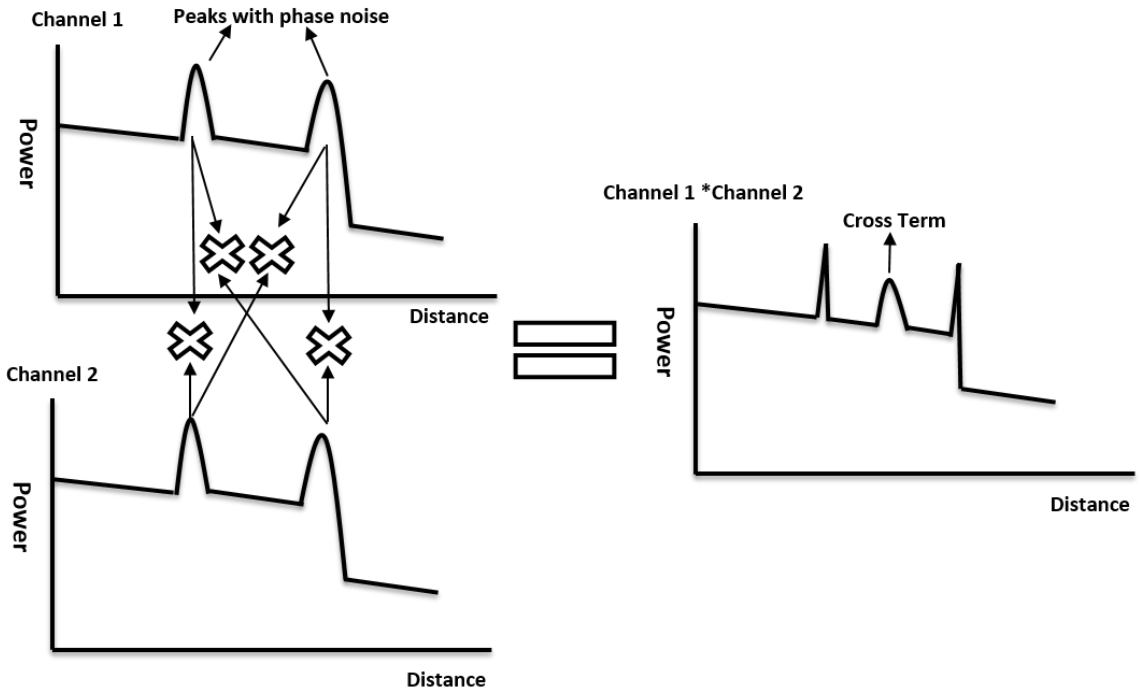

Figure 6.1 Two breakpoints scenario

In derived equation above the first and second terms are the two reflection peaks at two different locations without any phase noise and the third and fourth terms are the cross term which will appear between two reflection peaks with phase noise equal to difference of phase noises at two reflecting points. Fig. 6.2 is the experimental result of the phenomenon described above. In this experiment two reflection peaks at 1 km apart from each other were detected, as it can be seen two reflecting points peaks are clear and cross term (ghost peak) exist between them with phase noise.

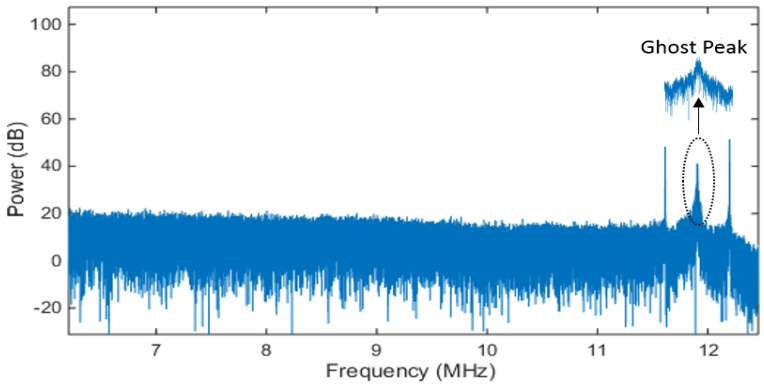

Figure 6.2 Two reflections 1 km apart from each other with a cross term between them

To solve this cross term problem a method was proposed [1] using spread spectrum, in which the phase of DSB-SC modulated signal was modulated with spreading code. The received signal from the spread spectrum technique has spreaded spectrum as a result the cross term is concealed in the spectrum and only reflection points appear.

6.2 Future works

The proposed theories in this thesis can be improved in terms of performance and there can be other applications for the DSB-PNC OFDR. Three possible future works are identified in this work which are described below.

6.2.1 Long range distributed optical sensing

Application of optical fiber in distributed optical sensing is a hot research topic in present times. There are a few advantages of using optical fiber over conventional sensors, such as optical fiber is robust, immune to external inference, provide distributed sensing. Recently, several techniques to use optical fiber as a sensors have been proposed. One technique to use optical fiber in distributed sensing is to measure the change in backscattered light pattern which can show accordance to the change in external environment such as temperature, strain, vibration [2, 3]. The backscattered pattern of every fiber is same all the time unless some external conditions are not changed or it can also be said as backscattered pattern of optical fiber is like its finger prints. Therefore, backscattered light can be considered as weak FBG which changes with the condition applied are changed. One technique using cross correlation can perform distributed sensing, in which backscattered light of each section taken at two different times are cross correlated, if external condition applied over optical fiber is not changed the correlation value for all the fiber sections

will remain high. If applied conditions are changed at any of the fiber section the backscattered pattern from that section will be changed from the one measured at earlier time and change in pattern can be recorded by obtaining reduced correlation value. This can be understood from fig. 6.3, where temperature applied on section 2 is changed at time 2 which will change the backscattered pattern from that section as compare to time 1, when backscattered pattern of same section taken at two different times are correlated the value obtained can give information of change in the temperature.

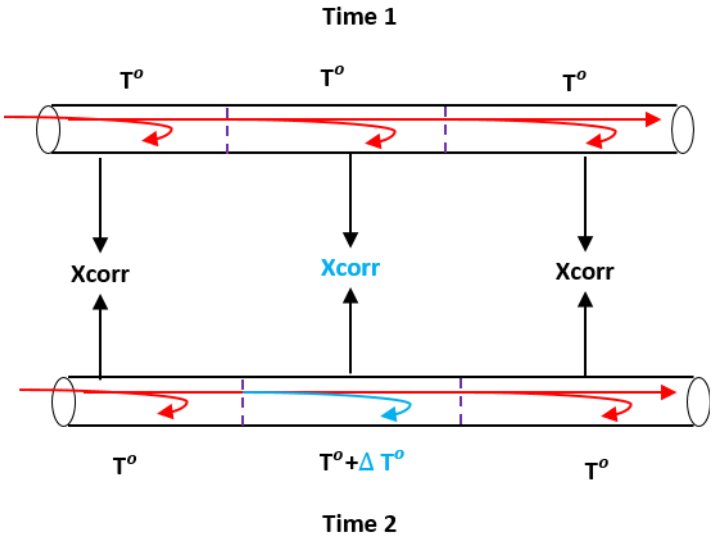

Figure 6.3 Backscattered light pattern in optical fiber as temperature applied at two different times

The backscattered pattern of an optical fiber is very sensitive which can be easily destroyed by different noises, therefore neutralizing all the possible noises is important. Since phase noise is not influential up to laser coherence length, however, beyond the laser coherence it increases drastically which can destroy the backscattered pattern, hence the correlation. Therefore optical fiber sensing is limited to short distance or within the laser coherence length, the longest optical fiber sensing reported was around 12 km [2]. For health monitoring of large structures such as bridges, tunnels, buildings need a long range sensing capability and DSB-PNC OFDR can be a right candidate for long range optical sensing because the phase noise influence is nullified which makes measurements beyond laser coherence length possible.

6.2.2 Frequency span broadening up to 12-times

A new method to increase frequency sweep span up to 3- times was proposed, as a result the spatial resolution was increase 3-times because there is a direct link between spatial resolution and frequency sweep span. The proposed method to increase spatial resolution was based on FWM and it is possible to

create cascaded two stages of FWM [4, 5]. In proposed method only one stage of FWM was created and obtained frequency span was broadened by 3-times in the form of newly generated two FWM frequency components. If both FWM components are separated using an optical filter and coupled together and used as two individual light signals for a cascaded second stage of FWM, it can result in two more new FWM frequencies with 9-times frequency sweep span broadening, if we consider Eq. (5) and (6) of chapter 4 as two signals and passed them through nonlinear medium obtained new frequency components can be described as below

$$E(t)_{FWM2} = E_{FWM}^{2}.\, E_{FWM}^{*}, \propto |E_{i2}|^{2}\left[\mathrm{e}^{j((\omega_c+9\omega_m)t+9\pi\beta t^{2}+\theta(t))}\right] \quad (6)$$

$$E(t)_{FWM2'} = E_{FWM'}^{2}.\, E_{FWM}^{*} \propto |E_{i2}'|^{2}\left[\mathrm{e}^{j((\omega_c-9\omega_m)t-9\pi\beta t^{2}+\theta(t))}\right] \quad (7)$$

Where $E(t)_{FWM2}$ and $E(t)_{FWM2'}$ are newly created FWM signals after second stage. The frequency broadening in first stage was 3-times and second stage resulted in 9-times of frequency span broadening, therefore the total frequency span was broadened by 12-times. Hence if cascaded two stages of FWM are created using proposed method frequency sweep span broadening capability can be increased from 3-times to 12-times.The configuration of two stages of FWM method can be seen in fig. 6.4.

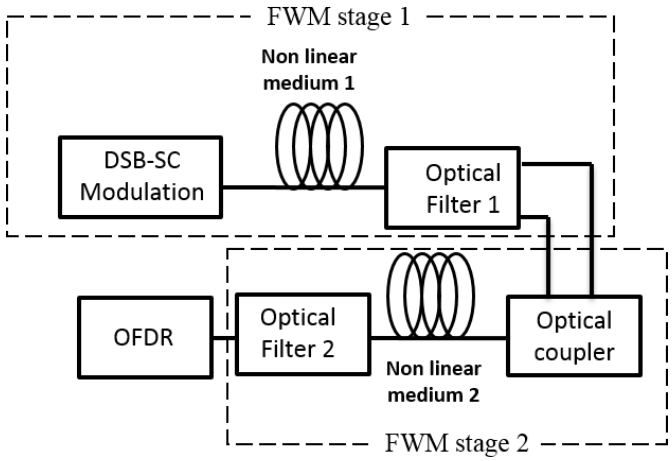

Figure 6.4 Frequency sweep span broadening based on cascaded two stages of FWM and DSB-SC modulation

6.2.3 Laser Spectral width measurement

Measuring laser linewidth has never been an easy task, especially with narrow linewidth lasers because finite delay cannot realize complete de-correlation. There are many techniques to measure laser linewidth,

measurement of laser linewidth using self-heterodyne or self-homodyne interferometry using a long optical delay is satisfactory method, however, in order to measure narrower linewidth by self-delayed heterodyne requires very long fiber delay as the coherence length of narrow linewidth laser is long. In this work a new method was proposed to estimate laser phase noise which can be used to measure the laser linewidth. The spectral analysis of estimated phase noise can reveal linewidth information. Since phase noise undergoes a random walk and the phase change follows Gaussian distribution, and laser linewidth can be known from the Gaussian distribution of estimated laser phase noise, as shown in fig. 6.5. In particular, the laser line width Δv is determined by the magnitude of the phase noise. This relationship between phase noise and linewidth is described analytically in the form of usual expression for the mean square error accumulated in a time τ

$$\sigma^2(\tau) = 2\pi\Delta v\tau$$

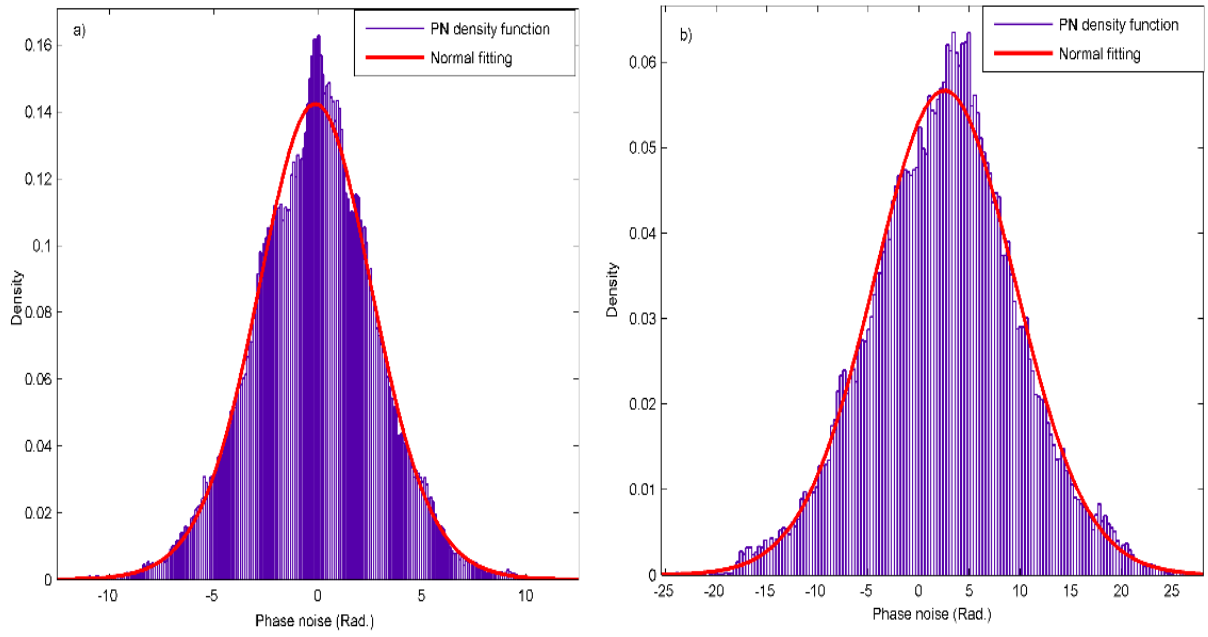

Figure 6.5 Density distribution of estimated phase noise, follows Gaussian distribution

6.3 References

[1] S. Hiramatsu and K. Iwashita, "Spatial Resolution Improved Phase-Noise Cancelled Optical Frequency Domain Reflectometry Using Spreading Code", P1-41, *17th Opto-electron. commun. Conf. (OECC 2012) Tech. Digest, Busan, Korea 2012*, pp.389-390.

[2]Z. Ding, Z. Yao, T. Liu, Y. Du, K. Liu, Q. Han, Z. Meng, H. Chen, “Long-range vibration based on correlation analysis of optical frequency-domain reflectometry signals”, Opt. Exp. **20** (27), 2012

[3] D. Zhou, Z. Qin, W. Li, L. Chen, X. Bao, “Distrubuted vibration sensing with time-resolved optical frequency-domain reflectometry”, Opt. Exp., **20** (12), 2012.

[4] J. Du, Lu. Li, X. Fan, Q. Li, and Z. He, “Sensitivity enhancement for fiber Bragg grating sensors by four wave mixing”, Photo. **2,** 426-439, (2015).

[5] S. Petit, T. Kurosu, M. Takahashi, T. Yagi, and S. Namiki, “Low penalty uniformly tunable wavelength conversion without spectral inversion over 30 nm using SBS-suppressed low-dispersion-slope highly nonlinear fibers,” Phot. Tech. Let. **23,** 546-548, (2011).

Appendix A

Here photo current equations for heterodyne detection are derived in detail.

DSB-SC Modulated light

$$E(t) = \left\{ e^{j\left((\omega_c+\omega_m)t+\pi\beta t^2+\theta(t)\right)} + e^{j\left((\omega_c-\omega_m)t-\pi\beta t^2+\theta(t)\right)} \right\}$$

Modulated light divided into two arms as below

$$E_{ref}(t) = \left\{ e^{j\left((\omega_c+\omega_m)t+\pi\beta t^2+\theta(t)\right)} + e^{j\left((\omega_c-\omega_m)t-\pi\beta t^2+\theta(t)\right)} \right\}$$

$$E_{FUT}(t) = \left\{ e^{j\left((\omega_c+\omega_m)(t-\tau_{FUT})+\pi\beta(t-\tau_{FUT})^2+\theta(t-\tau_{FUT})\right)} + e^{j\left((\omega_c-\omega_m)(t-\tau_{FUT})-\pi\beta(t-\tau_{FUT})^2+\theta(t-\tau_{FUT})\right)} \right\}$$

Before detection two sidebands are separated using optical filter in lower and higher frequency

Lower Frequency components

$$E_{refl}(t) = e^{j\left((\omega_c-\omega_m)t-\pi\beta t^2+\theta(t)\right)}$$

$$E_{FUTl}(t) = e^{j\left((\omega_c-\omega_m)(t-\tau_{FUT})-\pi\beta(t-\tau_{FUT})^2+\theta(t-\tau_{FUT})\right)}$$

Higher Frequency components

$$E_{refh}(t) = e^{j\left((\omega_c+\omega_m)t+\pi\beta t^2+\theta(t)\right)}$$

$$E_{FUTh}(t) = e^{j\left((\omega_c+\omega_m)(t-\tau_{FUT})+\pi\beta(t-\tau_{FUT})^2+\theta(t-\tau_{FUT})\right)}$$

And two separated frequency components are detected separately in a balance detector

Detected combined light with Lower Frequency Components

$$I_l(t) \propto \left|E_{refl}(t) + E_{FUTl}(t)\right|^2$$

$$= \left|E_{refl}(t)\right|^2 + |E_{FUTl}(t)|^2 + E_{FUTl}(t)^*.E_{refl}(t) + E_{FUTl}(t).E_{refl}(t)^* \quad (1)$$

For $\left|E_{refl}(t)\right|^2$

$$\left|E_{refl}(t)\right|^2 = E_{refl}(t).E_{refl}(t)^* = e^{j\left((\omega_c-\omega_m)t-\pi\beta t^2+\theta(t)\right)} * e^{-j\left((\omega_c-\omega_m)t-\pi\beta t^2+\theta(t)\right)} = 1$$

For $|E_{Futl}(t)|^2$

$$|E_{FUTl}(t)|^2 = E_{FUTl}(t).E_{FUTl}(t)^*$$
$$= e^{j\left((\omega_c-\omega_m)(t-\tau_{FUT})-\pi\beta(t-\tau_{FUT})^2+\theta(t-\tau_{FUT})\right)}$$
$$* e^{-j\left((\omega_c-\omega_m)(t-\tau_{FUT})-\pi\beta(t-\tau_{FUT})^2+\theta(t-\tau_{FUT})\right)} = 1$$

For $E_{FUTl}(t).E_{refl}(t)^*$

$$E_{FUTl}(t).E_{refl}(t)^* = e^{j\left((\omega_c-\omega_m)(t-\tau_{FUT})-\pi\beta(t-\tau_{FUT})^2+\theta(t-\tau_{FUT})\right)} * e^{-j\left((\omega_c-\omega_m)t-\pi\beta t^2+\theta(t)\right)}$$

$$= e^{j\left(\omega_c t-\omega_m t-\omega_c\tau_{FUT}+\omega_m\tau_{FUT}-\pi\beta t^2-\pi\beta{\tau_{FUT}}^2+2\pi\beta\tau_{FUT}t+\theta(t-\tau_{FUT})-\omega_c t+\omega_m t+\pi\beta t^2-\theta(t)\right)}$$

$$= e^{j\left(-(\omega_c-\omega_m)\tau_{FUT}-\pi\beta{\tau_{FUT}}^2+2\pi\beta\tau_{FUT}t+\theta(t-\tau_{FUT})-\theta(t)\right)}$$

$$= e^{j(2\pi\beta\tau_{FUT}t+\theta(t-\tau_{FUT})-\theta(t)+\emptyset_1)}$$

Where $\emptyset_1 = -(\omega_c-\omega_m)\tau_{FUT} - \pi\beta{\tau_{FUT}}^2$

For $E_{FUTl}(t)^*.E_{refl}(t)$

$$E_{FUTl}(t)^*.E_{refl}(t) = e^{-j\left((\omega_c-\omega_m)(t-\tau_{FUT})-\pi\beta(t-\tau_{FUT})^2+\theta(t-\tau_{FUT})\right)} * e^{j\left((\omega_c-\omega_m)t-\pi\beta t^2+\theta(t)\right)}$$

$$= e^{j\left(-\omega_c t+\omega_m t+\omega_c\tau_{FUT}-\omega_m\tau_{FUT}+\pi\beta t^2+\pi\beta{\tau_{FUT}}^2-2\pi\beta\tau_{FUT}t-\theta(t-\tau_{FUT})+\omega_c t-\omega_m t-\pi\beta t^2+\theta(t)\right)}$$

$$= e^{-j\left(-(\omega_c-\omega_m)\tau_{FUT}-\pi\beta{\tau_{FUT}}^2+2\pi\beta\tau_{FUT}t+\theta(t-\tau_{FUT})-\theta(t)\right)}$$

$$= e^{-j(2\pi\beta\tau_{FUT}t+\theta(t-\tau_{FUT})-\theta(t)+\emptyset_1)}$$

Putting all the calculated values in Eq. (1) and ignoring DC terms

$$I_l(t) \propto \left|E_{refl}(t) + E_{FUTl}(t)\right|^2$$
$$= 1 + 1 + e^{j(2\pi\beta\tau_{FUT}t+\theta(t-\tau_{FUT})-\theta(t)+\emptyset_1)} + e^{-j(2\pi\beta\tau_{FUT}t+\theta(t-\tau_{FUT})-\theta(t)+\emptyset_1)}$$

$$I_l(t) \propto \cos(2\pi\beta\tau_{FUT}t + \theta(t-\tau_{FUT}) - \theta(t) + \emptyset_1) \quad (2)$$

Detected combined light with Higher Frequency Components

$$I_h(t) \propto \left|E_{refh}(t) + E_{FUTh}(t)\right|^2$$

$$= \left|E_{refh}(t)\right|^2 + |E_{FUTh}(t)|^2 + E_{FUTh}(t)^*.E_{refh}(t) + E_{FUTh}(t).E_{refh}(t)^* \qquad (3)$$

For $\left|E_{refh}(t)\right|^2$

$$\left|E_{refh}(t)\right|^2 = E_{refh}(t).E_{refh}(t)^* = e^{j\left((\omega_c+\omega_m)t-\pi\beta t^2+\theta(t)\right)} * e^{-j\left((\omega_c+\omega_m)t-\pi\beta t^2+\theta(t)\right)} = 1$$

For $|E_{Futh}(t)|^2$

$$|E_{FUTh}(t)|^2 = E_{FUTh}(t).E_{FUTh}(t)^*$$

$$= e^{j\left((\omega_c+\omega_m)(t-\tau_{FUT})-\pi\beta(t-\tau_{FUT})^2+\theta(t-\tau_{FUT})\right)}$$

$$* e^{-j\left((\omega_c+\omega_m)(t-\tau_{FUT})-\pi\beta(t-\tau_{FUT})^2+\theta(t-\tau_{FUT})\right)} = 1$$

For $E_{FUTh}(t).E_{refh}(t)^*$

$$E_{FUTh}(t).E_{refh}(t)^* = e^{j\left((\omega_c+\omega_m)(t-\tau_{FUT})+\pi\beta(t-\tau_{FUT})^2+\theta(t-\tau_{FUT})\right)} * e^{-j\left((\omega_c+\omega_m)t+\pi\beta t^2+\theta(t)\right)}$$

$$= e^{j\left(\omega_c t+\omega_m t-\omega_c\tau_{FUT}-\omega_m\tau_{FUT}+\pi\beta t^2+\pi\beta{\tau_{FUT}}^2-2\pi\beta\tau_{FUT}t+\theta(t-\tau_{FUT})-\omega_c t-\omega_m t-\pi\beta t^2-\theta(t)\right)}$$

$$= e^{j\left(-(\omega_c+\omega_m)\tau_{FUT}+\pi\beta{\tau_{FUT}}^2-2\pi\beta\tau_{FUT}t+\theta(t-\tau_{FUT})-\theta(t)\right)}$$

$$= e^{-j(2\pi\beta\tau_{FUT}t-\theta(t-\tau_{FUT})+\theta(t)+\emptyset_2)}$$

Where $\emptyset_2 = (\omega_c + \omega_m)\tau_{FUT} - \pi\beta{\tau_{FUT}}^2$

For $E_{FUTh}(t)^*.E_{refh}(t)$

$$E_{FUTh}(t)^*.E_{refh}(t) = e^{-j\left((\omega_c+\omega_m)(t-\tau_{FUT})+\pi\beta(t-\tau_{FUT})^2+\theta(t-\tau_{FUT})\right)} * e^{j\left((\omega_c+\omega_m)t+\pi\beta t^2+\theta(t)\right)}$$

$$= e^{j\left(-\omega_c t-\omega_m t+\omega_c\tau_{FUT}+\omega_m\tau_{FUT}-\pi\beta t^2-\pi\beta{\tau_{FUT}}^2+2\pi\beta\tau_{FUT}t-\theta(t-\tau_{FUT})+\omega_c t+\omega_m t+\pi\beta t^2+\theta(t)\right)}$$

$$= e^{j\left((\omega_c+\omega_m)\tau_{FUT}-\pi\beta{\tau_{FUT}}^2+2\pi\beta\tau_{FUT}t-\theta(t-\tau_{FUT})+\theta(t)\right)}$$

$$= e^{j(2\pi\beta\tau_{FUT}t-\theta(t-\tau_{FUT})-\theta(t)+\emptyset_2)}$$

Similarly inserting all the calculated values in Eq.3 and ignoring DC terms

$$I_h(t) \propto \left|E_{refh}(t) + E_{FUTh}(t)\right|^2 = 1 + 1 + e^{j(2\pi\beta\tau_{FUT}t - \theta(t-\tau_{FUT}) + \theta(t) + \emptyset_2)} + e^{-j(2\pi\beta\tau_{FUT}t - \theta(t-\tau_{FUT}) + \theta(t) + \emptyset_2)}$$

$$I_h(t) \propto \cos(2\pi\beta\tau_{FUT}t - \theta(t-\tau_{FUT}) + \theta(t) + \emptyset_2)$$

$$\propto \cos(2\pi\beta\tau_{FUT}t - \{\theta(t-\tau_{FUT}) - \theta(t)\} + \emptyset_2) \quad (4)$$

As Eq. (2) and Eq. (4) has same frequency components and equal but opposite phase noise, therefor phase is noise term canceled out on multiplying two equations together, as below

$$I_h(t) * I_l(t) \propto \cos(4\pi\beta\tau_{FUT}t + \emptyset_1 + \emptyset_2)$$

$\emptyset_1 \& \emptyset_2$ are constant terms so can be ignored.

Appendix B

Here photo current equations of phase diversity are derived in detail

After modulating light source by double side band suppress carrier, the optical field we get is like below

$$E(t) = \frac{E_o}{2}\left\{e^{j\left(\omega_+ t+\pi\beta t^2+\theta(t)\right)} + e^{j\left(\omega_- t-\pi\beta t^2+\theta(t)\right)}\right\} \quad (1)$$

Linearly polarized reference light signal is divided into two inphase signals $E_{refA}(t)$ *and* $E_{refB}(t)$ *in 90 degree hybrid, they are described below*

$$E_{ref}(t) = \frac{1}{\sqrt{2}}\,E(t)$$

$$E_{refA}(t) = \frac{1}{\sqrt{2}}\,E_{ref}(t) = \frac{1}{2}\,E(t)$$

$$E_{refA}(t) = E_{refB}(t) = \frac{E_o}{4}\left\{e^{j\left(\omega_+ t+\pi\beta t^2+\theta(t)\right)} + e^{j\left(\omega_- t-\pi\beta t^2+\theta(t)\right)}\right\} = \frac{E_o}{4}\left\{e^{j\theta_{r1}} + e^{j\theta_{r2}}\right\} \quad (2)$$

Circularly polarized backscattered light from FUT is divided into two 90 degree out of phase signals $E_{FUTA}(t)$ *and* $E_{FUTB}(t)$ *in 90 degree hybrid, which are represented as below*

$$E_{FUT}(t) = \frac{\alpha}{\sqrt{2}}E(t-\tau_{FUT})$$

$$E_{FUTA}(t) = \frac{1}{\sqrt{2}}E_{FUT}(t) = \frac{\alpha}{2}E(t-\tau_{FUT})$$

$$E_{FUTA}(t) = \alpha\frac{E_o}{4}\left\{e^{j\left(\omega_+(t-\tau_{FUT})+\pi\beta(t-\tau_{FUT})^2+\theta(t-\tau_{FUT})\right)} + e^{j\left(\omega_-(t-\tau_{FUT})-\pi\beta(t-\tau_{FUT})^2+\theta(t-\tau_{FUT})\right)}\right\}$$

$$= \alpha\frac{E_o}{4}\left\{e^{j\theta_{F1}} + e^{j\theta_{F2}}\right\} \quad (3)$$

$$E_{FUTB}(t) = \alpha\frac{E_o}{4}\left\{e^{j\left(\omega_+(t-\tau_{FUT})+\pi\beta(t-\tau_{FUT})^2+\theta(t-\tau_{FUT})+\frac{\pi}{2}\right)} + e^{j\left(\omega_-(t-\tau_{FUT})-\pi\beta(t-\tau_{FUT})^2+\theta(t-\tau_{FUT})+\frac{\pi}{2}\right)}\right\}$$

$$= \alpha\frac{E_o}{4}\left\{e^{j\theta_{F3}} + e^{j\theta_{F3}}\right\} \quad (4)$$

where α is the fiber loss and the reflectivity of the reflected signal

and

$\omega_+ = \omega_c + \omega_m\,, \qquad \omega_- = \omega_c - \omega_m$

$\theta_{r1} = \omega_+ t + \pi\beta t^2 + \theta(t), \qquad \theta_{r2} = \omega_- t - \pi\beta t^2 + \theta(t)$

$\theta_{F1} = \omega_+(t - \tau_{FUT}) + \pi\beta(t - \tau_{FUT})^2 + \theta(t - \tau_{FUT})$

$\theta_{F2} = \omega_-(t - \tau_{FUT}) - \pi\beta(t - \tau_{FUT})^2 + \theta(t - \tau_{FUT})$

$\theta_{F3} = \omega_+(t - \tau_{FUT}) + \pi\beta(t - \tau_{FUT})^2 + \theta(t - \tau_{FUT}) + \frac{\pi}{2}$

$\theta_{F4} = \omega_-(t - \tau_{FUT}) - \pi\beta(t - \tau_{FUT})^2 + \theta(t - \tau_{FUT}) + \frac{\pi}{2}$

As it should be noted here that $E_{refA}(t)\ and\ E_{FUTA}(t)$ are two inphase light signals and $E_{refB}(t)$ & $E_{FUTB}(t)$ are two $\pi/2$ out of phase signals. Two inphase signals are detected together in a balance detector, as shown below

$$I_I(t) \propto \left|E_{refA}(t) + E_{FUTA}(t)\right|^2$$

$$= \left|E_{refA}(t)\right|^2 + |E_{FUTA}(t)|^2 + E_{FUTA}(t)^*.E_{refA}(t) + E_{FUTA}(t).E_{refA}(t)^* \qquad (5)$$

Here

$$\left|E_{refA}(t)\right|^2 = \left|\frac{E_o}{4}\left\{e^{j\theta_{r1}} + e^{j\theta_{r2}}\right\}\right|^2 = \frac{{E_o}^2}{16}\left\{1 + 1 + e^{j(\theta_{r1} - \theta_{r2})} + e^{j(\theta_{r2} - \theta_{r1})}\right\}$$

$$= \frac{{E_o}^2}{16}\left\{1 + 1 + e^{j(2\omega_m t + 2\pi\beta t^2)} + e^{-j(2\omega_m t + 2\pi\beta t^2)}\right\} \qquad (6)$$

Similarly

$$|E_{FUTA}(t)|^2 = \left|\alpha\frac{E_o}{4}\left\{e^{j\theta_{F1}} + e^{j\theta_{F2}}\right\}\right|^2 = \alpha^2\frac{{E_o}^2}{16}\left\{1 + 1 + e^{j(\theta_{F1} - \theta_{F2})} + e^{j(\theta_{F2} - \theta_{F1})}\right\}$$

$$` \quad = \alpha^2\frac{{E_o}^2}{16}\left\{1 + 1 + e^{j(2\omega_m(t - \tau_{FUT}) + 2\pi\beta(t - \tau_{FUT})^2)} + e^{-j(2\omega_m(t - \tau_{FUT}) + 2\pi\beta(t - \tau_{FUT})^2)}\right\} \qquad (7)$$

After ignoring DC components Eq. (6) and Eq. (7) becomes

$$\left|E_{refA}(t)\right|^2 \propto \frac{{E_o}^2}{16}\left\{e^{j(2\omega_m t + 2\pi\beta t^2)} + e^{-j(2\omega_m t + 2\pi\beta t^2)}\right\} \qquad (8)$$

$$|E_{FUTA}(t)|^2 \propto \alpha^2 \frac{{E_o}^2}{16}\left\{e^{j(2\omega_m(t-\tau_{FUT})+2\pi\beta(t-\tau_{FUT})^2)} + e^{-j(2\omega_m(t-\tau_{FUT})+2\pi\beta(t-\tau_{FUT})^2)}\right\} \quad (9)$$

And

$$E_{FUTA}(t).E_{refA}(t)^* = \alpha\frac{{E_o}^2}{16}\{\, e^{-jA} + e^{-jB} + e^{jC} + e^{jD}\} \quad (10)$$

While

$$E_{FUTA}(t)^*.E_{refA}(t) = \alpha\frac{{E_o}^2}{16}\{e^{jA} + e^{jB} + e^{-jC} + e^{-jD}\} \quad (11)$$

where

$$A = \theta_{r1} - \theta_{F1} = 2\pi\beta\tau_{FUT}t + \theta(t) - \theta(t-\tau_{FUT}) + \emptyset_2$$

$$B = \theta_{r2} - \theta_{F2} = 2\pi\beta\tau_{FUT}t - \theta(t) + \theta(t-\tau_{FUT}) - \emptyset_1$$

$$C = \theta_{r1} - \theta_{F2} = 2\omega_m t - 2\pi\beta\tau_{FUT}t + 2\pi\beta t^2 + \theta(t) - \theta(t-\tau_{FUT}) + \emptyset_1$$

$$D = \theta_{r2} - \theta_{F1} = 2\omega_m t - 2\pi\beta\tau_{FUT}t + 2\pi\beta t^2 - \theta(t) + \theta(t-\tau_{\mathrm{FUT}}) - \emptyset_2$$

$$\emptyset_1 = \omega_-\tau_{FUT} + \pi\beta{\tau_{FUT}}^2,\ \emptyset_2 = \omega_+\tau_{FUT} - \pi\beta{\tau_{FUT}}^2$$

After putting all simplified terms in Eq. (5), it becomes

$$I_I(t) \propto \frac{{E_o}^2}{16}\left\{e^{j(2\omega_m t+2\pi\beta t^2)} + e^{-j(2\omega_m t+2\pi\beta t^2)}\right\} + \alpha^2\frac{{E_o}^2}{16}\left\{e^{j(2\omega_m(t-\tau_{FUT})+2\pi\beta(t-\tau_{FUT})^2)} + e^{-j(2\omega_m(t-\tau_{FUT})+2\pi\beta(t-\tau_{FUT})^2)}\right\} + \alpha\frac{{E_o}^2}{16}\{e^{-jA} + e^{-jB} + e^{jC} + e^{jD} + e^{jA} + e^{jB} + e^{-jC} + e^{-jD}\} \quad (12)$$

As in our experiment the ω_m has frequency in GHz, while $2\pi\beta\tau_{FUT}$ is in MHz. Therefore after passing signal through low pas filter and filtering out GHz frequency terms, only low frequency terms will remain, which are A and B. Then Eq. (12) will become

$$I_I(t) \propto \alpha\frac{{E_o}^2}{16}\{e^{-jA} + e^{jB} + e^{jA} + e^{j-B}\}$$

$$I_I(t) \propto \alpha\frac{{E_o}^2}{16}\{2\cos(A) + 2\cos(B)\} = \alpha\frac{{E_o}^2}{8}\{\cos(A) + \cos(B)\} \quad (13)$$

List of publications

Journals

[1] **Mudabbir Badar**, Takuya Hino, and Katsushi Iwashita, "Phase noise cancelled OFDR with cm-Level Spatial Resolution Using Phase Diversity", *IEEE Photonics Technology Letters*, Vol. 26, No.9, pp. 858-861, 2014.

[2] **Mudabbir Badar**, Hirokazu Kobayashi, and Katsushi Iwashita, "Chromatic dispersion measurement with double sideband phase noise canceled OFDR*", Optics Communications*, vol. 356, pp.350-355, 2015.

[3] **Mudabbir Badar**, Hirokazu Kobayashi, and Katsushi Iwashita, "Demonstration of format free wavelength conversion for optical networks*", Optical and Quantum Electronics*, vol. 48, no. 1, 2016.

[4] **Mudabbir Badar**, Hirokazu Kobayashi, and Katsushi Iwashita, "Spatial resolution improvement in optical frequency domain reflectometry using four wave mixing and DSB-SC modulation*", "under review".*

Conferences/Presentations

[1] **M. Badar** and I. Katsushi, "Phase Fluctuation Extraction from Optical Frequency-Domain Reflectometry," *in Frontiers in Optics 2014, OSA Technical Digest , (Optical Society of America, 2014), paper JW3A.22.*

[2] **Mudabbir Badar**, Takuya Hino, and Katsushi Iwashita, "Phase Noise Cancelled Optical Frequency Domain-Reflectometry with cm-Level Spatial Resolution" *in Proceedings of the 2014 IEICE General Conference, B-13-34, Niigata 2014.*

[3] **Mudabbir Badar** and Katsushi Iwashita, "Phase Noise Extraction and Cancellation in Optical Frequency Domain Reflectometry", *in China-Japan Innovation Forum on New Energy Utilization and Sustainable Development academic symposium 2014.*

[4] **Mudabbir Badar**, Hirokazu Kobayashi, and Katsushi Iwashita," Format Free Wavelength Conversion by OSSB Modulator and AWG*", in Proceedings 20th Opto-electronics and communication (OECC), PWe.44, Shanghai, 2015.*

[5] **Mudabbir Badar**, Hirokazu Kobayashi, and Katsushi Iwashita, "Frequency Span Broadening in OFDR using FWM and DSB-SC Modulation", *in Proceedings of the 2016 IEICE General Conference, B-13-12, Fukuoka, 2016.*